THE AQUEOUS GEOCHEMISTRY OF THE LIGHTNING DOCK KNOWN GEOTHERMAL RESOURCE AREA, ANIMAS VALLEY, HIDALGO COUNTY, NEW MEXICO

BY

MARK J. LOGSDON

A.B., Geology, Princeton University, 1972

THESIS

Submitted in Partial Fulfillment of the
Requirements for the Degree of

Master of Science in Geology

The University of New Mexico
Albuquerque, New Mexico

May, 1981

ACKNOWLEDGEMENTS

Dr. G. P. Landis suggested the stable isotope study of the Lightning Dock system, provided the hydrogen isotope data, and provided many instructions, suggestions and ideas during the course of the research. Water samples and chemical analyses of the samples were provided by Dr. C. A. Swanberg. Mssrs. Roy Northrop and Ronald Churchill assisted with mass spectrometry. The thesis has profited from discussions with Drs. J. F. Callender, W. E. Elston, R. O. Fournier, H. D. Holland, S. G. Wells, and C. J. Yapp. I would like to acknowledge the use of analytical and computer facilities of the University of New Mexico. WATEQF was made available by and run on the computer facilities of the U.S. Geological Survey - Water Resources Division in Albuquerque, New Mexico. I am particularly grateful to Mr. Scott Anderholm of the U.S. Geological Survey for his assistance with the computer modeling. I would like to thank Ms. Sheri Bearse for typing the thesis and Ms. Judy Salas for drafting the figures. Financial support for the thesis was provided by the New Mexico Geological Society, the Department of Geology of the University of New Mexico and the New Mexico Energy Research and Development Program through Project Number 68R-2102.

THE AQUEOUS GEOCHEMISTRY OF THE LIGHTNING DOCK KNOWN GEOTHERMAL RESOURCE AREA, ANIMAS VALLEY, HIDALGO COUNTY, NEW MEXICO

BY

Mark J. Logsdon

ABSTRACT OF THESIS

Submitted in Partial Fulfillment of the
Requirements for the Degree of

Master of Science in Geology

The University of New Mexico
Albuquerque, New Mexico

May, 1981

THE AQUEOUS GEOCHEMISTRY OF THE LIGHTNING DOCK KNOWN GEOTHERMAL RESOURCE AREA, ANIMAS VALLEY, HIDALGO COUNTY, NEW MEXICO

Mark J. Logsdon
A.B., Geology, Princeton University, 1972
M.S., Geology, University of New Mexico, 1981

The Lightning Dock Known Geothermal Resource Area, located approximately 30 km southwest of Lordsburg, Hidalgo County, New Mexico, is on the east side of the lower Animas Valley, a north-trending graben in the Basin and Range tectonic province of southwestern New Mexico. Shallow wells produce 70° to 85°C water from Quaternary piedmont deposits which are underlain by approximately 1800 m of Oligocene ash-flow tuff, 400 m of Paleozoic sediments and Precambrian granitic basement. A 140,000-year-old basalt flow is located 15 km southwest of the hot wells.

The aqueous geochemistry of 55 water samples from shallow wells was modeled using graphical techniques and equilibrium analytical calculations, including chemical geothermometers, the computer program WATEQF and mineral stability diagrams. Fourteen of the samples were analyszed for oxygen and hydrogen isotopes.

The sample waters are mixtures of dilute sodium bicarbonate water with waters rich in calcium and sulfate and, to a lesser degree, chloride. Alkali and silica geothermometers indicate a shallow reservoir temperature of approximately 165°C. The silica - enthalpy mixing model suggests that the waters of the hot wells are mixed waters containing about 25% deep geothermal water of 250°C. Equilibrium calculations indicate that alteration phases should include magnesian calcite, smectites,

illite, zeolites, alkali feldspar, quartz, anhydrite, fluorite, and Fe-sulfides and -oxides. The $\delta^{18}O$ values of the lower Animas Valley water samples range from -9.0‰ to -11.4‰; δD values range from -65‰ to -80‰. The isotopic values indicate that the waters are meteoric in origin but may have been modified by evaporation and boiling.

Spatial analysis of the geochemistry of the water samples suggests that 250°C water moves up and along a major northeast-trending fault from a deep reservoir located southwest of the hot wells, mixing with shallow, cold aquifer waters to produce the mixed waters sampled in the shallow wells. The heat source for the geothermal system is probably basaltic magma.

TABLE OF CONTENTS

Page

List of Figures ix

List of Tables. xiii

Introduction. 1

Geologic Setting. 4

Methods and Procedures. 10

Water Chemistry 12

Composition. 12

Processes Affecting the Solvent. 44

Water-Rock Interaction 58

Mixing Model 94

The Geothermal Reservoir. 104

Physicochemical Environment. 104

Charge Balance. 104

Ionic Strength. 108

Activity Coefficients 108

P_{CO_2} and pH of Solution 109

Geometry and Hydrodynamics of the Geothermal System. 126

Conclusions 140

Appendices

Appendix 1 Chemical Analyses. 141

Appendix 2 Calculating Chemical Equilibrium of Natural Waters 162

Part I: The Aqueous Chemical Model 163

Mass Action Equilibrium Equations. 163

Table of Contents cont'd

	Page
Activity Coefficients	164
Solution of Mass Action and Mass Balance Equations	166
Ion Activity Products and Solubility Products	168
Effects of Temperature and Pressure	170
Redox Reactions	171
Gas Partial Pressures	173
Part II: WATEQF	174
Appendix 3 Computer-Modeled Geothermometry	187
Appendix 4 Mineral Stability Diagrams	198
Appendix 5 Oxygen and Hydrogen Isotope Relationships in Geothermal and Related Groundwaters	205
Isotopic Notation and Standards	205
Analytical Methods	206
Isotope Fractionation Processes	210
δD and $\delta^{18}O$ Systematics in Groundwater	219
Apparent and True Fractionation Factors for a Mixture of Waters	223
References	228

FIGURE CAPTIONS

Figure		Page
1	Index map of the Animas Valley, Hidalgo County, New Mexico and vicinity (after Elston and Deal, 1978)	3
2	Generalized structural setting of the lower Animas Valley.	7
3	Locations of the P-series and LD-series water samples in the Animas and adjacent Lordsburg and Playas valleys. . .	14
4	Locations of P-series (•) and An-series (+) water samples in the lower Animas Valley.	16
5	Trilinear plot of the water samples from the Animas Valley.	40
6	Ca-Mg-Na+K and HCO_3-Cl-SO_4 plots from Fig. 5 with P-series (•), LD-series (+), and An-series (▲) waters plotted separately.	42
7	δD and $\delta^{18}O$ values for the P-series waters.	47
8	Graphical solution for α_{model} in equation (3a) given $\alpha_{app} = 0.9962$ and $f_2 = 0.76$	57
9	Isopleths drawn for $\delta^{18}O$ values of P-series sample waters.	60
10	Isopleths drawn for best estimate shallow reservoir temperatures of P-series (•) and An-series (+) waters . .	67
11	Plot of boron concentration against calculated alkali temperatures for all water samples and for calculated geothermal reservoir compositions R2, R3, and R4.	75

Figure Captions cont'd

Figure		Page
12	Plot of chloride concentration against calculated alkali temperatures for all water samples and for calculated geothermal reservoir compositions R2, R3, and R4.	77
13	Plot of concentration of calcium and magnesium against concentration of total dissolved solids (TDS) for all water samples	79
14	Plot of concentration of sulfate and bicarbonate against concentration of total dissolved solids (TDS) for all water samples	81
15	Isopleths drawn for boron/calcium molar ratios (x 10^3) in P-series (•) and An-series (+) waters.	89
16	Isopleths drawn for boron/sodium molar ratios (x 10^3) in P-series (•) and An-series (+) waters.	91
17	Isopleths drawn for sulfate/fluoride molar ratios in P-series (•) and An-series (+) waters	93
18	Plot of dissolved silica versus enthalpy used to estimate the temperature and fraction of hot-water component in a mixed water	99
19	Plots of (log a_{K^+}/log a_{H^+}) and (log a_{Na^+}/log a_{H^+}) versus log $a_{H_4SiO_4}$ for representative water samples and for calculated geothermal reservoir waters R2, R3, and R4 . .	116

Figure Cations cont'd

Figure		Page
20	Compositions of low-temperature sample waters plotted on the mineral stability diagram for the system HCl-H_2O-Al_2O_3-K_2O-Na_2O-SiO_2 at 25°C and log $a_{H_4SiO_4}$ = -4.00 = quartz saturation (phase boundaries after Helgeson and others, 1969).	118
21a	Compositions of hot well samples P2, P3, and P4 plotted on the mineral stability diagram for the system HCl-H_2O-Al_2O_3-MgO-Na_2O-SiO_2 at 150°C and log $a_{H_4SiO_4}$ = -2.67 = quartz saturation (phase boundaries after Helgeson and others, 1969)	120
21b	Compositions of geothermal reservoir waters R2, R3, and R4 plotted on the mineral stability diagram for the system HCl-H_2O-Al_2O_3-MgO-Na_2O-SiO_2 at 250°C and log $a_{H_4SiO_4}$ = -2.11 = quartz saturation (phase boundaries after Helgeson and others, 1969).	120
22a	Compositions of hot well samples P2, P3, and P4 plotted on the mineral stability diagram for the system HCl-H_2O-Al_2O_3-K_2O-Na_2O-SiO_2 at 150°C and log $a_{H_4SiO_4}$ = -2.67 = quartz saturation (phase boundaries after Helgeson and others, 1969)	122
22b	Compositions of calculated geothermal reservoir waters R2, R3, and R4 plotted on the mineral stability diagram for the system HCl-H_2O-Al_2O_3-K_2O-Na_2O-SiO_2 at 250°C and	

Figure Captions cont'd

Figure		Page
22b	log $a_{H_4SiO_4}$ = -2.11 = quartz saturation (phase boundaries after Helgeson and others, 1969)	122
23	Calculated trends of pH with temperature for waters of three salinities (M_a), where $M_a = m_{Na^+} + m_{K^+}$.	125
24a	Total field apparent resistivity map of the Lightning Dock KGRA (after Jiracek, in Callender, 1980)	128
24b	Simple Bouguer anomaly gravity map of the Lightning Dock KGRA and vicinity (after Jiracek, in Callender, 1980) . .	128
25	Simple high-temperature hot-spring system with deeply circulating meteoric water assumed to be heated entirely by conduction (after White, 1968)	131
26	Diagrammatic representation of a thermal-spring system largely in fractured crystalline rocks.	134
27	Schematic block diagram of the geothermal system in the lower Animas Valley	138
A3.1	Silica solubility along the liquid-vapor water pressure curve for alpha quartz (A), chalcedony (B), and amorphous silica (C).	193

LIST OF TABLES

Table		Page
1	Chemical Data	17
2	Comparison of Calculated Reservoir Temperatures [°C]	62
3A	Multiple Linear Regression-Correlation Coefficients, Lightning Dock KGRA Data	68
3B	Multiple Linear Regression-Correlation Coefficients, Lightning Dock KGRA P-Series Data	71
4	Minerals Calculated by WATEQF to be in Equilibrium with the Waters of the Lower Animas Valley	86
5	Aqueous Silica Solubility	96
6	Mixing Estimates and Calculated Reservoir Chemistry (ppm)	101
7	Post-Mixing Composition Shift of P4	103
8	Physicochemical Parameters	105
9	Equilibrium and Solubility Constants	110
A1.1	Sample Locations of P- An- LD-Series	142
A1.2	Analyses of Iron, Fluoride, Boron, Phosphorus, and Silica in Samples	144
A1.3	Analyses of Iron, Fluoride, Boron, Phosphorus, and Silica in Samples	148
A1.4	Analyses of Nitrogen Species, Nickel, Lead, Antimony, Selenium, Strontium, and Zinc in Samples	151
A1.5	Analyses of Cadmium, Cobalt, Chromium, Copper, Mercury, Hydrogen Sulfide, Lithium, Manganese, Molybdenum, Ammonium, Silver, Aluminum, Arsenic, Barium, and Bromine in Samples	153

List of Tables cont'd

Table		Page
A1.6	Gram-Formula-Weights Used to Convert Analyzed Concentrations to Molality.	155
A1.7	Whole-Rock Chemistry of Samples from the Pyramid Mountains	157
A1.8	Summary of Analytical Techniques for Water Chemistry. . .	159
A2.1	Descriptive Program Features of WATEQF.	175
A2.2	Comparison of pE, EH, and Calculated Concentrations of Fe^{2+} and Fe^{3+} of Sample P3 for Imposed Redox Postentials.	181
A3.1	Na-K-Ca Alkali Geothermometer Curve-Fitting Data.	189
A3.2	Reservoir Temperature After Apply Mg^{++} Correction	197

INTRODUCTION

The Lightning Dock Known Geothermal Resource Area (KGRA) and adjacent portions of the Animas Valley (Fig. 1) were selected for a detailed geochemical study of a geothermal system in New Mexico. The Lightning Dock system is one of two geothermal systems (the other is the Valles Caldera system) in New Mexico with indicated subsurface temperatures above 150°C (White and Williams, 1975). Recent geophysical and geological studies of the Lightning Dock area (Jiracek and Smith, 1976; Smith, 1978; Elston and Deal, 1978) provide important information which can be refined and supplemented by a study of the aqueous and stable isotope geochemistry of the system. The study has three major objectives: first, evaluation of several important parameters which characterize a potential geothermal resource area, including reservoir temperature, reservoir location and extent, source of geothermal waters, and residence time for waters in the system; second, examination of the chemical evolution of low temperature (< 300°C) natural waters as they interact with reservoir rock, mix with other waters, and undergo physical changes of state; and third, delineation of the basic chemical and physical parameters of the reservoir to develop a model for the geothermal system in the Animas Valley.

Figure 1. Index map of the Animas Valley, Hidalgo County, New Mexico and vicinity (after Elston and Deal, 1978).

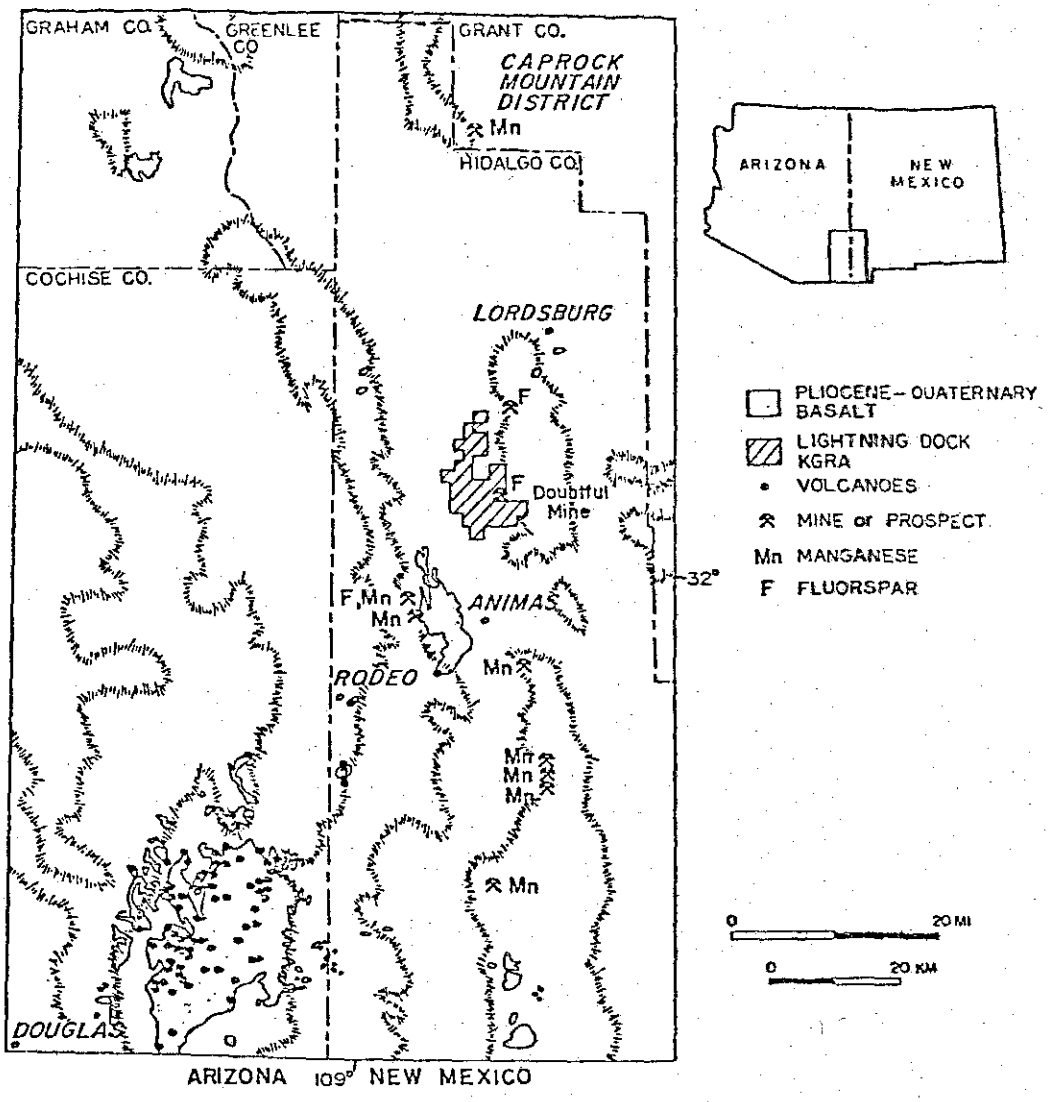
GRAHAM CO.
GREENLEE CO.
GRANT CO.
CAPROCK MOUNTAIN DISTRICT
Mn
HIDALGO CO.
COCHISE CO.
LORDSBURG
F
F
Doubtful Mine
F, Mn
Mn
ANIMAS
32°
Mn
RODEO
Mn
Mn
Mn
Mn
DOUGLAS
ARIZONA
109°
NEW MEXICO
ARIZONA
NEW MEXICO
PLIOCENE–QUATERNARY BASALT
LIGHTNING DOCK KGRA
VOLCANOES
MINE or PROSPECT
Mn MANGANESE
F FLUORSPAR
0
20 MI
0
20 KM

GEOLOGIC SETTING

Attention was first drawn to the geothermal anomaly in the Animas Valley in 1948. Several shallow wells drilled in sec. 7, T. 25 S., R. 19 W. produced steam and boiling water at a depth of 27 meters. The thermal anomaly is restricted to an area within a radius of approximately 400 m of the hot wells. While there is no active surface expression of hot groundwater anywhere in the Animas Valley, there is evidence for numerous inactive hot springs, in the form of hot spring deposits, on both sides of the valley. Hot spring deposits grade into low-temperature veins of fluorite, psilomelane, calcite (including travertine) and opaline silica. The veins are localized in Basin and Range fault zones bordering the valley (Fig. 1) (Elston and Deal, 1978).

The Animas Valley forms an elongate, north-trending graben within the Basin and Range tectonic province of southwestern New Mexico. In the vicinity of the Lightning Dock KGRA, the valley is about 18 km wide; the hot wells are 5 km from its eastern edge. The Animas Valley is bordered by the Peloncillo Mountains to the west and by the Pyramid and Animas Mountains to the east. Pyramid Peak, the highest point in the Pyramid Mountains, has an elevation of 1830 m, 566 m higher than the playa floor of the adjacent valley.

Recent geologic investigations by Elston and Deal (1978) and Deal and others (1978) show that the Pyramid Mountains are a complex of mid-Tertiary volcanic rocks on which Basin and Range tectonism has been superimposed. Some of the volcanic rocks are part of the Muir cauldron, an Oligocene ash-flow tuff eruptive center which is only partially preserved in the Pyramid Mountains. Basin and Range faulting

has dropped the western half of the Muir cauldron below the sedimentary cover of the Animas Valley. Wells (1978) has documented geomorphic evidence for continued recent movements along Basin and Range faults near the hot wells. The Muir cauldron is defined by cauldron fill intruded by a composite stock, ring-fracture zones, and associated ring-fracture domes, moat fill and outflow sheets (Elston and Deal, 1978). Elston and Deal propose that the location of the Lightning Dock KGRA is structurally controlled by the intersection of the ring-facture margin of the mid-Tertiary cauldron with active Holocene Basin and Range faults (Fig. 2). This interpretation, corroborated by electrical resistivity and gravity surveys (Jiracek and Smith, 1976; Smith, 1978), may be overly simplified, as will be shown below. Elston and Deal (1978) suggested that the heat source for the geothermal system was the northeast-trending basaltic volcanism seen in Fig. 1.

The valley contains surficial Quaternary piedmont and valley-floor deposits. The piedmont deposits are primarily coalescing Pleistocene and Holocene alluvial fans and pediment deposits and local modern or active sheetwash sediments. The bolson fill of the valley floor is capped by irregularly distributed fluviodeltaic, lacustrine, and playa sediments associated with Pleistocene Lake Animas (Reeder, 1957; Fleischauer, 1978). The total depth of the valley fill is highly variable, depending largely on the location of Tertiary and Holocene faults. In the vicinity of the hot wells, the valley fill is only 27 m thick, while drilling of the Cockrell #1 Forest Federal oil test well, in sec 31, T. 24 W., R. 19 W., 3 km to the north of the hot wells, penetrated 576 m of valley fill.

Figure 2. Generalized structural setting of the lower Animas Valley. Ball and bar are on the downthrown side of high angle faults. The hot wells are located near the intersection of the ring fracture margin and the Animas Valley fault (after Elston and Deal, 1978). The eastward-dippling high angle fault along the flank of the Peloncillo Mountains is reported by S. G. Wells (personal communication, 1980).

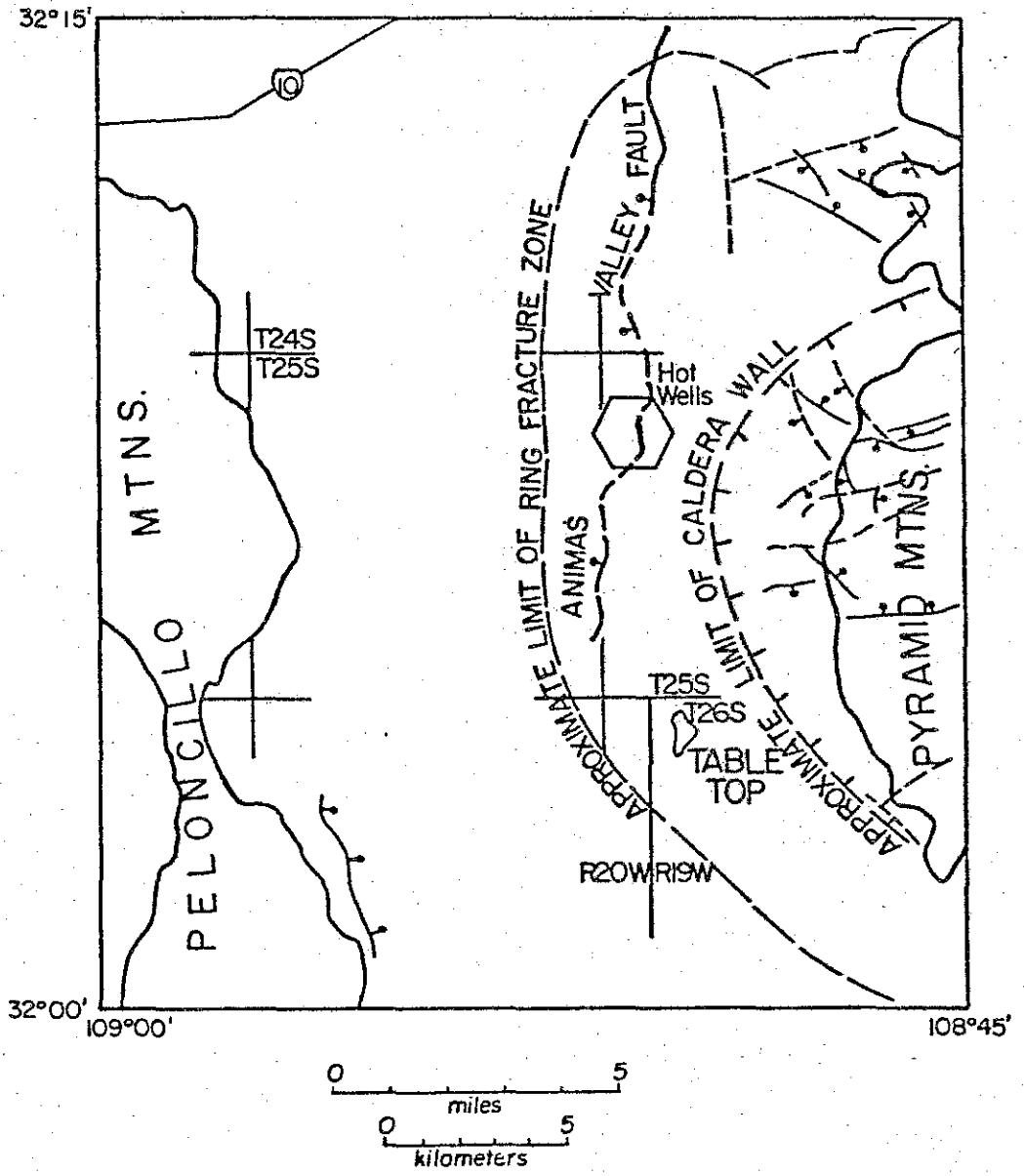
32°15'
10
T24S
T25S
PELONCILLO MTNS.
VALLEY FAULT
Hot Wells
APPROXIMATE LIMIT OF RING FRACTURE ZONE
ANIMAS
APPROXIMATE LIMIT OF CALDERA WALL
PYRAMID MTNS.
T25S
T26S
TABLE TOP
R20W R19W
32°00'
109°00'
108°45'
0 5
miles
0 5
kilometers

A shallow, one- to two-meter temperature and temperature gradient survey (Kintzinger, 1956) and a hydrologic survey (Reeder, 1957) were conducted in the Animas Valley several years after the hot wells were drilled. The flow of groundwater in the valley is from south to north, with local contributions from the flanking Peloncillo and Pyramid Mountains. A northerly-moving shallow flow of low-temperature groundwater mixes with thermal waters rising along a favorable structural zone near the hot wells to produce the northerly-spreading, fan-shaped anomaly reported by Kintzinger (1956). Heat flow measurements from shallow (< 70 m) observation wells show very high temperature gradients at shallow depths; the observation wells become isothermal at depth (Dellechaie, 1977). Thus, there is geological, geophysical and hydrologic evidence for the mixing of waters in the area of the Lightning Dock KGRA.

Fumarolic alteration of rocks in the Pyramid Mountains is associated with the pre-34 m.y. Muir cauldron, not with the modern Lightning Dock geothermal activity (Elston and Deal, 1978). A period of geothermal activity younger than a 20.6 $\pm$ 1.5 m.y. basalt flow produced the extensive hot spring deposits and hydrothermal veins which border the Animas Valley (Elston and others, 1973). Fluid inclusion studies by E. E. Erb and T. J. Bornhorst of fluorite and calcite from the near-surface veins indicate a range of depositional temperatures from 140°C to 350°C, which compare favorably with calculated reservoir temperatures for the modern geothermal system (Callender, 1981).

Various lines of evidence suggest that the modern geothermal anomaly at Lightning Dock may be a relict of a much larger, now-extinct hydrothermal system. The source of heat for the system is not known: all rhyolite domes in the area are Oligocene or older. The distribution of the Plio-Pleistocene San Bernardino basalt field in southeastern Arizona, of basalt cones near Rodeo, New Mexico, and of a Quaternary basalt flow, dated at 140,000 years (Marvin and others, 1978), in the Animas Valley southwest of the KGRA (Fig. 1) suggests that deep-seated basalt near the liquidus may be the ultimate heat source (Elston and Deal, 1978).

METHODS AND PROCEDURES

Fifty-five water samples were collected from wells under the supervision of C. A. Swanberg as part of an initial geothermal investigation of the Animas Valley (Landis, 1976; Callender, 1980). The water chemistry was analyzed at New Mexico State University under the supervision of A. L. Bristol using standard analytical procedures (see Appendix 1). The physicochemical properties of the waters were studied using WATEQF, a FORTRAN IV computer program that calculates the inorganic chemical equilibrium of natural waters (Plummer and others, 1978). Geothermometry was calculated using GEOTHM, a FORTRAN computer program written specifically for this work. The computer programs are described and critically evaluated in Appendices 2 and 3. Possible alteration phases in the geothermal reservoir were determined by means of mineral stability diagrams constructed after the methods of Helgeson and others (1969); the diagrams are discussed in Appendix 4.

Oxygen isotope analyses were performed on a standard 3-inch, 60°-sector Nier-type gas ratio mass spectrometer at the University of New Mexico. Data output was interpreted graphically and numerically by means of a digital integrator interfaced to a minicomputer. Oxygen isotope gas samples of the waters were prepared by the CO_2-H_2O equilibration method of Epstein and Mayeda (1953). The hydrogen isotope analyses were performed on a similar 3-inch mass spectrometer at the United States Geological Survey Isotope Branch laboratories in Denver, Colorado by G. P. Landis. The hydrogen isotope samples were prepared by the reduction-of-water technique of Bigeleisen and others

(1952). Details of the analytical procedures for both oxygen and hydrogen are given in Appendix 5. Precision of the oxygen analyses is better than $\pm$ 0.2 permil; the precision of the hydrogen analyses is better than $\pm$ 2 permil.

WATER CHEMISTRY

Composition

The water samples from the Animas Valley comprise three suites, the P-series, the AN-series, and the LD-series. The three suites were collected and named by three different field assistants working under the supervision of C. A. Swanberg. Sample locations are given in Table A1.1 and are shown in Figures 3 and 4. Chemical analyses for the major aqueous species in the water samples are presented in Table 1, which also lists the hydrogen and oxygen isotopic data and several calculated parameters. The results of the chemical analyses are shown graphically in the trilinear plot of Figure 5. The samples can be classified as sodium bicarbonate waters with variable proportions of calcium, sulfate, and chloride. The apparent scatter of values in the diagram can be resolved by plotting the three suites of samples separately. In Fig. 6 the Ca-Mg-Na+K and HCO_3-Cl-SO_4 plots indicate that the sample waters are mixtures of dilute sodium bicarbonate water with waters rich in calcium and sulfate and, to a lesser degree, chloride. One mixing line is apparently sufficient to describe the mixing process in the Ca-Mg-Na+K plot, but two distinct mixing lines are needed to describe the relations seen in the HCO_3-Cl-SO_4 plot.

Laboratory experiments (Ellis and Mahon, 1964, 1977; Hemley and Jones, 1964), theoretical calculations (Helgeson, 1967; 1969), and mineralogical and field studies (Browne and Ellis, 1970; Truesdell, 1975; Mariner and Willey; 1976) indicate that the concentrations of sparingly soluble species such as SiO_2, Na, K, Ca, Mg, Fe, HCO_3, SO_4, and F in geothermal reservoir waters are controlled by mineral-solution

Figure 3. Locations of the P-series and LD-series water samples in the Animas and adjacent Lordsburg and Playas valleys. Box shows location of Figure 4.

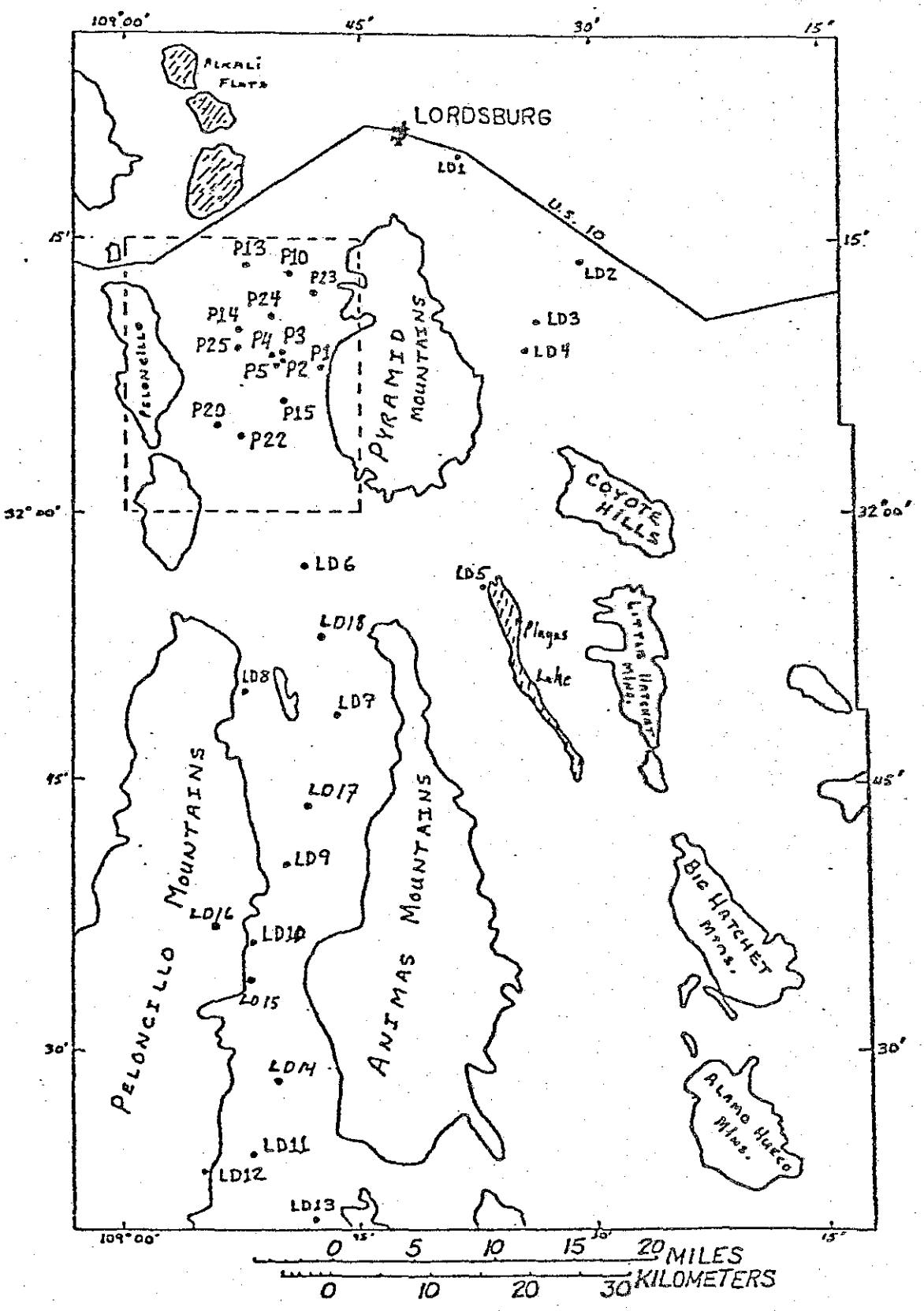
109°00'
45'
30'
15'
ALKALI FLATS
LORDSBURG
LD1
U.S. 10
LD2
LD3
LD4
P13
P10
P23
P24
P14
P25
P4
P3
P1
P5
P2
P20
P15
P22
PELONCILLO
PYRAMID MOUNTAINS
COYOTE HILLS
32°00'
LD6
LD5
Playas Lake
LITTLE HATCHET MTNS.
LD18
LD8
LD7
LD17
LD9
LD16
LD10
LD15
LD14
LD11
LD12
LD13
PELONCILLO MOUNTAINS
ANIMAS MOUNTAINS
BIG HATCHET MTNS.
ALAMO HUECO MTNS.
0 5 10 15 20 MILES
0 10 20 30 KILOMETERS

Figure 4. Locations of P-series (•) and An-series (+) water samples in the lower Animas Valley. Samples P2, P3, and P4 are from the hot wells.

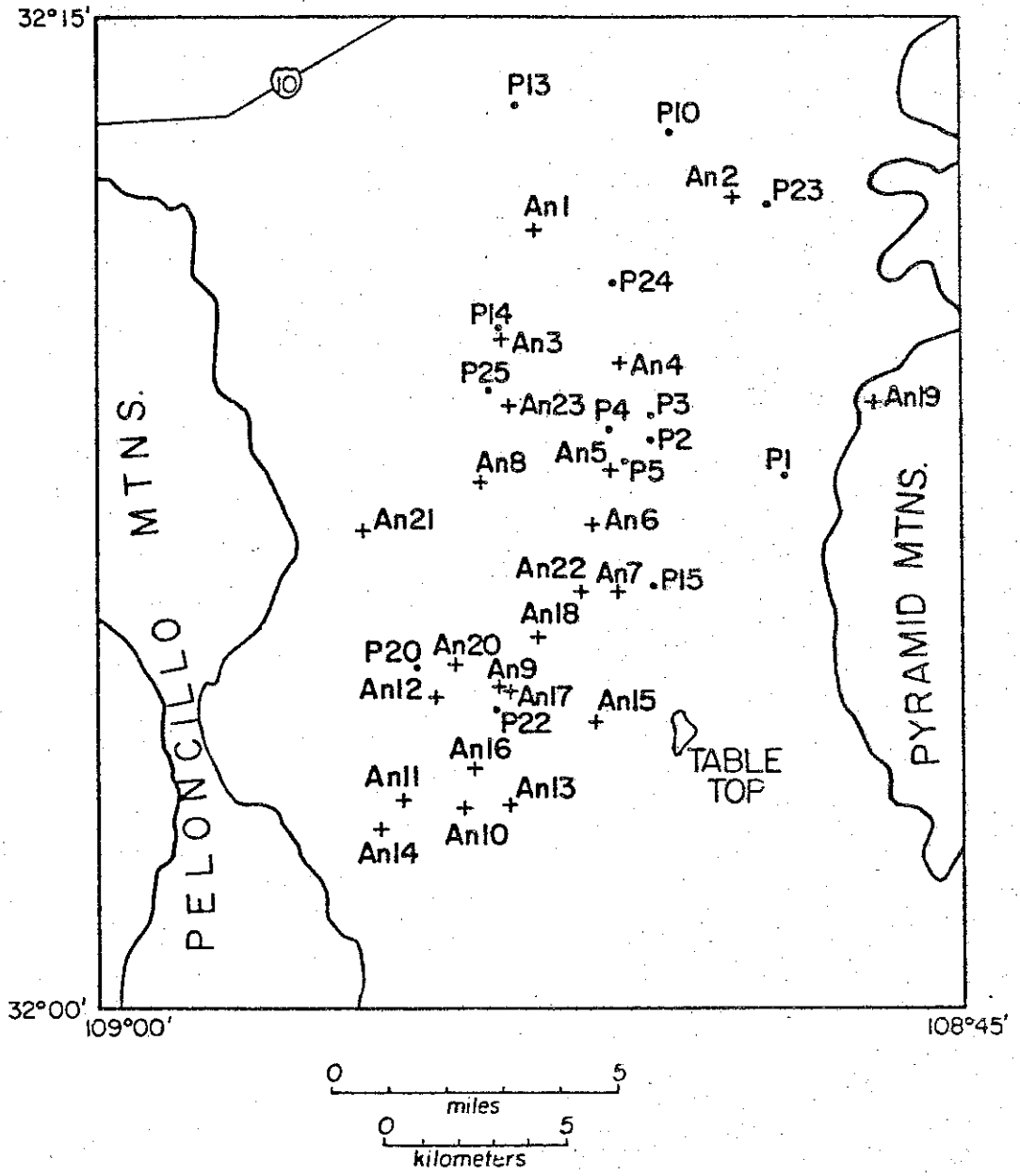
32°15'
10
P13
P10
An2
P23
An1
P24
P14
An3
An4
P25
An23
P4
P3
An19
P2
An8
An5
P5
P1
An21
An6
An22
An7
P15
An18
P20
An20
An9
An12
An17
An15
P22
An16
TABLE TOP
An11
An13
An10
An14
PELONCILLO MTNS.
PYRAMID MTNS.
32°00'
109°00'
108°45'
0
5
miles
0
5
kilometers

Table 1

Chemical Data

P-Series	P 1	P 2	P 3	P 4	P 5
TDS	484	1116	1024	1608	1660
pH	8.20	7.71	8.16	7.84	8.08
Major Cations, (mg/l):					
Ca^{++}	28.0	22.0	23.2	67.3	159.3
Mg^{++}	7.3	0.5	0.5	5.3	34.9
Na^{+}	68.7	333.6	338.6	493.1	231.7
K^{+}	1.9	23.5	21.1	27.8	9.0
Major Anions, (mg/l):					
F^{-}	0.35	12.6	12.0	7.25	3.55
HCO_3^{-}	183.1	106.8	103.7	118.9	209.3
Cl^{-}	20.5	88.3	87.6	111.3	181.9
SO_4^{--}	79.3	497.1	480.0	893.4	956.3
(mg/l):					
Fe^{++}	1.10	0.20	0.40	0.83	<.10
B	0.08	0.48	0.50	0.42	0.25
P	0.01	0.02	0.02	0.01	0.01
SiO_2 (mg/l)	31.3	147.5	143.0	115.6	42.3
$\bar{I}$	0.010	0.020	0.019	0.032	0.037
Surface Temp. °C	23.0	85.0	81.0	71.0	22.0

Table 1 cont'd

P-Series	P 1	P 2	P 3	P 4	P 5
Molal Ratio:					
B/Na $*10^3$	2.5	3.1	3.3	1.8	2.3
B/Ca $*10^3$	10.6	80.9	79.9	23.1	5.8
SO_4/F	44.8	7.8	7.9	24.4	53.3
Isotopic Values, (SMOW):					
$\delta^{18}O$ (‰)	-10.2	-10.5	-10.3	-10.5	-10.3
δD (‰)	-71	-78	-78	-78	-75

Table 1 cont'd

P-Series	P 10	P 13	P 14	P 15	P 20
TDS	1708	756	668	868	632
pH	8.18	7.90	8.00	8.07	8.02
Major Cations, (mg/l):					
Ca^{++}	67.9	38.3	47.9	78.6	43.2
Mg^{++}	17.1	2.7	4.4	12.6	4.1
Na^{+}	366.2	105.5	71.0	152.2	97.0
K^{+}	6.3	3.1	2.7	5.9	2.3
Major Anions, (mg/l):					
F^{-}	7.25	3.90	0.85	2.35	2.65
HCO_3^{-}	255.0	237.9	209.3	201.4	192.2
Cl^{-}	133.6	16.7	23.0	80.5	21.3
SO_4^{--}	939.0	298.7	289.6	483.7	305.0
(mg/l):					
Fe^{++}	0.53	1.31	0.16	<.10	<.10
B	0.51	0.10	0.06	0.18	0.10
P	0.01	0.01	0.01	0.01	0.01
SiO_2 (mg/l)	60.7	74.1	48.4	34.3	50.4
$\bar{I}$	0.034	0.015	0.014	0.021	0.014
Surface Temp. °C	23.0	19.0	20.0	24.0	22.0

Table 1 cont'd

P-Series	P 10	P 13	P 14	P 15	P 20
Molal Ratio:					
B/Na $*10^3$	3.0	2.0	1.8	2.5	2.2
B/Ca $*10^3$	27.9	9.6	4.6	8.5	8.6
SO_4/F	25.6	15.1	67.4	40.7	22.8
Isotopic Values, (SMOW):					
$\delta^{18}O$ (‰)	-11.4	-9.8	-9.7	-10.5	-10.2
δD (‰)	−79	−67	−67	−77	−67

Table 1 cont'd

P-Series	P 22	P 23	P 24	P 25
TDS	600	640	1348	604
pH	7.90	8.08	7.92	8.35
Major Cations, (mg/l):				
Ca^{++}	49.3	18.6	38.5	38.1
Mg^{++}	4.4	2.4	1.8	5.7
Na^{+}	111.3	120.2	321.4	78.8
K^{+}	2.7	1.6	18.0	3.5
Major Anions, (mg/l):				
F^{-}	1.20	1.15	9.35	3.55
HCO_3^{-}	192.2	250.2	275.8	183.1
Cl^{-}	38.6	29.1	79.8	8.9
SO_4^{--}	311.7	308.3	768.5	285.8
(mg/l):				
Fe^{++}	<.10	7.66	21.18	0.36
B	0.06	0.12	0.05	0.12
P	0.01	0.01	0.01	0.01
SiO_2 (mg/l)	43.3	29.3	149.7	34.3
$\bar{I}$	0.015	0.015	0.029	0.013
Surface Temp. °C	22.0	24.0	---	23.0

Table 1 cont'd

P-Series	P 22	P 23	P 24	P 25
Molal Ratio:				
B/Na $*10^3$	1.1	2.1	3.3	3.2
B/Ca $*10^3$	4.5	23.9	48.2	11.7
SO_4/F	51.4	53.0	16.3	15.9
Isotopic Values, (SMOW):				
$\delta^{18}O$ (‰)	-9.6	-9.8	-10.4	-9.0
δD (‰)	−67	−74	−80	−65

Table 1 cont'd

An-Series	An 1	An 2	An 3	An 4	An 5
TDS	300	360	380	1372	1184
pH	7.88	8.00	8.29	7.59	7.82
Major Cations, (mg/l):					
Ca^{++}	26.2	13.0	39.7	79.7	122.0
Mg^{++}	2.2	1.6	8.8	8.3	25.3
Na^{+}	54.0	115.4	66.9	353.3	178.6
K^{+}	2.0	2.0	2.7	14.1	8.2
Major Anions, (mg/l):					
F^{-}	1.60	1.60	0.66	2.85	3.48
HCO_3^{-}	151.3	151.3	207.4	228.8	172.1
Cl^{-}	7.1	7.1	15.6	122.7	144.3
SO_4^{--}	42.0	42.0	64.8	492.8	351.9
(mg/l):					
Fe^{++}	<.10	14.30	14.92	<.10	.10
B	0.12	0.17	0.02	0.59	0.18
P	0.05	0.01	0.04	0.01	0.01
SiO_2 (mg/l)	58.5	15.5	68.5	97.5	50.5
$\bar{I}$	0.007	0.011	0.011	0.027	0.023
Surface Temp. °C	23.0	18.0	16.0	24.0	19.0

Table 1 cont'd

An-Series	An 1	An 2	An 3	An 4	An 5
Molal Ratio:					
B/Na $*10^3$	4.7	3.1	0.6	3.6	2.1
B/Ca $*10^3$	11.7	35.1	1.9	27.5	5.5
SO_4/F	5.2	9.2	19.4	3.4	20.0

Table 1 cont'd

An-Series	An 6	An 7	An 8	An 9	An 10
TDS	1020	624	272	384	524
pH	8.00	7.52	7.83	7.85	7.92
Major Cations, (mg/l):					
Ca^{++}	125.2	60.5	28.8	19.8	29.8
Mg^{++}	14.6	9.7	2.7	4.7	8.5
Na^{+}	161.4	134.3	55.6	98.2	112.2
K^{+}	6.6	4.3	2.3	3.1	3.5
Major Anions, (mg/l):					
F^{-}	1.98	2.28	1.14	0.84	0.63
HCO_3^{-}	83.6	195.2	170.8	81.1	156.8
Cl^{-}	117.0	68.1	3.5	59.2	53.9
SO_4^{--}	369.0	167.0	51.6	107.3	111.7
(mg/l):					
Fe^{++}	74.58	1.73	3.01	47.69	8.54
B	0.78	0.17	0.05	0.01	0.02
P	0.00	0.00	0.00	0.00	0.00
SiO_2 (mg/l)	30.0	29.5	33.5	0.95	37.5
$\bar{I}$	0.023	0.015	0.015	0.009	0.011
Surface Temp. °C	19.0	20.0	---	18.0	18.0

Table 1 cont'd

An-Series	An 6	An 7	An 8	An 9	An 10
Molal Ratios:					
B/Na $*10^3$	10.3	2.7	1.9	0.2	0.4
B/Ca $*10^3$	23.1	10.4	6.4	1.9	2.5
SO_4/F	36.9	14.5	9.0	25.3	35.1

Table 1 cont'd

An-Series	An 11	An 12	An 13	An 14	An 15
TDS	688	384	420	340	240
pH	7.68	7.73	8.26	7.75	7.93
Major Cations, (mg/l):					
Ca^{++}	81.8	34.5	25.0	26.0	18.2
Mg^{++}	9.1	3.0	1.8	1.8	2.5
Na^{+}	110.6	77.9	103.4	70.3	49.6
K^{+}	4.3	2.7	3.9	2.3	2.0
Major Anions, (mg/l):					
F^{-}	2.85	2.28	3.03	3.45	0.63
HCO_3^{-}	202.0	185.5	167.8	176.3	139.1
Cl^{-}	38.3	8.5	27.3	1.8	6.4
SO_4^{--}	198.6	74.8	84.1	58.8	38.4
(mg/l):					
Fe^{++}	<.10	10.31	21.85	<.10	17.93
B	0.19	0.00	0.12	0.04	0.00
P	0.00	0.01	0.02	0.01	0.00
SiO_2 (mg/l)	44.5	45.0	32.0	44.0	30.00
$\bar{I}$	0.016	0.010	0.010	0.009	0.005
Surface Temp. °C	19.0	21.0	26.0	20.0	24.0

Table 1 cont'd

An-Series	An 11	An 12	An 13	An 14	An 15
Molal Ratio:					
B/Na $*10^3$	3.7	---	2.5	1.2	---
B/Ca $*10^3$	8.6	---	17.8	5.7	---
SO_4/F	13.8	6.5	5.5	3.4	12.1

Table 1 cont'd

An-Series	An 16	An 17	An 18	An 19	An 20
TDS	384	524	352	675	628
pH	8.39	8.17	8.43	8.33	7.41
Major Cations, (mg/l):					
Ca^{++}	30.7	30.7	31.3	81.0	76.1
Mg^{++}	3.0	5.7	3.2	23.5	7.2
Na^{+}	89.9	129.2	67.8	74.5	91.7
K^{+}	2.7	7.0	2.7	2.7	3.5
Major Anions, (mg/l):					
F^{-}	1.32	4.02	1.71	---	0.69
HCO_3^{-}	178.8	237.4	157.4	181.8	187.9
Cl^{-}	19.8	29.4	27.3	42.5	64.2
SO_4^{--}	86.9	113.3	58.8	197.0	124.9
(mg/l):					
Fe^{++}	0.29	<.10	<.10	3.63	0.68
B	0.00	0.13	0.18	0.04	0.05
P	0.01	0.01	0.01	0.01	0.00
SiO_2 (mg/l)	37.0	30.0	37.5	40.0	49.5
$\bar{I}$	0.010	0.013	0.009	0.016	0.014
Surface Temp. °C	20.0	22.0	21.0	---	20.0

Table 1 cont'd

An-Series	An 16	An 17	An 18	An 19	An 20
Molal Ratio:					
B/Na $*10^3$	---	2.1	5.6	1.1	1.2
B/Ca $*10^3$	---	15.7	21.3	1.8	2.4
SO_4/F	13.0	5.6	6.8	---	35.8

Table 1 cont'd

An-Series	An 21	An 22	An 23
TDS	402	396	384
pH	8.27	8.41	8.44
Major Cation, (mg/l):			
Ca^{++}	39.9	25.4	22.0
Mg^{++}	6.3	2.5	2.1
Na^{+}	74.5	93.8	53.4
K^{+}	3.5	2.3	2.0
Major Anions, (mg/l):			
F^{-}	3.81	2.16	0.93
HCO_3^{-}	186.7	172.1	148.0
Cl^{-}	9.6	20.9	2.1
SO_4^{--}	88.5	76.4	51.6
(mg/l):			
Fe^{++}	<.10	0.83	0.65
B	0.04	0.05	0.00
P	0.01	0.01	0.01
SiO_2 (mg/l)	37.5	32.5	37.0
$\bar{I}$	0.011	0.009	0.007
Surface Temp. °C	19.0	19.0	18.0

Table 1 cont'd

An-Series	An 21	An 22	An 23
Molal Ratio:			
B/Na $*10^3$	1.1	1.1	---
B/Ca $*10^3$	3.7	7.3	---
SO_4/F	4.5	7.0	11.0

Table 1 cont'd

LD-Series	LD 1	LD 2	LD 3	LD 4	LD 5
TDS	564	816	740	592	796
pH	8.09	7.86	7.48	7.94	7.82
Major Cation, (mg/l):					
Ca^{++}	7.6	28.0	117.4	10.2	15.6
Mg^{++}	1.4	2.7	18.7	1.8	1.3
Na^{+}	143.2	216.1	98.6	159.3	234.5
K^{+}	5.9	11.7	10.2	1.5	5.5
Major Anions, (mg/l):					
F^{-}	3.66	6.90	0.44	2.67	7.11
HCO_3^{-}	234.3	314.8	218.4	301.4	400.3
Cl^{-}	27.6	47.5	116.6	33.0	50.7
SO_4^{--}	93.7	223.8	181.5	104.2	154.6
(mg/l):					
Fe^{++}	<.15	<.15	<.15	0.37	<.15
B	0.46	0.46	0.32	0.50	0.64
P	0.00	0.01	0.01	0.01	0.01
SiO_2 (mg/l)	33.5	39.6	43.4	32.3	47.2
$\bar{I}$	0.012	0.019	0.019	0.014	0.019
Surface Temp. °C	25.3	33.0	---	---	---

Table 1 cont'd

LD-Series	LD 1	LD 2	LD 3	LD 4	LD 5
Molal Ratio:					
B/Na $*10^3$	6.8	4.5	6.9	6.7	5.8
B/Ca $*10^3$	224.4	60.9	10.1	18.2	15.2
SO_4/F	5.1	6.4	81.5	7.7	4.3
Isotopic Values, (SMOW):					
$\delta^{18}O$ (‰)	-11.1	-11.1	-9.3	-11.2	-10.1

Table 1 cont'd

LD-Series	LD 6	LD 7	LD 8	LD 9	LD 10
TDS	208	208	184	175	156
pH	7.92	7.82	7.57	7.39	7.31
Major Cations, (mg/l):					
Ca^{++}	22.0	40.3	26.0	21.0	17.8
Mg^{++}	7.3	4.9	2.2	3.2	3.3
Na^{+}	27.6	15.2	21.1	6.2	6.9
K^{+}	2.0	2.0	1.2	4.5	6.2
Major Anions, (mg/l):					
F^{-}	0.30	0.16	1.34	0.12	0.11
HCO_3^{-}	147.7	156.2	109.8	65.9	57.3
Cl^{-}	3.5	2.5	2.8	0.7	1.4
SO_4^{--}	19.2	4.3	4.3	33.6	40.3
(mg/l):					
Fe^{++}	0.62	4.70	6.39	<.15	0.56
B	0.12	0.12	0.06	0.04	0.04
P	0.01	0.02	0.01	0.14	0.01
SiO_2 (mg/l)	38.1	47.6	45.2	47.6	39.3
$\bar{I}$	0.007	0.007	0.005	0.004	0.003
Surface Temp. °C	---	24.4	21.2	18.7	---

Table 1 cont'd

LD-Series	LD 6	LD 7	LD 8	LD 9	LD 10
Molal Ratio:					
B/Na $*10^3$	9.2	16.8	6.0	13.7	12.3
B/Ca $*10^3$	20.2	11.0	8.6	7.1	8.3
SO_4/F	12.7	5.3	0.6	55.4	72.5
Isotopic Values, (SMOW):					
$\delta^{18}O$ (‰)	-9.2	-10.0	-9.5	-8.6	-8.8

Table 1 cont'd

LD-Series	LD 11	LD 12	LD 13
TDS	200	136	132
pH	7.74	6.88	7.00
Major Cations, (mg/l):			
Ca^{++}	16.6	15.8	8.2
Mg^{++}	4.8	2.9	1.7
Na^{+}	36.8	13.8	15.2
K^{+}	5.1	3.5	2.7
Major Anions, (mg/l):			
F^{-}	1.12	0.18	0.14
HCO_3^{-}	173.8	37.8	22.0
Cl^{-}	1.4	0.7	1.4
SO_4^{--}	3.8	52.8	40.3
(mg/l):			
Fe^{++}	5.77	<.15	<.15
B	0.12	0.06	0.06
P	0.01	0.01	0.01
SiO_2 (mg/l)	32.4	35.7	39.3
I^{-}	0.007	0.003	0.002
Surface Temp. °C	18.3	18.0	17.0

Table 1 cont'd

LD-Series	LD 11	LD 12	LD 13
Molal Ratio:			
B/Na $*10^3$	6.9	9.2	8.4
B/Ca $*10^3$	26.8	14.1	27.1
SO_4/F	0.7	58.0	56.9
Isotopic Values, (SMOW):			
$\delta^{18}O$ (‰)	-9.1	-8.1	-10.0

Figure 5. Trilinear plot of the water samples from the Animas Valley. Chemical analyses of water are represented as percentages of total equivalents per liter.

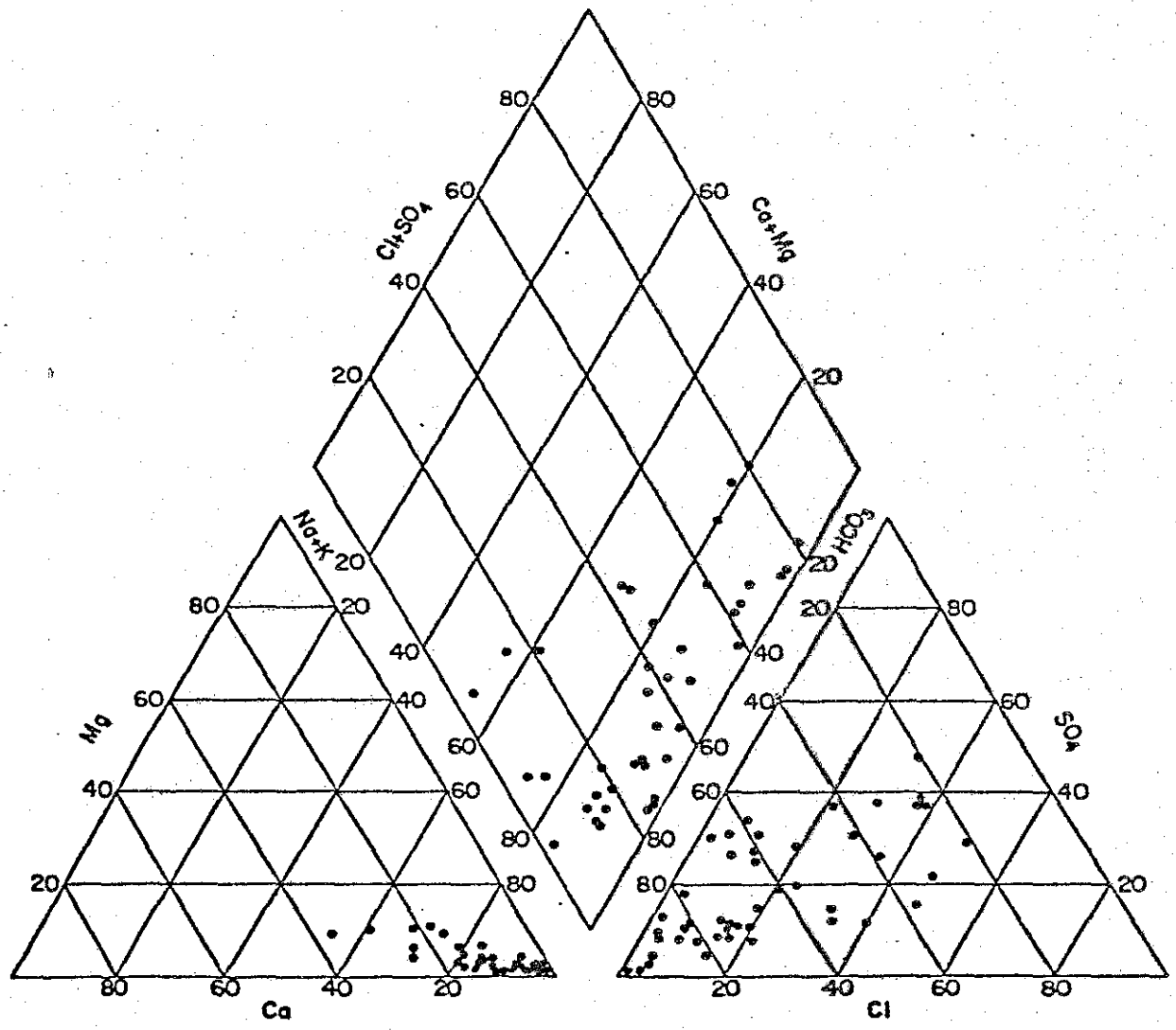
Cl+SO4
Ca+Mg
Na+K
HCO3
Mg
SO4
Ca
Cl
80
60
40
20

Figure 6. Ca-Mg-Na+K and HCO_3-Cl-SO_4 plots from Figure 5 with P-series (•), LD-series (+), and An-series (▲) waters plotted separately.

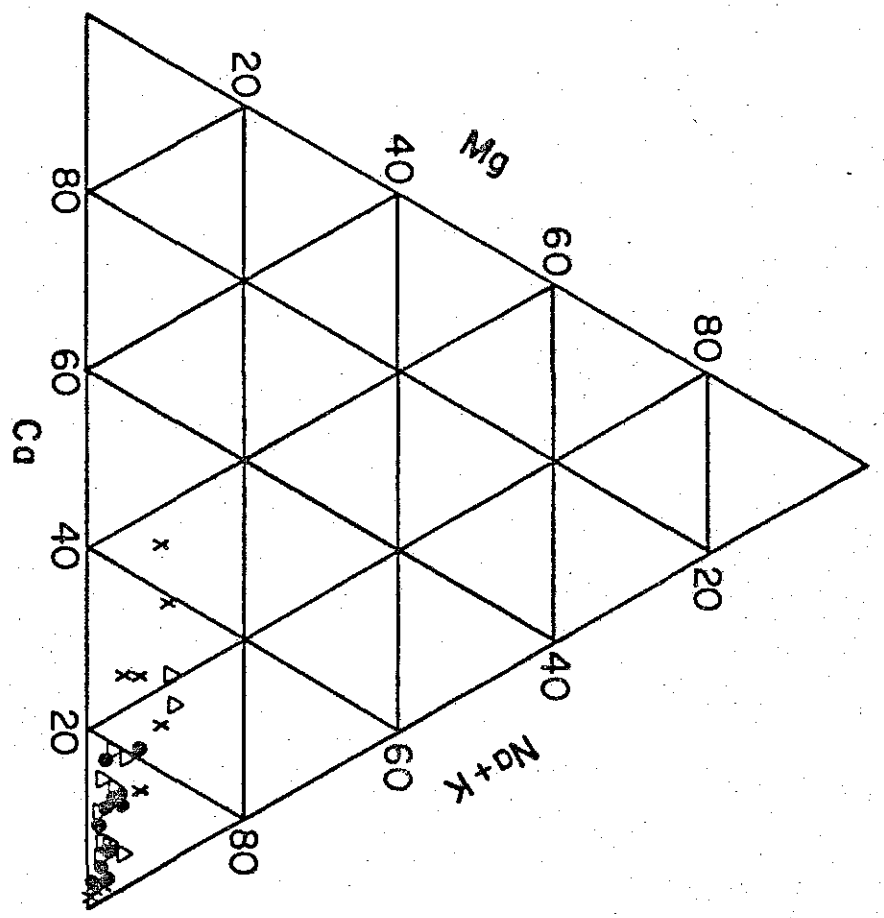
Ca
Mg
Na+K
20
40
60
80

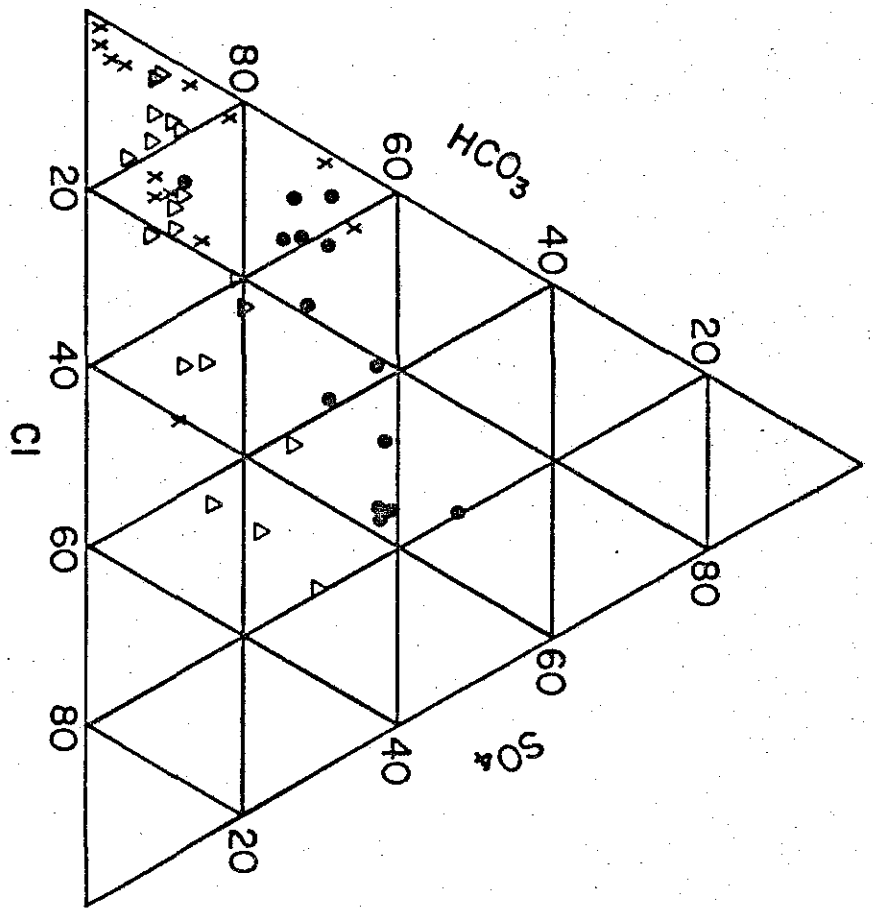
Cl
HCO3
SO4
20
40
60
80

equilibria. In contrast, the concentrations of soluble elements such as Cl, B, Br, I. Li, Cs, and As in geothermal reservoir waters are primarily the result of temperature dependent rock-leaching (Ellis and Mahon, 1964; Ellis, 1977). Waters actually sampled at or near the surface, whether from wells or springs, are typically modified by a variety of processes. Broadly speaking, one can classify the possible processes into three categories: (1) processes in which the solvent, water, is added to or removed from the solution; (2) processes in which the solution reacts with the surrounding rocks; and (3) mixing of solutions of different compositions and concentrations. Within each of the three classes of processes, more specific processes may be of greater or lesser significance in determining the chemical composition of a sampled water:

1. Changes in the solvent
    a. Boiling
    b. Evaporation
    c. Membrane filtration
2. Water-rock interaction
    a. Dissolution
    b. Precipitation
    c. Ion exchange
    d. Biologic activity
3. Mixing

Since no shale units were observed in microscopic examination of the Cockrell #1 oil test well drill chips, membrane filtration probably is not a significant process in the Lightning Dock system. The

chemical analyses of the water samples did not include any data on bacteria in the waters. Therefore, the effects of biologic activity on the composition of the fluids will be neglected.

Because of the complexity of the geologic, hydrologic, and geochemical processes which affect the waters, it is typically impossible to derive a fully quantitative analysis of the chemical evolution of waters sampled from a geothermal system. However, by applying some concepts of chemical equilibria to the regularities observed in the water analyses, it is possible to develop models which describe some of the processes quantitatively and others semi-quantitatively or qualitatively.

Processes Affecting the Solvent

Isotopic analyses of hydrogen and oxygen in Table 1 are reported as δD or $\delta^{18}O$ values in the conventional permil notation,

$$\delta = \frac{R_{spl} - R_{std}}{R_{std}} \times 10^3,$$

where R_{spl} = D/H or $^{18}O/^{16}O$ ratio in the sample and R_{std} is the corresponding ratio in the standard. The standard for both hydrogen and oxygen is Standard Mean Ocean Water (Craig, 1961).

The results of the Animas Valley stable isotope study are presented in Table 1. All groundwater samples are from relatively shallow (< 40 m) wells. Since sample LD1-LD5 are from the adjacent Lordsburg and Playas Valleys, which probably are not in hydraulic continuity with the lower Animas Valley (Reeder, 1957), they will not be considered in

this discussion. The P-series was chosen for analyses of both hydrogen and oxygen isotopes because the chemistry and the geologic setting of the samples indicated that they would yield the greatest amount of information about the geothermal system. Only oxygen isotopic analyses are available for the LD-series, the cool, dilute waters of the upper Animas Valley.

The $\delta^{18}O$ values of groundwaters from the KGRA and adjacent parts of the lower Animas Valley range from -9.0 permil to -11.4 permil. Groundwaters from the upper Animas Valley range from -8.1 permil to -10.1 permil. Summer rainwater has a $\delta^{18}O$ value near -5 permil. δD values for the lower valley groundwaters range from -65 permil to -80 permil. The δD of the summer rainwater is near -21 permil. Interpretation of these data is complex and requires some knowledge of the hydrology of the valley and of the meteorology of southwestern New Mexico.

The isotopic data for the P-series waters are plotted on a δD-$\delta^{18}O$ diagram in Fig. 7; the meteoric water line of Craig (1961) is plotted along with the data (see Appendix 5). Linear regression on the isotopic values yields an equation

$$\delta D = 7.51\ \delta^{18}O + 3.3, \qquad (1)$$

with a correlation coefficient of 0.8. The groundwaters of the Animas Valley, including the KGRA, are meteoric in origin.

While a 50 to 60 percentage of the precipitation in the Animas Valley falls during the summer rains (Reeder, 1957), the groundwaters do not represent samples of the present-day summer rains. This paradox

Figure 7. δD and $\delta^{18}O$ values for the P-series waters. The meteoric water line is from Craig (1961).

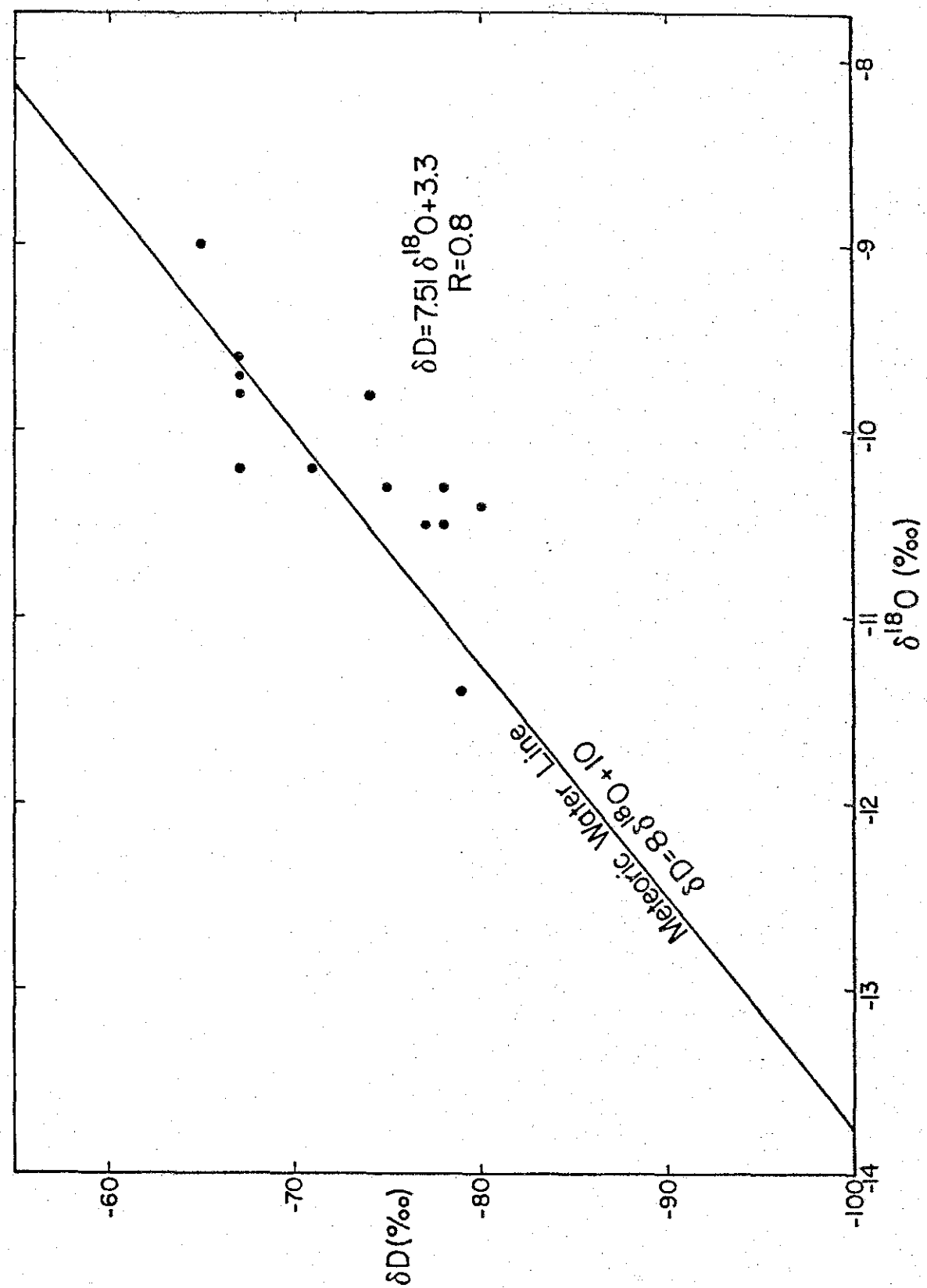
δD=7.51 δ18O+3.3
R=0.8
Meteoric Water Line
δD=8δ18O+10
δD(‰)
δ18O (‰)
-60
-70
-80
-90
-100
-8
-9
-10
-11
-12
-13
-14

is not hard to resolve. Summer rainstorms are typically high intensity, short duration convective storms. Rain which falls on the valley floor is unlikely to add significantly to recharge because the valley floor is an area of net discharge due to high rates of evapotranspiration and low rates of infiltration which result from the presence of a caliche hardpan in the soil (Reeder, 1957; D. B. Stevens, personal communication, 1980). Much of the rain which falls on the steeper terrain of recharge areas in the mountains during high intensity storms will run off to the playas of the valley floor, where the water will be lost to evapotranspiration. The principal source of meteoric water recharge to the Animas Valley is believed to be winter precipitation which falls in the surrounding mountains, as is the case in other southwestern valleys (e.g., Wells, 1977). Winter storms are typically frontal storms of relatively long duration. Because of lower temperature of condensation, winter precipitation should have more negative δD and $\delta^{18}O$ values than the summer rains, and proportionally more of the precipitation should infiltrate to the water table because of lower evaporation rates. This hypothesis is supported by a detailed study of a similar valley in southern Arizona (Simpson and others, 1972). Samples P13, P14, and P22 are cool, dilute waters with tightly grouped δD and $\delta^{18}O$ values (-67 permil and -9.6 permil) which can be taken as representative of effective modern meteoric recharge water. The deuterium value agrees very closely with the regional study of Taylor (1974).

The groundwaters of the Animas Valley typically are present in unconfined aquifers in the poorly consolidate valley-fill sediments. Locally, perched or confined conditions are encountered due to clay

lenses in the playa deposits of Pleistocene Lake Animas (Reeder, 1957). Most of the wells in the upper Animas Valley supply water from shallow, perched aquifers (Reeder, 1957). Groundwater samples which have $\delta^{18}O$ values near -9.6 permil and, where available, δD values near -67 permil represent samples from shallow aquifers recharged by modern meteoric waters. $\delta^{18}O$ values which are significantly more positive than -9.6 permil may represent modern meteoric water which has undergone evaporation before or during infiltration.

Waters which have $\delta^{18}O$ and δD values significantly more negative than -9.6 permil and -67 permil, respectively, present more complex and problematical histories. Analysis of the chemical, isotopic and temperature data indicates that there is a negative correlation between $\delta^{18}O$ and δD values and subsurface temperature, concentration of chlorine, and concentration of boron (Table 2). The deeper, high temperature reservoir water is more depleted in ^{18}O and D than the shallow aquifer water. This is a surprising result, since higher temperature should favor increased ^{18}O exchange with the enclosing rock and a shift to more positive $\delta^{18}O$ values with essentially constant δD values (Craig, 1963). Instead of the expected "oxygen shift" pattern, the isotopic data of Figure 6 may represent a mixing line between a modern meteoric water ($\delta^{18}O$ = -9.0 permil; δD = -65 permil), which may have undergone some evaporation, and a deep reservoir water ($\delta^{18}O$ = -13.4 permil; δD = -97 permil), with a small oxygen shift for the hot wells which accounts for much of the scatter in the data. The small oxygen shift, about 0.5 permil, is similar to that observed at Wairakei and Long Valley (Marriner and Willey, 1977), and probably indicates that the

Animas Valley geothermal system is moderately to very old and has isotopically well-flushed conduits. This interpretation is consistent with the observed record of hydrothermal activity in the region (Elston and Deal, 1978).

The isotopic value of the deep water is substantially too negative to be locally derived meteoric water. There are at least three reasonable interpretations for the very negative $\delta^{18}O$ and δD water required by the data. First, the reservoir water may be a paleometeoric water within the deep gravels or even within the fractured volcanic rocks below the valley fill. If such a water were representative of a colder climate than modern, it would have more negative isotopic values than modern waters. Such paleowaters have been described from arid and semiarid regions (Gat and Dansgaard, 1972; Gat and Issar, 1974) and have been proposed for the geothermal system at Yellowstone (Truesdell and others, 1977). Deep circulations times for many geothermal systems have been estimated at > 30,000 years (e.g., Craig, 1963; Elder, 1976). For a steady-state model of the Animas Valley, given known recharge rates and porosities based on geologic and geophysical evidence, the residence time for basin waters is 5,000 to 50,000 years. Therefore, Pleistocene water is probably present in the deeper portions of the basin. However, it is not clear that paleometeoric waters in this portion of North America, at least as far back as approximately 20,000 years P.B., had isotopic values more negative than modern meteoric water. Although there are no data specifically from southwestern New Mexico, studies of the δD of cellulose in trees suggest that except very close to the margins of the Pleistocene ice sheets, average

annual meteoric water isotopic values were probably little different from modern values (C. J. Yapp, personal communication, 1980).

Paleobotanical studies of ancient packrat middens indicate that woodland communities were present in most of the Chihuahuan, Sonoran and Mojave deserts during the late Wisconsinian (22,000 to 11,000 years B.P.) (Van Devender and Spaulding, 1979). On the basis of the paleobotanical evidence and model water budgets for playa lakes, Van Devender and Spaulding (1979) propose that the late Wisconsinian climate in the southwest was characterized by mild, wet winters and cool summers and that the climatic pattern of predominantly winter precipitation probably continued until about 8,000 years B.P. Therefore, a second possible interpretation of the isotopically depleted waters is that they represent groundwater recharge from a climatic regime with a significantly higher percentage of winter precipitation than modern recharge. Simple mass balance considerations indicate that as the fraction of winter precipitation in the total groundwater recharge approaches one, the isotopic composition of the groundwater approaches the value of the winter component. This mechanism would produce older, deeper waters with significantly more negative isotopic values than modern waters only if summer precipitation is an important part of the recharge to modern groundwater. The relative proportions of winter and summer infiltration, not precipitation, is the factor which will determine the weighted isotopic composition of the groundwater. As discussed above, modern groundwater is dominated by winter precipitation, and a shift to relatively more winter precipitation probably would have little effect on the isotopic composition of the water. Furthermore, cooler summers would imply lower evaporation rates and more infiltration of

summer precipitation. While such summer meteoric waters would be more negative than modern summer rainwater, they would be more positive than modern winter precipitation and would tend to offset the increased proportion of negative winter precipitation in the mixture. A careful, long-term study of the seasonal distribution of recharge and the isotopic composition of the recharge is needed to quantitatively test the hypothesis of increased winter contribution as the source of the isotopically depleted water.

The third possibility for the origin of the isotopically depleted waters is that they are associated with a recondensed vapor phase on the distal edge of a boiling geothermal system in which the isotopic composition of the reservoir water is close to that of modern meteoric water. Hot waters originating in geothermal reservoirs at temperatures above surface boiling must lose heast as they ascend. The heat loss may take place by conduction to the surrounding rock, by mixture with cooler waters, or by loss of steam. Conductive cooling will not affect the isotopic composition of the water. With the assumption that the initial isotopic composition of the reservoir water is nearly the same as that of modern meteoric water, mixing also will not affect the isotopic composition of the sample waters. However, below 220°C, $H_2O_{(vapor)}$ is depleted in both D and ^{18}O relative to $H_2O_{(liquid)}$ (C. J. Yapp, personal communication, 1980), indicating that boiling followed by recondensation of the vapor phase is consistent with the data. The potential isotopic consequences of boiling and recondensation are very complex (Truesdell and others, 1977; C. J. Yapp, personal communication, 1980). Uncertainties concerning initial conditions, mechanisms of boiling and

recondensation, and degree of post-recondensation mixing make quantitative evaluation of the possibilities difficult and the drawing of conclusions dangerous. However, one may consider a limiting case as a semi-quantitative check on the consistency of the potential process. The treatment which follows is based on a formally identical treatment of the isotopic systematics of coexisting sulfides and sulfates, presented in classwork at the University of New Mexico by C. J. Yapp.

The observed mixed water system can be considered to include two coexisting species, the modern meteroic water ($\delta^{18}O$ = -9.6 permil; δD = -67 permil) and the deep reservoir water ($\delta^{18}O$ = -13.4 permil; δD = -97 permil). To define the limiting case, one must make two critical and stringent assumptions. First, the isotopic composition of the presumed reservoir water represents the isotopic composition of the aggregate distillate. That is, either all the steam recondensed to liquid water in one step, or step-wise recondensation was followed by mixing which reestablished the isotopic composition of the bulk distillate. Second, the isotopic composition of modern meteoric water is identical to the isotopic composition of the residual liquid. Working with these assumptions, the $\delta^{18}O$ values of the two model species define an apparent fractionation factor,

$$\alpha_{app} = \frac{1 + \frac{\delta^{18}O_r}{1000}}{1 + \frac{\delta^{18}O_m}{1000}}, \qquad (2)$$

where $\delta^{18}O_r$ = $\delta^{18}O$ value of the geothermal reservoir fluid and $\delta^{18}O_m$ = $\delta^{18}O$ value of modern meteoric water. If one applies the Rayleigh model to describe the boiling process which leads to this α_{app} and treats the $\delta^{18}O_r$ as a value which is integrated over the fraction of water which is removed from the initial reservoir by boiling, it can be shown that

$$\alpha_{app} = \frac{f_2^{\alpha} - f_1^{\alpha}}{f_2^{\alpha-1}\,(f_2 - f_1)} \qquad (3)$$

where f_1 = the fraction of the original water left in the reservoir when boiling begins, f_2 = the fraction of water left in the system when boiling ends, and α = the true α of the boiling process, assumed to be constant for the purposes of the derivation (see Appendix 5). Assuming that there has been no significant loss of water prior to boiling, f_1 = 1 and equation (3) simplifies to

$$\alpha_{app} = \frac{f_2^{\alpha} - 1}{f_2^{\alpha-1}\,(f_2 - 1)} \,. \qquad (3a)$$

The value of f_2 can be estimated by considering the mass balance of the mixture observed in the hot wells,

$$\delta^{18}O_{total} = (1-x)\ \delta^{18}O_r + x\ \delta^{18}O_m, \qquad (4)$$

where x is identically equal to f_2. Setting $\delta^{18}O_{total}$ = -10.5 permil, the approximate $\delta^{18}O$ value of the waters collected from the hot wells (samples P2, P3, and P4), f_2 = 0.76. For the given $\delta^{18}O_r$ and $\delta^{18}O_m$, α_{app} = 0.9962. Using these values for f_2 and α_{app}, a graphical solution of equation (3a) yields a model α = 0.9965 (Fig. 8). Taking the reciprocal and using the data of Bottinga in Friedman and O'Neil (1977), the model α value corresponds to a temperature of approximately 170°C. Therefore, for the limiting case represented by this model, the hypothesized boiling occured at or above approximately 170°C.

The principal limitation of this model is probably the assumption that the deep reservoir component truly represents the aggregate distillate. Unless all the vapor recondensed to give this end-point component, the recondensed water would be more positive than the original vapor. If this were true, quantitative evaluation of the data would require some knowledge of the recondensation process. However, it has been shown that in the limiting case of the model presented here, the required negative isotopic values observed in the system could be produced by boiling.

The relatively low salinity of the Lightning Dock area waters is consistent with the boiling hypothesis. Since most of the solutes derived from water-rock interactions will be partitioned into the liquid phase during boiling, the recondensed vapor phase would have an initially low concentration of dissolved solids and would develop significant salinity again over time as the recondensed liquid interacted with the rock at elevated temperature. On the other hand, there is no geologic evidence for recent boiling at or near the surface in the Animas Valley, except for the initial boiling of McCant's well when the locally

Figure 8. Graphical solution for α_{model} in equation (3a) given $\alpha_{app} = 0.9962$ and $f_2 = 0.76$.

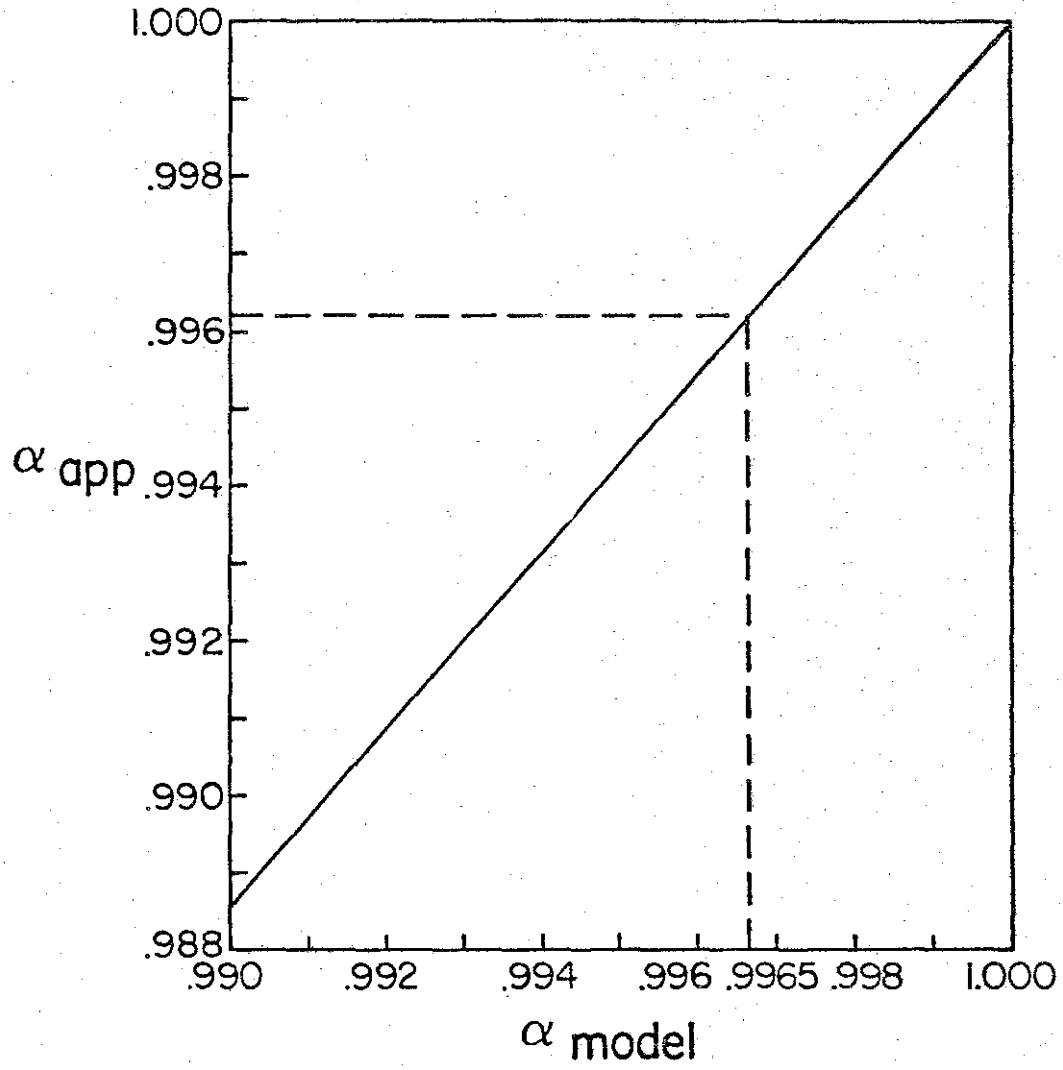
1.000
.998
.996
.994
.992
.990
.988
α app
.990
.992
.994
.996
.9965
.998
1.000
α model

confining clay layer was pierced during drilling (Summers, 1965). This is perhaps reconcilable if the boiling system is now extinct and all evidence of fumarolic alteration is buried by recent sediments or if the fluids mixed in a deep aquifer, so that no evidence of the vapor phase can be found at the surface.

In summary, the isotopic composition of hydrogen and oxygen in the waters of the Animas Valley indicates that the groundwaters originated as meteoric water, which may have been modified by evaporation and mixing. While it is not possible on the basis of present geochemical and geologic data and isotopic systematics to choose unequivocally between the "old, cold" water hypothesis and the boiling hypothesis, it is possible that boiling has played a role in modifying the isotopic and chemical composition of the geothermal reservoir water.

In Figure 9 the $\delta^{18}O$ values for the P-series samples are plotted and contoured on a sketch map of the lower Animas Valley. Although there are not many data points, the $\delta^{18}O$ isopleths do outline a northeast-trending linear feature with an apparent dispersion pattern to the north of the hot wells. Because of the relationship between $\delta^{18}O$ and δD, a plot of δD values would give a very similar pattern. The significance of the pattern will be discussed below, in the section on the geothermal reservoir.

Water-Rock Interaction

Because water-rock interactions are typically temperature dependent, it is useful to estimate subsurface temperatures. Reservoir temperatures were estimated using the silica geothermometer, proposed by Fournier and Rowe (1966) but using the recent silica solubility of Walther and

Figure 9. Isopleths drawn for $\delta^{18}O$ values of P-series sample waters.

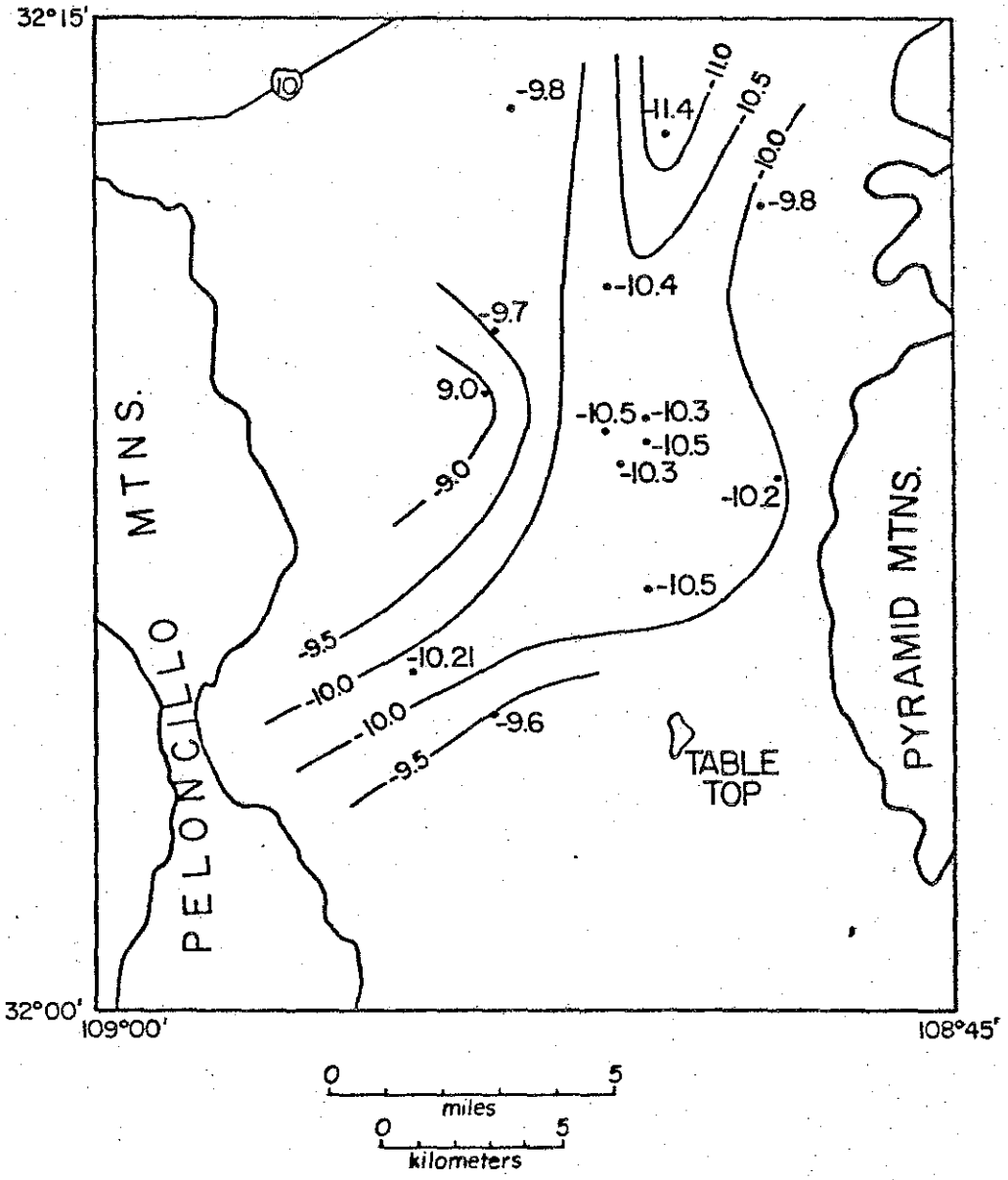
32°15'
32°00'
109°00'
108°45'
10
-9.8
-11.4
-11.0
-10.5
-10.0
-9.8
-10.4
-9.7
9.0
-9.0
-10.5
-10.3
-10.5
-10.3
-10.2
-10.5
-9.5
-10.0
-10.21
-10.0
-9.6
-9.5
MTNS.
PELONCILLO
PYRAMID MTNS.
TABLE TOP
0
5
miles
0
5
kilometers

Helgeson (1977), and the alkali geothermometers of Fournier and Truesdell (1973) and Fournier and Potter (1979). A comparison of the temperatures calculated by various methods using the computer program GEOTHM is given in Table 3. The last column lists a "Best Estimate" reservoir temperature, which is a subjective but value based on comparison of the values computed by the alkali and either alpha quartz (L-V) or chalcedony silica models. Best estimate temperatures from the samples in the lower Animas Valley in the vicinity of the KGRA are plotted and contoured on Figure 10.

In Figure 10 the isopleths define a recognizable hot spot around the hot wells, from which the chemical temperatures indicate a northerly thermal dispersion similar to that originally described by Kintzinger (1956) from the temperature and temperature gradient survey. The apparent thermal ridge and continued evidence for high-temperature water to the southwest of the hot wells will be discussed below.

To help evaluate water-rock interactions, multiple linear regression and correlation matrix calculations were performed on selected physicochemical parameters of P-series and LD-series data (Table 3A and 3B). Speculation on the physical significance of the observed correlations provides some insight into possible interpretations of the water chemistry.

Chlorine and boron were selected as conservative or nonreactive elements, the concentrations of which are indicative of sources of components and fluids, of mixing processes, and of dissolution of evaporite minerals from the sedimentary section (Fournier and Truesdell, 1974; Mariner and Willey, 1977). Boron concentration shows a very strong

Table 2

Comparison of Calculated Reservoir Temperatures [°C]

Sample	Na-K	Na-K-Ca [F&T]	Na-K-Ca [UNM]	Alpha Quartz (BARS) L-V	500	1500	2000	Alpha Cristoba.	Chalced.	Best Estimate
P-Series:										
P 1	109	38	32	80	71	59	53	38	59	38
P 2	169	174	169	168	152	128	118	110	137	169
P 3	164	170	165	165	150	126	116	108	135	165
P 4	153	160	156	150	136	114	105	95	122	153
P 5	129	60	53	94	84	69	63	48	70	50
P 10	85	71	65	112	100	83	76	63	87	64
P 13	112	49	43	123	111	92	84	72	97	97
P 14	128	38	32	100	90	74	68	53	76	76
P15	129	58	51	85	75	62	56	41	62	60
P 20	101	39	32	102	92	76	69	55	78	78
P 22	102	42	35	95	85	70	64	49	71	71
P 23	73	46	39	77	69	56	51	36	56	38

Table 2 cont'd

Sample	Na-K	Na-K-Ca [F&T]	Na-K-Ca [UNM]	Alpha Quartz (BARS) L-V	500	1500	2000	Alpha Cristoba.	Chalced.	Best Estimate
P 24	152	157	154	169	153	129	118	111	138	142
P 25	137	50	43	85	75	62	56	41	62	56
An-Series:										
An 1	126	39	32	110	98	82	74	62	85	62
An 2	85	58	52	53	47	39	35	17	35	52
An 3	131	41	34	119	107	89	81	69	93	69
An 4	130	94	87	140	126	105	96	86	112	86
An 5	139	60	53	102	92	76	69	55	78	54
An 6	132	52	46	78	70	57	52	36	57	54
An 7	117	52	46	78	69	57	51	36	56	54
An 8	133	41	34	83	74	61	56	40	61	40
An 9	117	61	54	---	---	---	---	---	---	55
An 10	116	58	51	89	78	65	59	44	66	62
An 11	129	45	38	96	86	71	65	50	72	47

Table 2 cont'd

Sample	Na-K	Na-K-Ca [F&T]	Na-K-Ca [UNM]	Alpha Quartz (BARS) L-V	500	1500	2000	Alpha Cristoba.	Chalced.	Best Estimate
An 12	122	45	38	97	87	72	66	50	73	47
An 13	127	64	57	81	72	59	54	39	59	58
An 14	119	45	38	96	86	71	65	49	72	47
An 15	131	44	37	78	70	57	52	37	57	37
An 16	114	48	41	88	78	64	59	44	65	46
An 17	150	81	73	78	70	57	52	36	57	80
An 18	130	45	38	89	78	65	59	44	66	45
An 19	125	30	23	91	81	67	62	46	68	60
An 20	128	39	32	101	91	75	69	54	77	70
An 21	141	49	42	89	78	65	59	44	66	60
An 22	103	48	41	82	73	60	55	39	60	55
An 23	127	42	35	88	78	64	59	44	65	43

Table 2 cont'd

Sample	Na-K	Na-K-Ca [F&T]	Na-K-Ca [UNM]	Alpha Quartz (BARS) L-V	500	1500	2000	Alpha Cristoba.	Chalced.	Best Estimate
LD-Series:										
LD 1	133	143	139	83	74	61	56	40	61	87
LD 2	150	151	100	91	81	67	61	46	68	95
LD 3	199	62	54	95	85	70	64	49	71	52
LD 4	58	58	52	82	72	60	54	39	60	58
LD 5	100	95	88	99	89	73	67	52	75	93
LD 6	171	36	29	89	79	65	60	45	66	45
LD 7	220	21	14	99	89	74	67	53	75	53
LD 8	154	19	12	97	87	72	66	50	73	50
LD 9	---	45	36	99	98	74	67	53	75	45
LD 10	---	58	49	91	81	67	61	46	67	48
LD 11	225	70	62	104	93	77	71	58	80	60
LD 12	289	50	42	86	76	63	58	42	64	42
LD 13	250	56	49	91	81	67	61	46	67	48

Figure 10. Isopleths drawn for best estimate shallow reservoir temperatures of P-series (•) and An-series (+) waters. Values are calculated from the water chemistry and listed in Table 3.

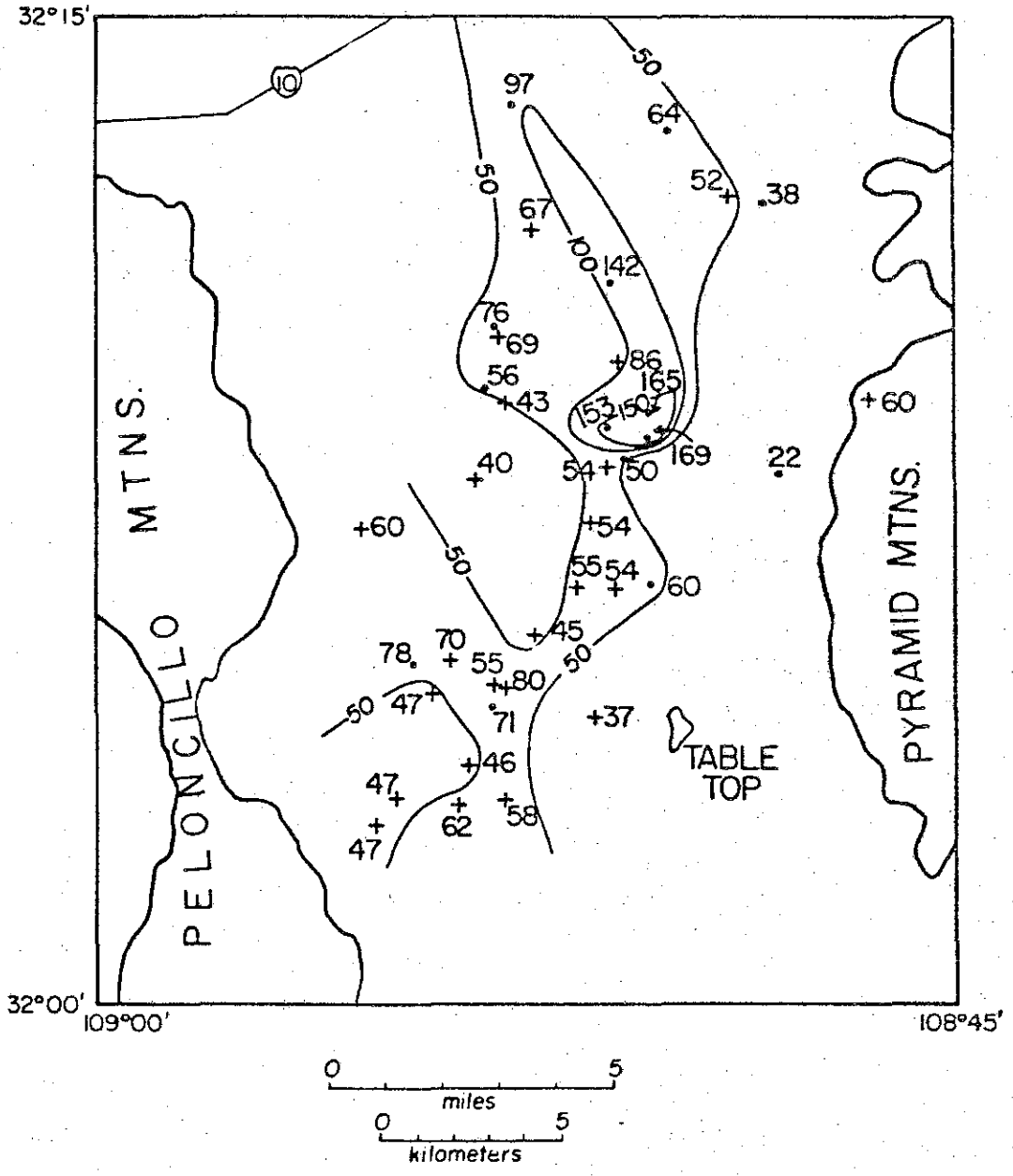
32°15'
32°00'
109°00'
108°45'
10
97
64
52
38
67
100
142
76
69
56
43
86
165
153
150
169
22
60
40
54
50
54
60
55
54
45
78
70
55
80
47
71
37
46
58
62
47
47
50
MTNS.
PELONCILLO
PYRAMID MTNS.
TABLE TOP
0
5
miles
0
5
kilometers

Table 3A

Multiple Linear Regression-Correlation Coefficients Lightning Dock KGRA Data

	T°C Alkali	T°C Silica	Cl	B	Cl/B	HCO_3^-	SO_4^-	$HCO_3^-/SO_4^=$	$\delta^{18}O°/\infty$ (SMOW)
P-Series and LD-Series:					Multiple Correlation = 0.66				
T°C Meas.	0.741	0.736	0.400	0.481	0.054	-0.210	0.394	-0.171	-0.294
T°C Alk.		0.703	0.448	0.770	-0.037	0.140	0.450	-0.278	-0.511
T°C Sil.			0.406	0.466	0.035	-0.101	0.542	-0.081	-0.203
Cl				0.585	0.686	0.279	0.855	-0.353	-0.488
B					0.016	0.557	0.457	-0.247	-0.703
Cl/B						0.218	0.611	-0.345	-0.227
HCO_3							0.215	-0.113	-0.558
SO_4								-0.400	-0.460
HCO_3/SO_4									-0.198

Table 3A cont'd

	T°C Alkali	T°C Silica	Cl	B	Cl/B	HCO_3^-	SO_4^-	$HCO_3^-/SO_4^=$	$\delta^{18}O°/\infty$ (SMOW)
P-Series: [14 samples]					Multiple Correlation = 0.79				
T°C meas.	0.844	0.728	0.312	0.655	-0.245	-0.849	0.220	-0.399	-0.278
T°C Alk.		0.926	0.445	0.871	-0.305	-0.305	0.484	-0.523	-0.408
T°C Sil.			0.332	0.806	-0.344	-0.388	0.423	-0.514	-0.382
Cl				0.679	0.473	-0.107	0.911	-0.585	-0.699
B					-0.218	-0.248	0.703	-0.593	-0.700
Cl/B						0.098	0.271	-0.095	-0.118
HCO_3^-							0.065	0.155	0.007
SO_4^-								-0.695	-0.661
HCO_3/SO_4									-0.289

Table 3A cont'd

	T°C Alkali	T°C Silica	Cl	B	Cl/B	HCO_3^-	SO_4^-	$HCO_3^-/SO_4^=$	$\delta^{18}O°/\infty$ (SMOW)
LD-Series:	[13 samples]				Multiple Correlation = 0.87				
T°C meas.	0.625	-0.216	0.427	0.618	0.285	0.675	0.664	-0.136	-0.379
T°C Alk.		-0.296	0.375	0.702	0.169	0.588	0.711	-0.391	-0.662
T°C Sil.			-0.060	-0.296	0.014	-0.063	-0.247	0.622	-0.397
Cl				0.620	0.951	0.586	0.822	-0.387	-0.284
B					0.359	0.939	0.782	-0.387	-0.729
Cl/B						0.339	0.661	-0.308	-0.091
HCO_3							0.698	-0.127	-0.669
SO_4								-0.596	-0.528
HCO_3/SO_4									-0.182

Table 3B

Multiple Linear Regression-Correlation Coefficients Lightning Dock KGRA P-Series Data

[Atom Ratio]

	Cl/Ca	Cl/Mg	Cl/K	Cl/Na	Cl/F	Cl/SO_4	Cl/HCO_3	Ca/Mg	$\frac{Na}{Cl+HCO_3}$	$\delta^{18}O°/\infty$
T°C meas.	0.827	0.838	-0.483	-0.171	-0.314	0.324	0.755	0.776	0.901	-0.278
T°C Alk.	0.848	0.784	-0.520	-0.155	-0.396	0.230	0.725	0.781	0.920	-0.414
T°C Sil.	0.757	0.740	-0.566	-0.242	-0.465	0.083	0.586	0.819	0.821	-0.361
Cl/Ca		0.908	-0.196	0.005	-0.298	0.428	0.708	0.810	0.780	-0.507
Cl/Mg			-0.434	-0.144	-0.354	0.309	0.562	0.955	0.677	-0.251
Cl/K				0.667	0.510	0.277	-0.010	-0.583	-0.410	-0.335
Cl/Na					0.691	0.518	0.425	-0.281	-0.145	-0.350
Cl/F						0.697	0.046	-0.480	-0.338	-0.129
Cl/SO_4							0.499	0.110	0.250	-0.518
Cl/HCO_3								0.437	0.812	-0.580
Ca/Mg									0.639	-0.125
$\frac{Na}{Cl + HCO_3}$										-0.451

Multiple Correlation = 0.898

Table 3B cont'd

	B/C	B/Mg	B/K	B/Na	B/F	B/SO_4	B/HCO_3	Ca/Mg	$\frac{Na}{B+HCO_3}$	$\delta^{18}O°/\infty$
T°C meas.	0.809	0.824	-0.409	0.286	-0.239	0.659	0.944	0.777	0.910	-0.281
T°C Alk.	0.865	0.791	-0.400	0.491	-0.317	0.641	0.924	0.782	0.484	-0.408
T°C Sil.	0.807	0.753	-0.424	0.400	-0.456	0.538	0.823	0.818	0.716	-0.383
B/Ca		0.941	-0.149	0.636	-0.252	0.793	0.880	0.875	0.663	-0.360
B/Mg			-0.319	0.513	-0.280	0.735	0.826	0.958	0.616	-0.241
B/K				0.116	-0.259	-0.088	-0.297	-0.441	-0.351	-0.287
B/Na					-0.109	0.638	0.484	0.364	0.225	-0.309
B/F						0.285	-0.292	-0.410	-0.077	-0.098
B/SO_4							0.694	0.597	0.617	-0.365
B/HCO_3								0.752	0.907	-0.483
Ca/Mg									0.559	-0.125
$\frac{Na}{B+HCO_3}$										-0.478

Multiple Correlation = 0.990

correlation with the calculated alkali temperature and with the silica temperature in P-series waters, suggesting that boron is derived primarily from the deep, high-temperature water component in the sample (Table 3A; Fig. 11). The relatively poor correlation between temperature and chloride concentration, which would have been expected on the basis of the experimental results of Ellis and Mahon (1964), is probably due to addition of chloride to the samples by the dissolution of evaporites in the playa sediments (Table 3A; Fig. 12). This hypothesis is corroborated by the very strong correlation between Cl^- and SO_4^{2-} concentrations (Table 3A).

Regression of the atom ratios of chlorine and boron with other components of the P-series waters suggests further relations (Table 3B). The strong positive correlations of temperature with B/Ca, B/Mg, Cl/Ca, and Cl/Mg may result from loss of carbon dioxide and precipitation of carbonate phases. The increase in Ca/Mg ratio with temperature suggests that magnesian calcite may be the carbonate phase which is precipitating; the Ca/Mg ratio is too high for dolomite to be the stable carbonate.

However, carbonates probably do not account for the removal of most of the Mg^{2+} from solution. Figure 13 is a plot of Ca^{2+} and Mg^{2+} concentrations against the concentration of total dissolved solids (TDS) in the solution. While calcium and magnesium behave in a grossly similar fashion, there is substantially better trend in calcium than in magnesium. Furthermore, the calcium concentration increases more strongly than the magnesium, especially up to approximately 1200 mg/l TDS. Figure 14, a plot of HCO_3^- and SO_4^{2-} concentrations against TDS, offers some insights into the Ca^{2+} and Mg^{2+} trends. The sulfate and bicarbonate

Figure 11. Plot of boron concentration against calculated alkali temperatures for all water samples and for calculated geothermal reservoir compositions R2, R3, and R4.

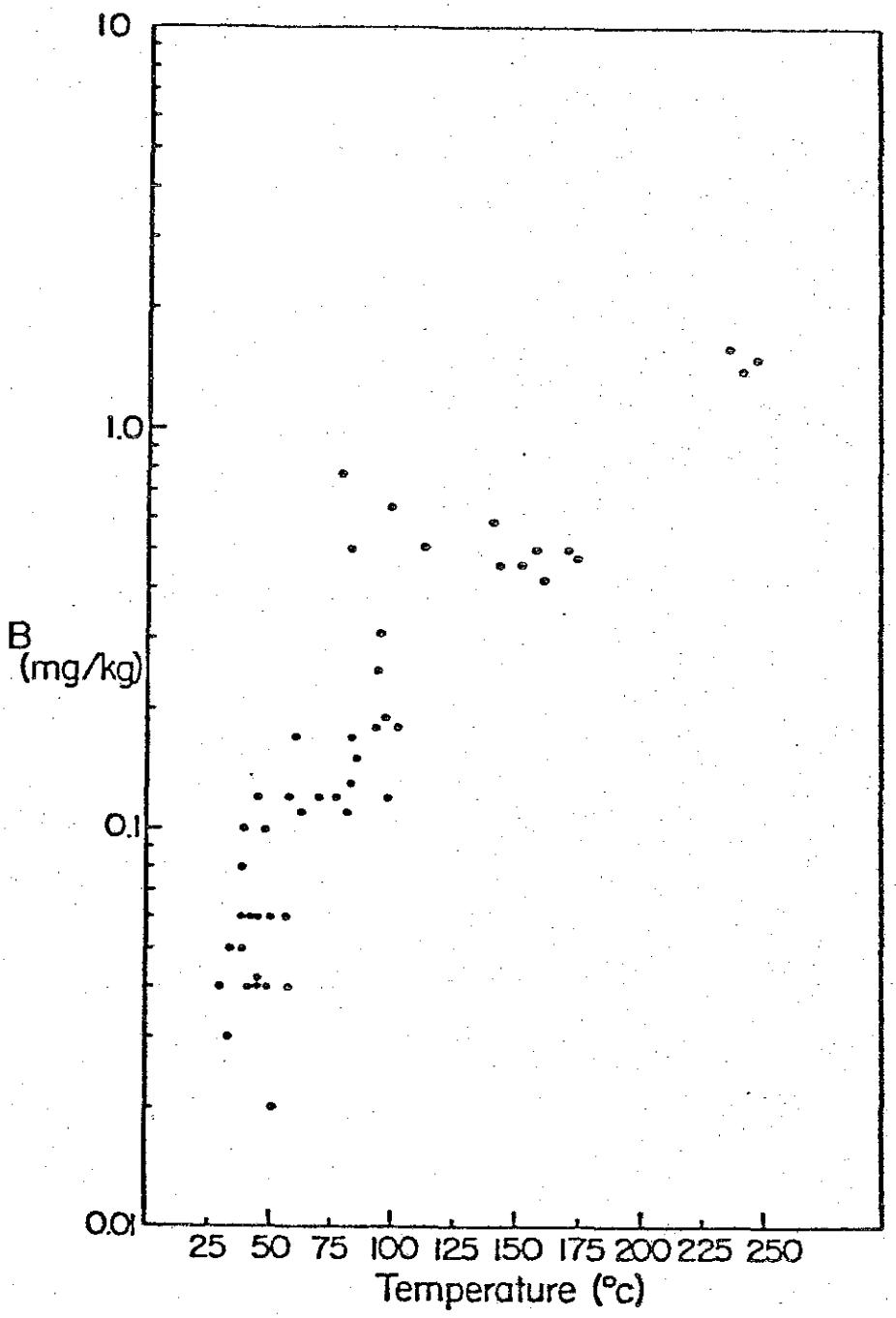
10
1.0
0.1
0.01
B
(mg/kg)
25 50 75 100 125 150 175 200 225 250
Temperature (°c)

Figure 12. Plot of chloride concentration against calculated alkali temperatures for all water samples and for calculated geothermal reservoir compositions R2, R3, and R4.

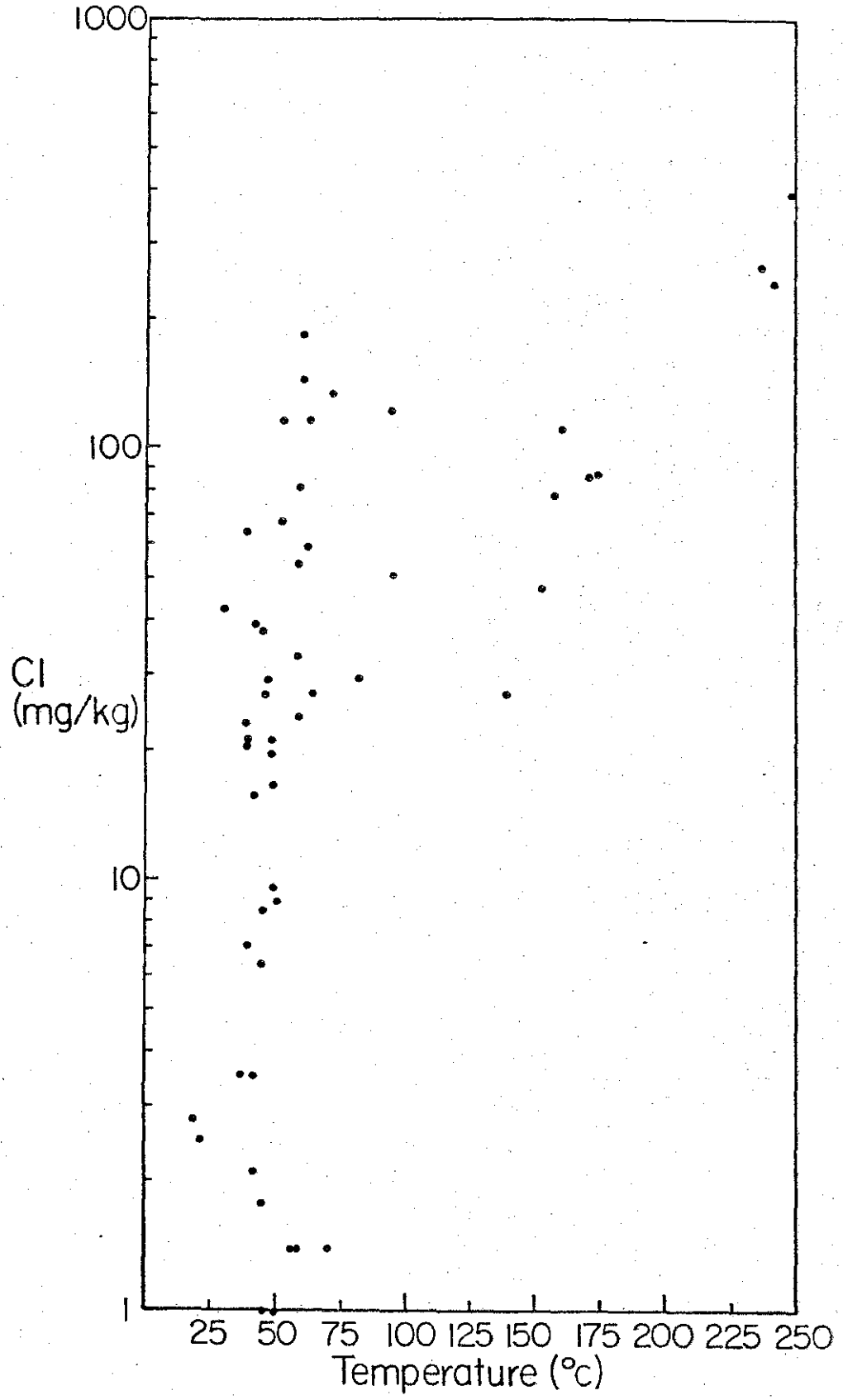
1000
100
10
1
Cl
(mg/kg)
25
50
75
100
125
150
175
200
225
250
Temperature (°C)

Figure 13. Plot of concentration of calcium and magnesium against concentration of total dissolved solids (TDS) for all water samples.

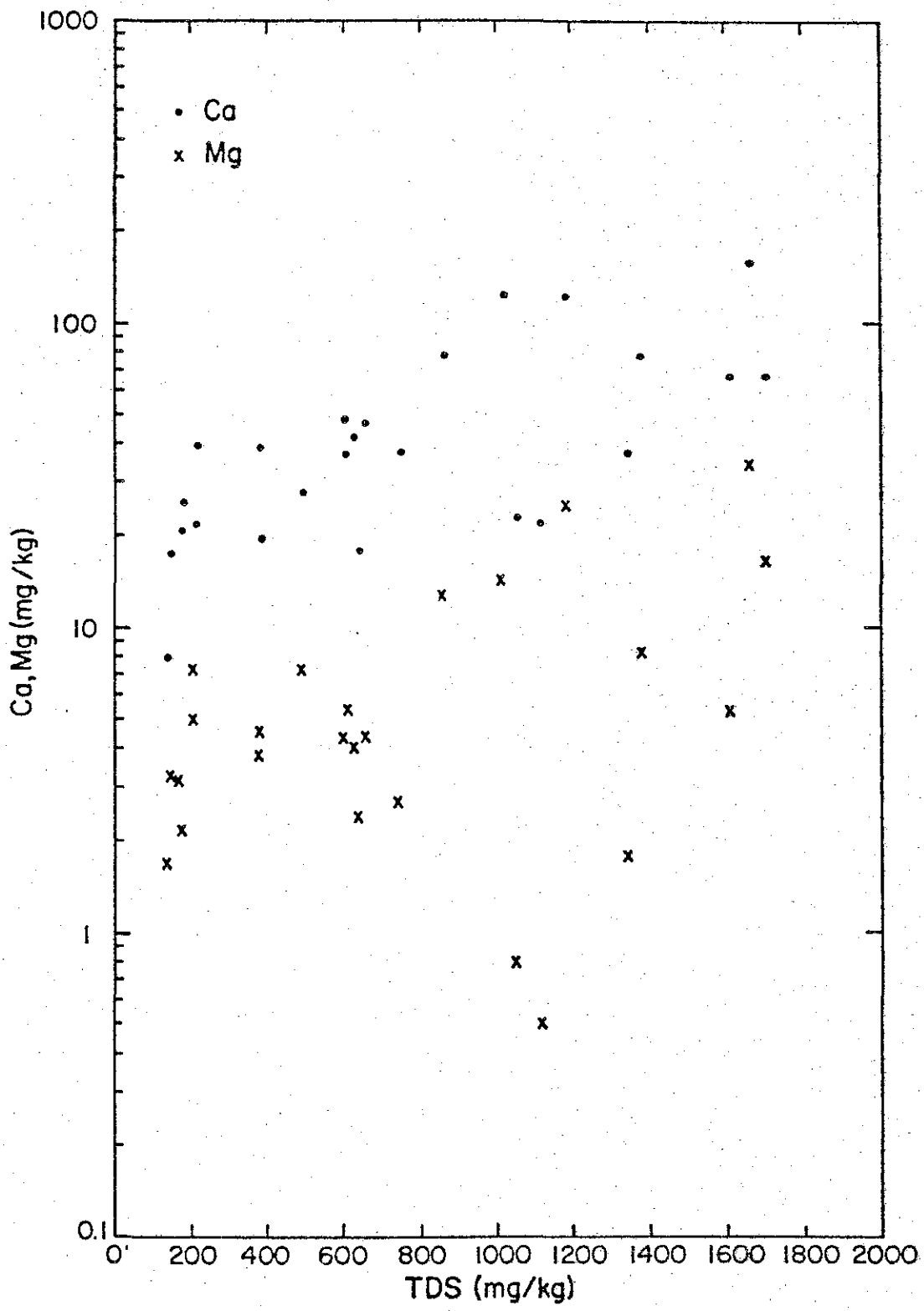
1000
100
10
1
0.1
Ca
Mg
Ca, Mg (mg/kg)
0
200
400
600
800
1000
1200
1400
1600
1800
2000
TDS (mg/kg)

Figure 14. Plot of concentration of sulfate and bicarbonate against concentration of total dissolved solids (TDS) for all water samples.

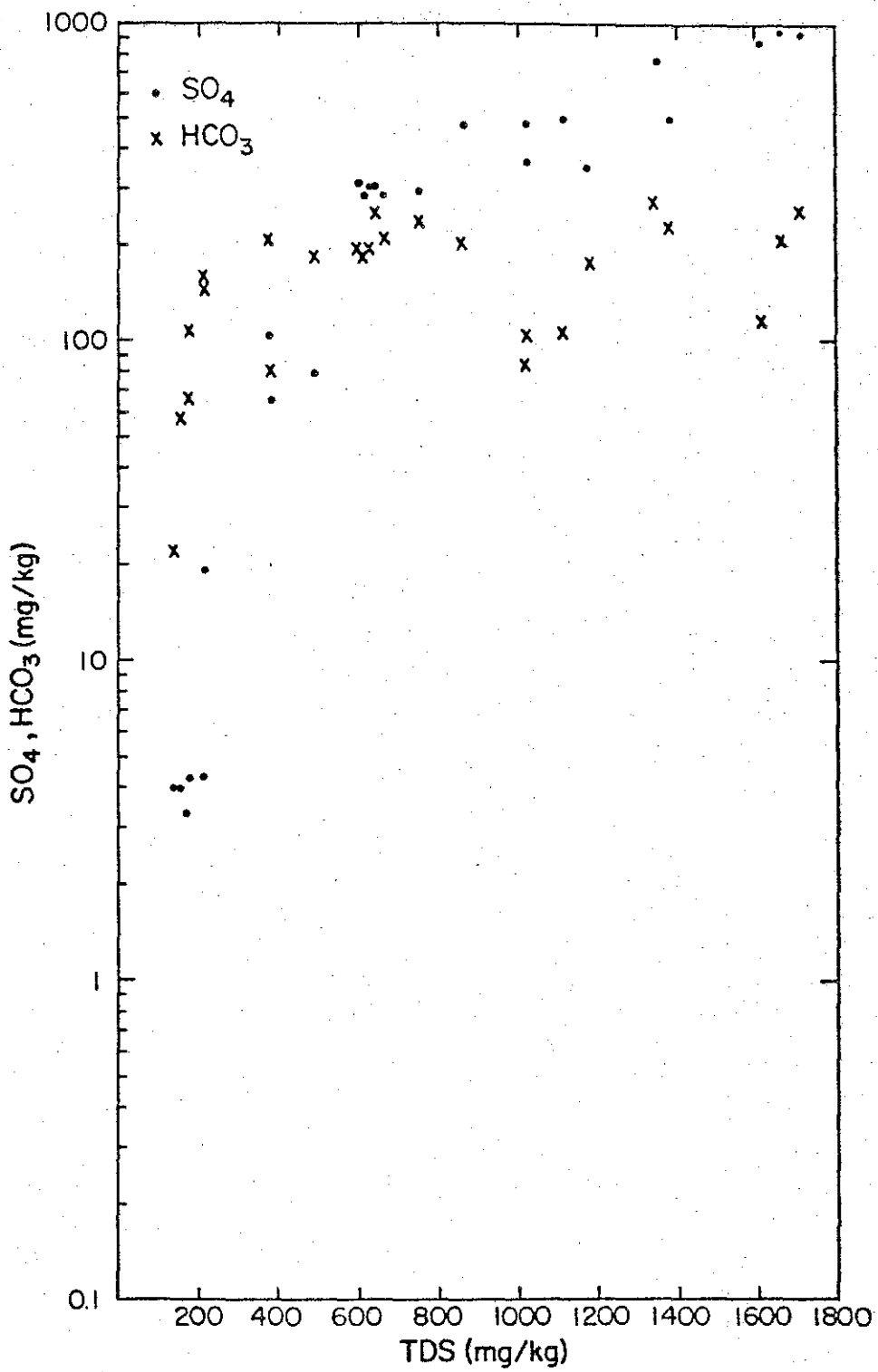
1000
100
10
1
0.1
SO4
HCO3
SO4, HCO3 (mg/kg)
200
400
600
800
1000
1200
1400
1600
1800
TDS (mg/kg)

concentrations behave qualitatively in a similar manner, but the concentration of sulfate increases much more rapidly with salinity than does the concentration of bicarbonate. The strong similarity between the Mg^{2+} and the HCO_3^- trends imply that magnesium is being incorporated in silicate minerals, particularly Mg-montmorillonite, in the formation of which HCO_3^- is consumed (Mackenzie and Garrels, 1966). This hypothesis is supported by calculation of saturation indices and mineral stability diagrams (to be described below), by the recognition of smectites and chlorite in alteration assemblages at numerous studied geothermal areas (Browne, 1978), and by the experimental results of seawater-basalt interaction, in which magnesium is removed from seawater quantitatively by the formation of Mg-montmorillonite (Mottl and Holland, 1978). The similarity of the Ca^{2+} and HCO_3^- trends suggests that the calcium concentrations of the solutions also may be affected by incorporation of Ca^{2+} into silicates, particularly zeolites and Ca-montmorillonites.

The increase in SO_4^{2-} with TDS already has been ascribed to dissolution of evaporites in the playa sediments. The difficulty that the Ca^{2+} concentration is much lower than that needed to balance the sulfate can be met by considering the $Ca/(SO_4^{2-} + HCO_3^-)$ molar ratio. For all the Animas Valley water samples, the ratio is less than one. In general, for any solution in which the ratio is less than one, precipitation of calcium carbonate or calcium sulfate will deplete the solution in calcium, but not in bicarbonate or sulfate. Calculated saturation indices for the waters show all the samples to be saturated with respect to calcite but strongly undersaturated with respect to

to gypsum and anhydrite. Dissolution of $CaSO_4$ from evaporites adds Ca^{2+} and SO_4^{2-} to the solution. A portion of the Ca^{2+} can be removed from the solution by reaction with HCO_3^-,

$$Ca^{2+} + 2HCO_3^- = CaCO_3 + CO_2 + H_2O. \quad (4)$$

As suggested above, HCO_3^- reaches a steady-state concentration buffered by silicate reactions of the general type,

$$n\ \text{H-silicate} + n\ HCO_3^- + R^{n+} = \text{R-silicate} + n\ CO_2 + n\ H_2O, \quad (5)$$

where R^{n+} is an arbitrary cation of charge n. The formation of Mg-montmorillonite and Ca-zeolite or Ca-montomorillonite would be examples of reaction (5). The potential charge imblanace due to loss of Ca^{2+} without equivalent loss of SO_4^{2-} is offset by the removal from solution of a larger molar proportion of anion than cation by reaction (4) and by reaction (5) when multiply-charged cations are involved. Gypsum and anhydrite are the only poorly soluble sulfate minerals that can control the concentration of SO_4^{2-} in natural solutions. Since calcium sulfate is being dissolved, not precipitated, the SO_4^{2-} concentration in the solution increases in proportion to the Ca^{2+} and HCO_3^- concentrations.

Alternatively, the SO_4^{2-} could be added to the waters by oxidation of deep H_2S, a process commonly observed in vapor-dominated geothermal systems (White, 1957). However, there is no indication that the modern geothermal system has any acid sulfate water affinities. In particular, none of the sample waters is saturated with respect to alunite, and the pH of the solutions seems to have been firmly buffered by reaction (5) at values in the neutral to slightly alkaline range. While the large

scale oxidation of H_2S seems unlikely and is not required to explain the chemical data, the hypothesis could be checked by a careful study of the isotopic systematics of sulfur in the system.

While a major portion of the Na^+ and Ca^{2+} in solution in the sample waters appears to be derived from the dissolution of evaporites, the agreement between reservoir temperatures calculated by the Na-K, Na-K-Ca, and SiO_2 geothermometers for the hot wells (samples P2, P3, P4, and P24) suggests that at elevated temperatures, the Na^+, K^+, and Ca^{2+} concentrations of the deep reservoir solution are controlled by equilibrium cation exchange reactions between feldspars and solution. The SiO_2 concentration of the fluids is controlled by the solubility of a silica phase. Alpha quartz solubility gives the best agreement of silica and alkali temperatures for temperatures greater than 100°C; below 100°C, the agreement is best for chalcedony solubility (Landis and Logsdon, 1980). This interpretation of the solubility control of silica is consistent with the detailed work on low temperature systems in Iceland (Arnorsson, 1975) and with the observations at numerous sites in western North America (R. O. Fournier, personal communication, 1979). For the waters sampled at the hot wells, Table 3 shows that quartz solubility and the alkali chemistry of the solutions require the fluids to be near the boiling curve for water in order to yield calculated temperatures in near agreement.

Fluoride ion in solution is controlled by the solubility of fluorite, CaF_2. Calculated saturation indices in Table 4 indicate that virtually all the waters of the lower Animas Valley are saturated with respect to fluorite. Green fluorite, similar to samples from the Animas Mine

along the eastern margin of the Animas Valley, can be seen in microscopic examination of drill chips from the Cockrell #1 well. The spatial association of the fluorite deposits and the high F^-, fluorite-saturated waters of the Lightning Dock area groundwater samples is probably the strongest piece of evidence linking the modern geothermal system to the older, more extensive hydrothermal activity in the valley.

If one assumes that the Animas Valley waters are at chemical equilibrium, it is possible to apply numerical and graphical techniques to the chemistry of the waters to calculate mineral phases with which the solutions could be in equilibrium. Calculated saturation indices for waters have already been referred to above. The saturation index (SI) for a mineral may be defined as the logarithm of the quotient of the ion activity product of the appropriate species in solution divided by the thermodynamic equilibrium constant of the mineral. At chemical equilibrium the quotient is one. Therefore, a saturation index greater than zero implies supersaturation; a saturation index less than zero implies undersaturation (see Appendix 2). The computer program WATEQF was used to compute saturation indices for mineral phases which might be controlling the chemical composition of the lower Animas Valley waters. Table 4 lists the calculated mineral phases which would be in chemical equilibrium with the groundwaters of the Animas Valley.

Truesdell (1976) has shown that a spatial analysis of the chemistry of geothermal waters can produce useful information on subsurface structures and the direction of flow in a geothermal system. The strong positive correlation between boron concentration and temperature suggests that the boron concentration reflects the contribution of the

Table 4

Minerals Calculated by WATEQF to be in Equilibrium with the Waters of the Lower Animas Valley. A Saturation Index (SI) Greater than Zero Implies Supersaturation; a Saturation Index Less than Zero Implies Undersaturation.

	Saturation Index	
	Minimum	Maximum
Quartz	-1.73	+1.19
Chalcedony	-2.22	+0.68
Kaolinite	-1.46	+7.05
Montmorillonite	-5.24	+10.69
Illite	-4.42	+7.56
Chlorite	-1.72	+7.90
Calcite	-0.07	+0.58
Siderite	-27.39	+0.62
Analcime	-10.57	+0.17
Wairakite	-16.15	+3.29
Laumontite	-5.71	+7.44
Prehnite	-6.27	+3.42
Adularia	-5.77	+3.76
Albite	-9.11	+2.70
Hematite	+0.86	+25.44
Pyrite	+5.47	+16.34
Fluorite	-1.54	+0.76

deep reservoir water. Boron should not enter into near surface stoichiometric reactions with gases or rocks, and the waters are not saturated with respect to any borate phases. The major cations potentially do enter into stoichiometric reactions. As discussed above, the strong positive correlation between the B/Ca ratio and temperature probably reflects loss of Ca^{2+} from solution due to precipitation of calcium carbonate at depth. The B/Ca ratio can also change as a result of mixing. The B/Na ratio shows a much weaker correlation with temperature than does the B/Ca ratio, since all the potential Na-bearing mineral phases have prograde solubility. Furthermore, there is a possible contribution of Na^{+} to the waters due to the dissolution of playa evaporites. Therefore, it seems likely that changes in the molar ratio of B/Na occur primarily by mixing and dilution. Similarly, the statistical treatment suggests that fluorine can be used to characterize the contribution of high temperature reservoir fluids but that sulfate characterizes low temperature waters of the shallow aquifers. The SO_4^{2-}/F^{-} ratio can be used as a qualitative index of the amount of reservoir fluid in a sample: low ratios indicate relatively more reservoir fluid; high ratios indicate relatively more shallow fluid.

B/Ca (Fig. 15), B/Na (Fig. 16), and SO_4/F (Fig. 17) molar ratios are plotted and contoured in the same manner as $\delta^{18}O$ values in Figure 9 and temperature values in Figure 10. Figures 9, 10, and 15 to 17 illustrate common features: (1) mixing and dilution of deep reservoir water by shallow aquifer water; (2) dispersion of deep reservoir components by the shallow flow regime to the north of the hot wells; and (3) leakage of deep reservoir components into the shallow aquifer in

Figure 15. Isopleths drawn for boron/calcium molar ratios (x 10^3) in P-series (•) and An-series (+) waters.

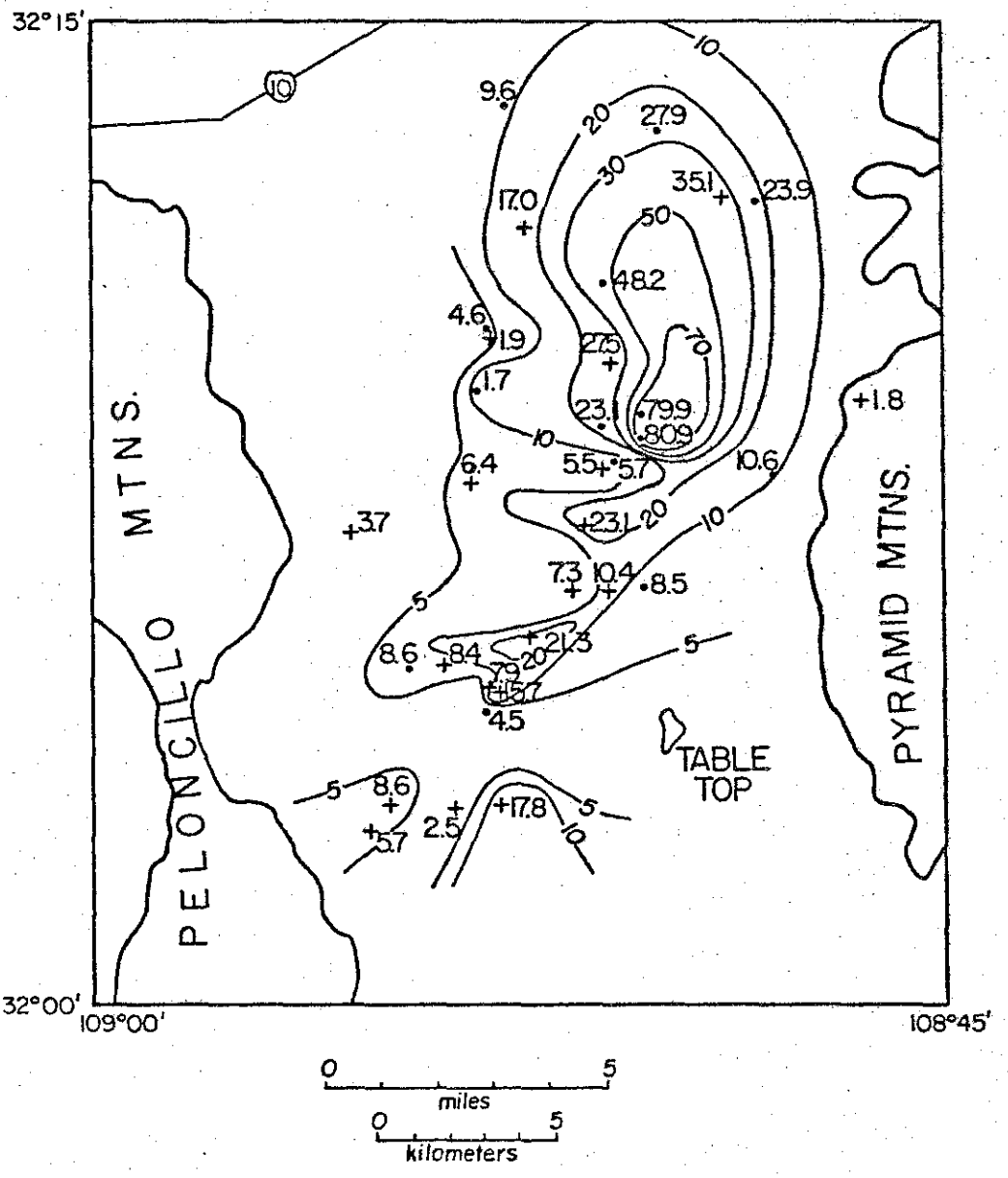
32°15'
32°00'
109°00'
108°45'
MTNS.
PELONCILLO
PYRAMID MTNS.
TABLE TOP
10
9.6
20
27.9
30
35.1
23.9
17.0
50
48.2
4.6
1.9
27.5
1.7
23.1
7.9
8.0
9
10
5.5
5.7
10.6
6.4
3.7
23.1
20
10
7.3
10.4
8.5
5
8.6
8.4
7.9
20
21.3
5
15.7
4.5
5
8.6
5.7
2.5
17.8
5
10
1.8
0
5
miles
0
5
kilometers

Figure 16. Isopleths drawn for boron/sodium molar ratios (x 10^3) in P-series (•) and An-series (+) waters.

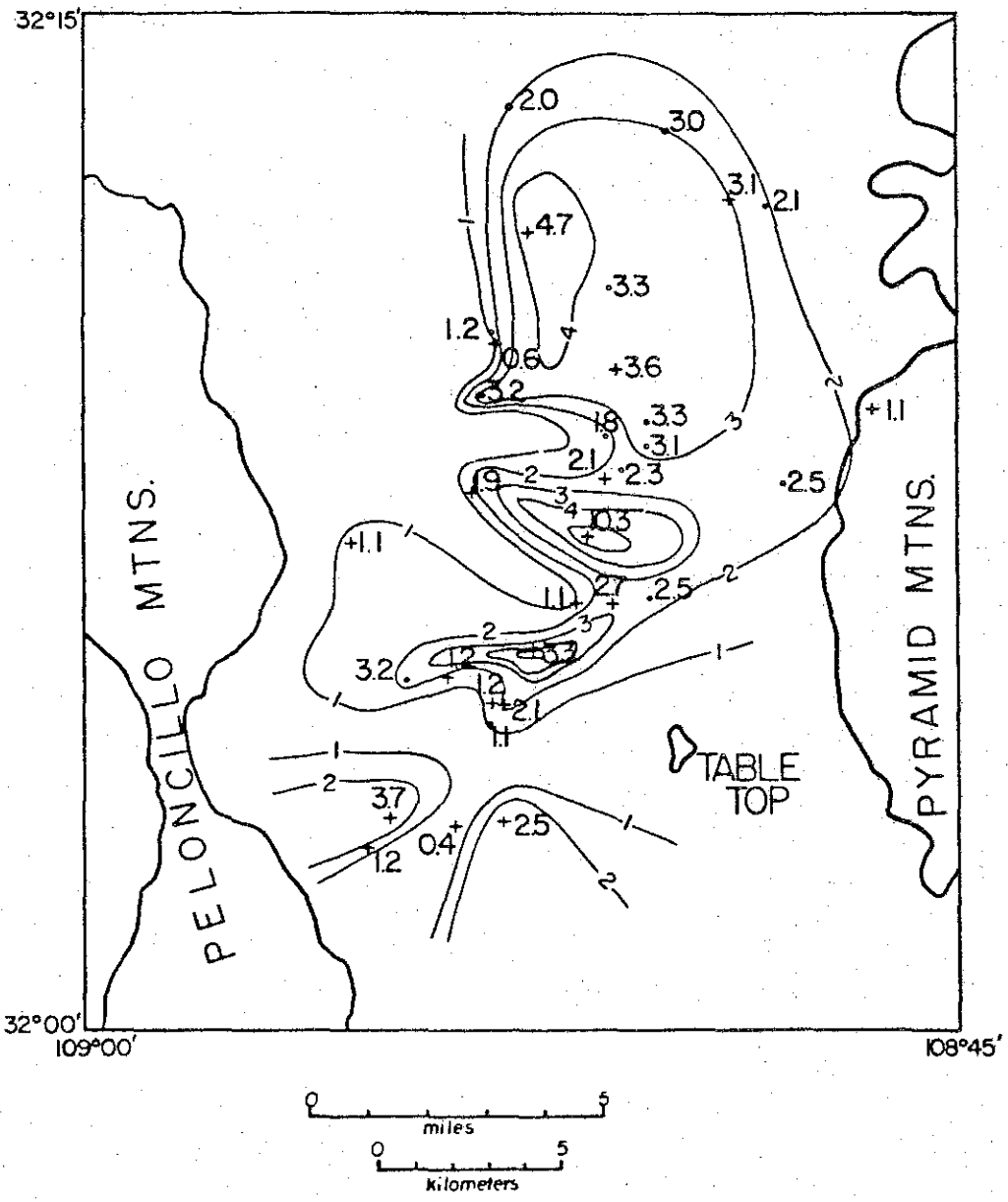
32°15'
32°00'
109°00'
108°45'
PELONCILLO MTNS.
PYRAMID MTNS.
TABLE TOP
2.0
3.0
3.1
2.1
4.7
3.3
1.2
0.6
3.6
3.2
1.8
3.3
3.1
2.1
2.3
1.9
2.5
1.1
0.3
2.7
2.5
1.1
3.2
2.1
1.1
3.7
1.2
0.4
2.5
miles
Kilometers

Figure 17. Isopleths drawn for sulfate/fluoride molar ratios in P-series (•) and An-series (+) waters.

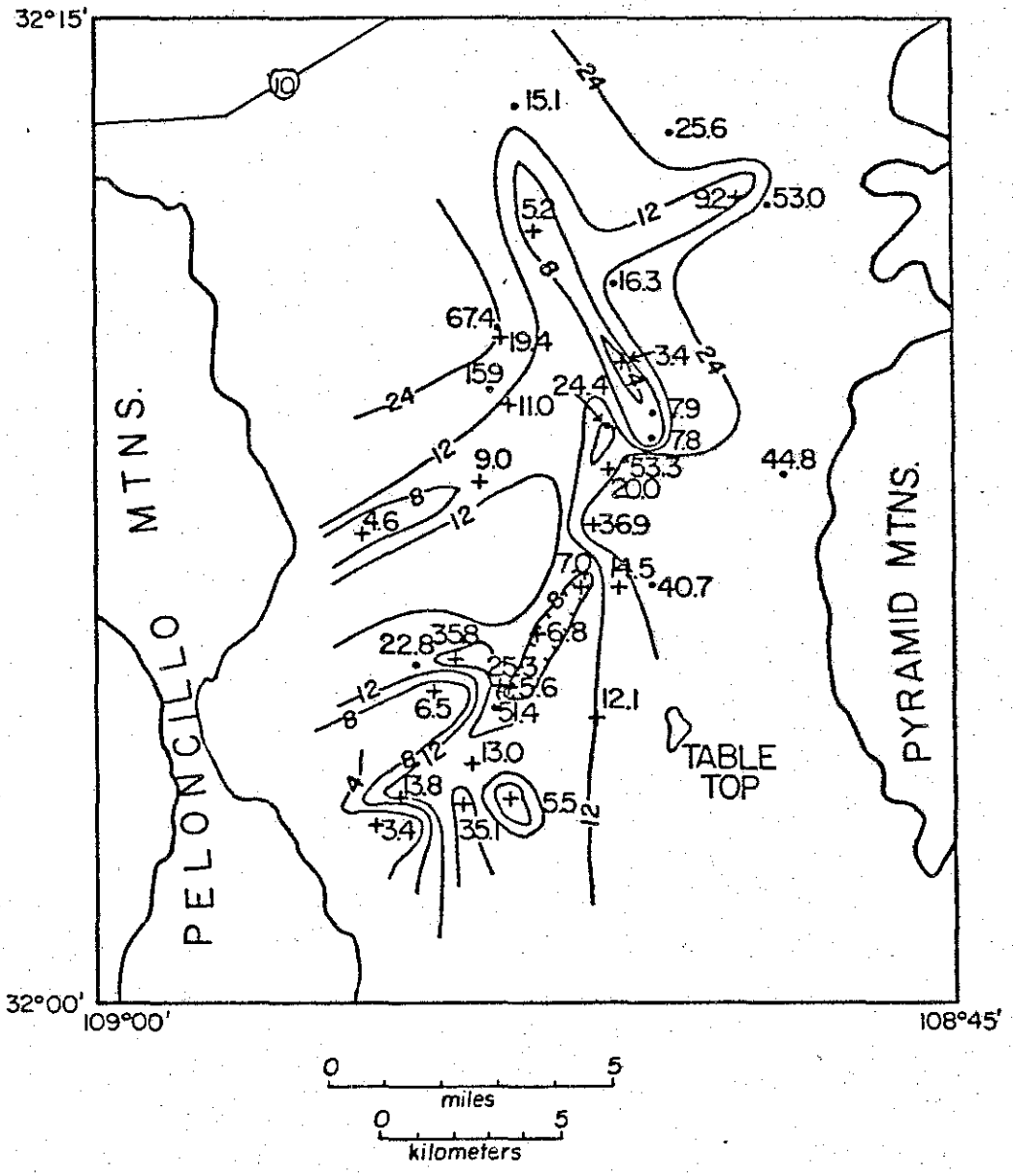
32°15'
32°00'
109°00'
108°45'
PELONCILLO MTNS.
PYRAMID MTNS.
TABLE TOP
15.1
25.6
53.0
16.3
67.4
19.4
15.9
11.0
24.4
7.9
7.8
44.8
9.0
4.6
53.3
20.0
36.9
7.0
14.5
40.7
22.8
35.8
6.8
25.3
25.6
51.4
6.5
12.1
13.0
13.8
55.5
3.4
35.1
0
5
miles
0
5
kilometers

an area southwest of the hot wells. The persistence of the linear trend in the isopleths constructed on the basis of major and minor chemical components and isotopic data is strong evidence that the trend is real and related to subsurface structure. The geothermal reservoir fluid is thermally evident only where it reaches the surface as a major percentage of the water mixture which is sampled in a well. Southwest of the hot wells, geothermal reservoir fluid that is leaking into the near surface aquifers can be documented only by the chemical signature preserved in the mixture. High temperatures are indicated chemically, but thermal evidence is absent because of the extreme dilution of the deep reservoir water by shallow groundwater. The nature of the subsurface structure which controls the leakage of deep reservoir components into the shallow aquifers will be discussed below in the section on the nature of the reservoir.

Mixing Model

The discussion of Figures 5 to 10 and 15 to 17 has already pointed out that mixing of solutions has been important in developing the physico-chemical nature of the groundwaters of the Animas Valley. The chemistry of the waters from the hot wells meets all the standard tests for mixed water in a geothermal system: variations in temperature, variations in content of relatively nonreactive components, variations in the ratios of nonreactive to reactive components, and significant deviation of chemically calculated temperatures from measured temperatures (Fournier and Truesdell, 1974; Fournier and others, 1974).

To determine the degree of mixing and to characterize the water chemistry of the high temperature geothermal reservoir, a mixing model described by Truesdell and Fournier (1977) was applied. Data on aqueous silica solubility controlled by alpha quartz (Fournier and Rowe, 1966) and by other silica forms and at various fluid pressures (Walther and Helgeson, 1977) were used (Table 5). The model is limited by three basic assumptions: (1) the concentration of silica does not change by dissolution or precipitation during or after mixing; (2) no heat is lost from the total fluid system by conduction, i.e., there is adiabatic cooling at constant enthalpy; and (3) a steam phase, if formed, does not separate (Fournier and others, 1974). Using these assumptions, the concentration of dissolved silica and all temperature changes are controlled solely by mixing.

Figure 18, after Truesdell and Fournier (1977), illustrates the application of the mixing model. The waters of the hot wells, P2, P3, and P4, are assumed to represent a two-component mixture, consisting of a cold, shallow aquifer component, represented by sample P1, and a high-temperature geothermal reservoir component. P1 was chosen as a geographically close, low-temperature sample which is located up hydrologic gradient from the hot wells, and which can be considered representative of the dilute shallow groundwater component. The silica concentration for each sample is given in milligrams per kilogram (ppm). Because the system is assumed to be isenthalpic, silica solubility is plotted as a function of enthalpy of liquid water, rather than of temperature. When the enthalpy of liquid water is calculated in International Table calories per gram, the numerical value of the

Table 5

Aqueous Silica Solubility*

Temperature-Enthalpy

Saturated SiO_2(aq) at L-V P_{H_2O}

Temperature °C	Enthalpy** Cal/gm IT	Alpha Quartz	Alpha Cristobalite	Beta Cristobalite	Chalcedony	Amorphous Silica	Quartz 0.5 kbar	Quartz 1.0 kbar
0	0.02	1.89	7.72	25.52	3.74	60.93	1.97	1.99
5	5.1	2.46	9.77	31.10	4.82	70.76	---	---
10	10.1	3.15	12.13	37.22	6.09	81.06	---	---
25	25.1	6.02	21.37	59.40	11.24	116.09	7.13	8.20
50	50.0	14.18	44.75	108.59	25.22	187.41	17.49	21.03
75	75.0	27.78	79.40	173.30	47.51	274.66	34.74	42.54
100	100.1	48.28	126.71	253.40	79.58	378.27	60.65	74.61
125	125.4	76.88	187.41	348.98	122.69	497.51	96.56	118.80
150	151.0	115.03	262.30	460.05	178.16	632.12	157.50	176.52
175	177.0	163.98	353.02	587.22	247.06	777.68	204.08	249.92
200	203.6	224.80	458.99	729.13	330.22	934.98	278.49	343.40
225	230.9	297.72	580.50	886.75	427.37	1093.46	367.96	447.51

Table 5 cont'd

Temperature °C	Enthalpy** Cal/gm IT	Saturated SiO_2(aq) at L-V P_{H_2O}						
		Alpha Quartz	Alpha Cristobalite	Beta Cristobalite	Chalcedony	Amorphous Silica	Quartz 0.5 kbar	Quartz 1.0 kbar
250	259.2	384.72	717.47	1058.77	536.79	1252.57	472.94	576.50
275	289.0	481.73	864.57	1241.09	657.36	1395.73	594.02	725.78
300	321.0	585.87	1013.45	1418.41	779.48	1516.36	729.13	894.96

*Data on Walther and Helgeson (1977) in Mg/l

**International Calories

Figure 18. Plot of dissolved silica versus enthalpy used to estimate the temperature and fraction of hot-water component in a mixed water. Samples P2, P3, and P4 are mixed waters from the hot wells; P1 is a geographically close, low-temperature water (after Truesdell and Fournier, 1977).

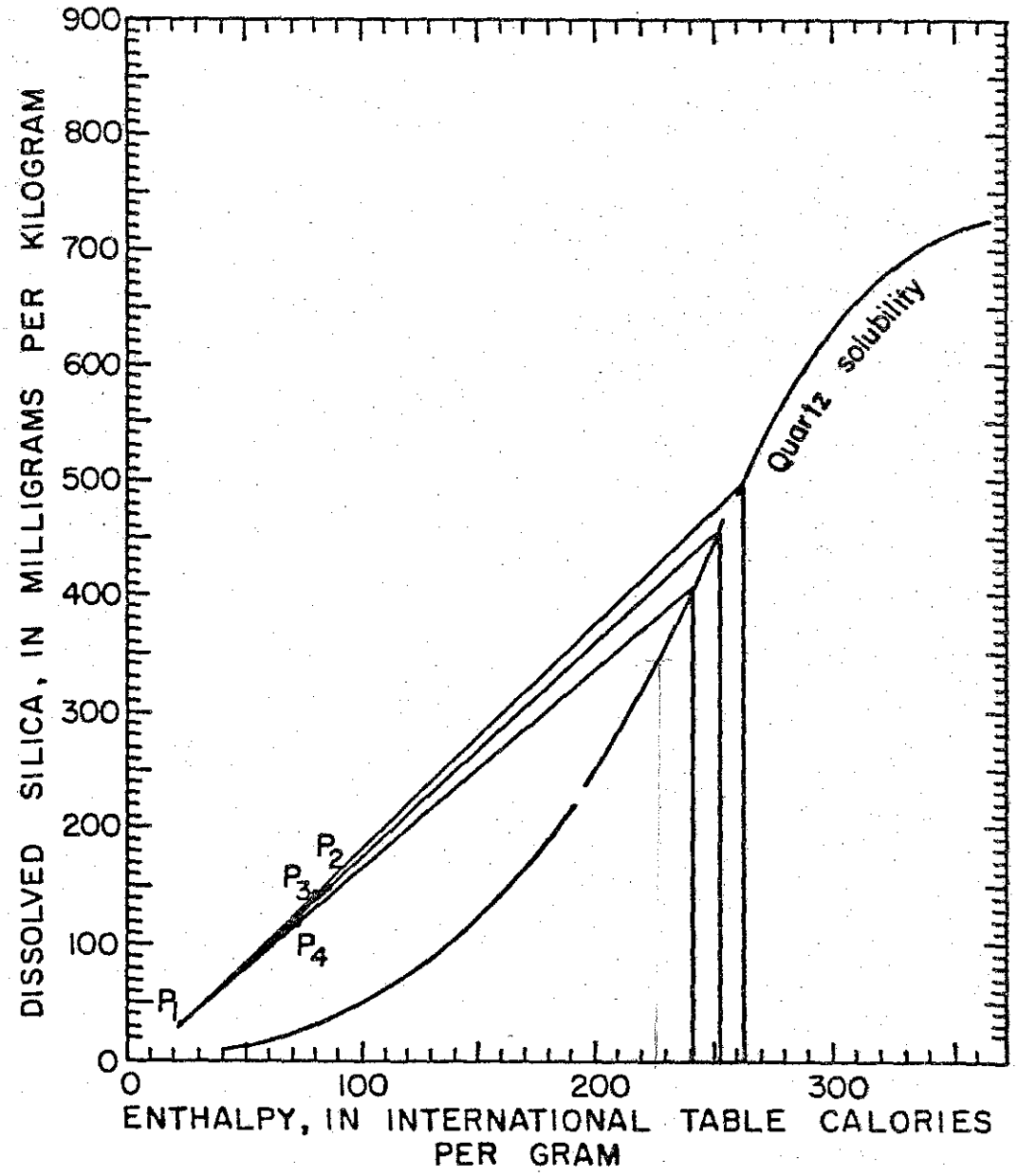
900
800
700
600
500
400
300
200
100
0
0
100
200
300
DISSOLVED SILICA, IN MILLIGRAMS PER KILOGRAM
ENTHALPY, IN INTERNATIONAL TABLE CALORIES PER GRAM
Quartz solubility
P1
P2
P3
P4

enthalpy is nearly identical to the temperature in degrees Celsius up to 250°C (see Table 5). Above 250°C, the Steam Tables can be used to convert rapidly between enthalpy and temperature. Projecting a line from P1 through a mixed-water point to the quartz solubility curve gives the silica concentration and the enthalpy (temperature) of the high-temperature component, called R, in the mixture. Further, the lever rule can be applied to determine the percentage of P1 and R in the mixture.

The graphical mixing technique yields a deep reservoir component of about 25 percent in the waters of the hot wells. A numerical mass balance calculation on the mixing trend of the isotopic data of Fig. 7, using a modern meteoric water of $\delta^{18}O = -9.6$ permil, a deep component of $\delta^{18}O = -13.4$ permil, and a mixed-water value of $\delta^{18}O = -10.5$ permil (sample P2),

$$-10.5‰ = x(-13.4‰) + (1-x)(9.6‰), \qquad (6)$$

yields a deep reservoir contribution of 24 percent. The close agreement between the two independent computations strongly supports the validity of the mixing model.

Table 6 presents mixing percentages, deep reservoir temperatures and calculated reservoir chemistries based on the application of the mixing model. The mixed waters of the hot wells contain about 25 percent deep geothermal reservoir water component which has a temperature of approximately 250°C. The reservoir fluid chemistry is calculated using the appropriate hot water fraction for each well and the analyzed chemistry of cold well P1 and the hot well of interest. From the

Table 6

Mixing Estimates and Calculated Reservoir Chemistry (ppm)

	P 1	P 2	R2Q	R2C	P 3	R3Q	R3C	P 4	R4Q	R4C
T°C Reservoir			250	232		262	238		241	221
X			0.27	0.30		0.24	0.27		0.23	0.24
T°C Alkali	32	169	246	241	165	240	237	156	211	211
Ca^{++}	28.0	22.0	5.8	8.0	23.2	8.0	10.2	67.3	198.9	191.8
Mg^{++}	7.3	0.5	-17.4	0.8	-15.4	-23.1	-16.8	5.3	-1.4	-1.0
Na^{+}	68.7	333.6	1049.8	951.7	318.6	1110.0	994.3	493.1	1913.9	1837.0
K^{+}	1.9	23.5	81.9	73.9	21.1	81.9	73.9	27.8	114.5	109.8
HCO_3^{-}	183.1	106.8	-99.5	-71.2	103.7	-147.7	-110.0	118.9	-96.0	-84.4
Cl^{-}	20.5	88.3	271.6	246.5	87.6	300.1	269.0	111.3	415.3	398.8
$SO_4^{=}$	79.3	497.1	1626.7	1476.0	480.0	1748.9	1563.4	893.4	3618.9	3471.4
SiO_2	31.3	147.5	461.7	418.6	143.0	496.7	445.0	115.6	397.8	382.6
B	0.08	0.48	1.56	1.41	0.5	1.83	1.64	0.42	1.56	1.50
F^{-}	0.35	12.6	45.7	41.2	12.0	48.9	43.5	7.3	30.6	29.3

calculated deep reservoir chemistry, temperature is determined by the Na-K-Ca geothermometer. For R2 and R3 the alkali temperature agrees very closely with the independently determined silica-enthalpy mixing model temperature. However, for R4 the agreement is not satisfactory.

Comparison of the chemistry of sample P4 with that of samples P2 and P3 suggests that components may have been added to P4 after mixing. The large increases in Ca^{2+}, Mg^{2+}, Na^{+}, SO_4^{2-}, and Cl^{-} suggests that the additional components are due to dissolution of evaporite minerals. By considering an average of the compositions of P2 and P3 to represent the composition of P4 prior to the post-mixing addition of dissolved solids, the amount of material added to P4 can be determined. Table 7 presents the calculation and shows that a comparison of total cation equivalence to total anion equivalence supports the interpretation. The alkali temperature calculated from the corrected reservoir (R4') chemistry is 248°C, in very good agreement with the mixing model temperature of 241°C.

The negative values of Mg^{2+} and HCO_3^{-} in the mass balance of the reservoir composition require that the concentrations of Mg^{2+} and HCO_3^{-} are too low in the P-series mixed waters. The most likely explanation is that Mg^{2+} and HCO_3^{-} were lost in chemical reactions which led to the formation of mineral phases after mixing. As suggested in the section on water-rock interaction, formation of Mg-montmorillinite probably controls the Mg^{2+} and HCO_3^{-} concentration in the mixed water solutions.

Table 7

Post Mixing Composition Shift of P 4

	Cations				Anions		
	Ca^{++}	Mg^{++}	Na^{+}	K^{+}	HCO_3^{-}	Cl^{-}	$SO_4^{=}$
P 4	67 .3	5.3	493.1	27.8	118.9	111.3	893.4
$\frac{(P2+P3)}{2}$	22.6	0.65	326.1	22.3	105.3	88.0	488.6
Δ(ppm)	44.7	4.7	167.0	5.5	13.7	23.4	404.9
meq.	2.23	0.38	7.26	0.14	0.22	0.66	8.43
Σ Ion Eq.		10.0				9.3	

R4Q' Corrected:

4.52 1187.8 90.6 = 248°C (T Alkali)

THE GEOTHERMAL RESERVOIR

Physicochemical Environment

The general features of the physicochemical environment of the deep geothermal reservoir can be modeled by assuming chemical equilibrium in the model reservoir waters. The calculation of chemical equilibrium in natural aqueous systems is described in detail in Appendix 2. WATEQF, which was used to model chemical equilibrium in the low- to moderate-temperature waters which were actually sampled, is not applicable to the deep reservoir waters at 250°C or even to the mixed waters at 150°-170°C because the Van't Hoff approximation cannot be applied accurately over such a wide temperature range. However, one can apply the principles of chemical equilibrium in hand calculations to determine important parameters and use mineral stability diagrams to predict mineral phases which would be in equilibrium with waters of the calculated compositions. The physicochemical data in Table 8 are used to characterize the shallow water, mixed water, and deep reservoir water. The calculatations of the water chemistry, here presented in molality, have already been described. The other parameters in Table 8 are described below.

Charge Balance. The ratio of the sum of cation equivalence to the sum of anion equivalence provides a good measure of the charge balance of an aqueous solution. Since the solution must be electrically neutral, the ratio is also a measure of the completeness of the chemical analysis. The 7 to 9 percent excess of cation to anion is within analytical error limits and may not be real (see Appendix 1). If the imbalance is real, it is probably due to the removal of bicarbonate ion.

Table 8

Physicochemical Parameters

	Shallow Aquifer	Mixed Water			Geothermal Reservoir			
	P 1	P 2	P 3	P 4	R2Q	R3Q	R4Q	R4Q'
Water Chemistry: [molal x 10^3]:								
Ca^{++}	0.70	0.55	0.58	1.68	0.14	0.20	4.96	0.11
Mg^{++}	0.30	0.02	0.03	0.22	---	---	---	---
Na^{+}	2.99	14.51	13.86	21.45	45.67	48.28	83.25	51.67
K^{+}	0.05	0.60	0.54	0.71	2.09	2.09	2.93	2.32
Fe^{++}	0.02	0.00	0.01	0.02	---	---	---	---
F^{-}	0,02	0.66	0.63	0,38	2.41	2.57	1.61	2.75
HCO_3^{-}	3.00	1.75	1.70	1.95	---	---	---	---
Cl^{-}	0.58	2.49	2.47	3.14	7.66	8.46	11.71	8.85
$SO_4^{=}$	0.83	5.18	5.00	9.30	16.93	18.21	37.67	19.35
H_4SiO_4	0.05	2.45	2.38	1.92	7.68	8.27	6.62	8.77

Table 8 cont'd

	Shallow Aquifer	Mixed Water			Geothermal Reservoir			
	P 1	P 2	P 3	P 4	R2Q	R3Q	R4Q	R4Q'
Miscellaneous:								
ΣCation/ΣAnion	9.96	1.07	1.06	1.08	1.09	1.07	1.08	1.08
T°C	23	85	81	71	248	251	226	245
$\bar{I}$	0.007	0.022	0.021	0.036	0.063	0.068	0.135	0.072
-log f_{CO_2} 7)	3.34	2.38	2.40	1.36	1.23	0.73	-2.80	1.62
10)	2.74	1.42	1.71	1.23	-1.10	-1.11	-2.57	-0.88
pH calc.	8.3	7.7	6.9	7.1	7.4	7.1	4.7	7.4
obs.	8.2	7.7	8.2	7.8				
$\gamma_{H_2CO_3}$	1.27	1.22	1.22	1.23	1.34	1.34	1.28	1.33
γ^{+}_{-}	0.914	0.845	0.850	0.819	0.652	0.654	0.601	0.645
γ^{++}_{--}	0.715	0.548	0.557	0.497	0.235	0.231	0.196	0.233

Table 8 cont'd

	Shallow Aquifer	Mixed Water			Geothermal Reservoir			
	P 1	P 2	P 3	P 4	R2Q	R3Q	R4Q	R4Q'
Activitiy Co-ordinates:								
log $a_{H_4SiO_4}$	-4.18	-2.52	-2.54	-2.63	-1.99	-1.96	---	-1.93
log a_K/a_H	3.96	4.41	3.56	3.86	4.53	4.23	---	4.58
log a_{Na}/a_H	4.74	5.82	4.97	5.35	5.87	5.59	---	5.92
log a_{Ca}/a_H^+	13.30	11.88	10.31	11.12	10.32	9.87	---	10.21
log a_{Mg}/a_H^+	12.93	10.44	9.02	10.24	9.60	8.99	---	9.59

Ionic Strength. The ionic strength (I) of an electrolyte solution is defined to be

$$I = \frac{1}{2} \sum_i z_i^2 m_i,$$

where z_i is the charge and m_i is the molality of the ith species, respectively. The ionic strength of all the sample waters is given in Table 1. All of the solutions, including the calculated reservoir fluids, are weak electrolytes, for which activity coefficients can be calculated using Debye-Huckel theory.

Activity Coefficients. The activity coefficient for neutral (molecular) complexes are based on H_2CO_3 behavior and Henry's Law coefficients for NaCl solutions (Helgeson, 1969). Mean activity coefficients ($\gamma_{\pm}$) for ionic species are calculated from the Debye-Huckel equation and the MacInnes assumption for symmetrical solutions,

$$\log \gamma_{\pm} = \frac{A z_i^2 \sqrt{I}}{1 + Ba\sqrt{I}},$$

where $\gamma_{\pm}$ is the mean activity coefficient of the ith ionic species, z_i is the charge on the ith species, I is the ionic strength of the solution and A, B, and a are constants (Lewis and Randall, 1923). For ionic strengths less than 0.1, the mean activity coefficients for all singly (or doubly) charged ions or complexes are nearly identical (Latimer, 1952; Garrels and Christ, 1965). Values of A and B used to

calculate activities in Table 8 are from Helgeson (1967) and Helgeson and Kirkham (1974); the ion size, a, is from Klotz (1950).

P_{CO_2} and pH of Solution. CO_2 solubility and carbonate equilibria can be used to compute P_{CO_2} and pH values for the solutions. Table 9 lists the equilibrium solubility data for the carbonate system. Chemical equilibrium involving water, carbon dioxide, and calcium carbonate requires that the following relationships be true:

$$m_{CO_2} = B\, P_{CO_2}, \tag{7}$$

where m_{CO_2} is the molal concentration of carbon dioxide in aqueous solution, P_{CO_2} is the partial pressure of carbon dioxide, and B is the Henry's Law constant at the temperature of interest;

$$H_2CO_3 = H^+ + HCO_3^- \tag{8}$$

$$K_1 = \frac{a_{H^+} \cdot a_{HCO_3^-}}{a_{H_2CO_3}}, \tag{8a}$$

where K_1 is the first ionization constant of carbonic acid and a_i is the activity of the ith component;

$$HCO_3^- = H^+ + CO_3^{2-} \tag{9}$$

$$K_2 = \frac{a_{H^+} \cdot a_{CO_3^{2-}}}{a_{HCO_3^-}}, \tag{9a}$$

where K_2 is the second ionization constant of carbonic acid;

Table 9

Equilibrium and Solubility Constants

T°C	p K_B [1]	p K_1 [2]	p K_2 [2]	p K_c [3]
0	1.11	6.58	10.62	8.340
20	1.41	6.38	10.38	8.385
25	1.46	6.35	10.33	8.40
50	1.70	6.31	10.17	8.62
60	1.78	6.32	10.15	8.74
100	1.97	6.45	10.16	9.39
150	2.07	6.73	10.29	10.25
200	2.06	7.08	10.68	11.37
250	1.98	7.63	11.43	12.72
300	1.83	8.86	13.38	14.0

[1] Harned and Davis (1943)

[2] Garrels and Christ (1965)

[3] Langmuir (1971)

and

$$CaCO_3 = Ca^{2+} + CO_3^{2-} \tag{10}$$

$$K_c = a_{Ca^{2+}} \cdot a_{CO_3^{2-}} , \tag{10a}$$

where K_c is the solubility product for calcite.

Further, for the system containing only H_2O, CO_2, and $CaCO_3$, the condition of electroneutrality of the solution requires that

$$2m_{Ca^{2+}} + m_{H^+} = m_{HCO_3^-} + 2m_{CO_3^{2-}} + m_{OH^-} . \tag{11}$$

For most natural waters $2m_{Ca^{2+}} >> m_{h^+}$ and $m_{HCO_3^-} >> (2m_{CO_3^{2-}} + m_{OH})$. Equation (11) can then be rewritten

$$2m_{Ca^{2+}} = m_{HCO_3^-}. \tag{11a}$$

Using the definition that

$$a_i = \gamma_i m_i ,$$

where γ_i is the activity coefficient of the ith component, equation (7), equation (11a), and rewriting equation (10a) to give $m_{CO_3^{2-}} = (K_c/m_{Ca^{2+}})$, one can divide equation (8a) by equation (9a) to yield

$$\frac{K_1}{K_2} = \frac{4\, a^3_{Ca^{2+}}\, \gamma^2_{HCO_3^-}}{B\, P_{CO_2}\, K_c\, \gamma_{H_2CO_3}\, \gamma^2_{Ca^{2+}}} \tag{12}$$

or

$$P_{CO_2} = \frac{4\ K_2\ a^3_{Ca^{2+}}\ \gamma^2_{HCO_3^-}}{K_1\ K_c\ B\ \gamma_{H_2CO_3}\ \gamma^2_{Ca^{2+}}} \cdot \qquad (12a)$$

For systems which include silicates, sulfates or carbonates other than calcite, the condition for electroneutrality becomes

$$2m_{Ca^{2+}} + \sum_i z_i m_i = m_{HCO_3^-} + \sum_j z_j m_j, \qquad (13)$$

where $\sum_i z_i m_i$ is the sum of the charges, z_i, times the concentration, m_i, of all cations except Ca^{2+}, and $\sum_j z_j m_j$ is the sum of the charges, z_j, times the concentrations, m_j, of all anions except HCO_3^-. Rearranging equation (13)

$$2m_{Ca^{2+}} + (\sum_i z_i m_i - \sum_j z_j m_j) = m_{HCO_3^-} \cdot \qquad (13a)$$

Now, let $(\sum_i z_i m_i - \sum_j z_j m_j) = Q$. When $Q = 0$, equation (13a) reduces to equation (11a). Using equation (13a), equation (12a) can be rewritten

$$P_{CO_2} = \frac{K_2\ a_{Ca^{2+}}}{K_1\ K_c\ B\ _{H_2CO_3}} [(2a_{Ca^{2+}}\ \gamma_{HCO_3^-})(\gamma_{Ca^{2+}} + \gamma_{HCO_3^-} - Q)]^2 \qquad (14)$$

The P_{CO_2} values of the fluids in Table 8 are calculated using both equations (12a) and (14). The P_{CO_2} values calculated by WATEQF for the sample waters P1 to P4 agree quite closely with the values calculated on the basis of equation (12a). However, equation (14)

more correctly characterizes the composition of the true water system and should give more nearly correct values for P_{CO_2}.

The pH of a water which is saturated with respect to calcite can be calculated by combining equations (9a) and (10a),

$$a_{H^+} = \frac{K_2}{K_c} (a_{HCO_3^-} \cdot a_{Ca^{2+}}). \qquad (15)$$

The agreement between calculated and observed pH for the shallow aquifer and the mixed aquifer is excellent (Table 8). In samples P3 and P4 the slightly higher observed pH is undoubtedly due to loss of CO_2 from the solution before the pH was measured in the field.

Using thermodynamic data, one may construct chemical potential or activity diagrams which show the stability fields of mineral phases in terms of the ratios of activities of aqueous species (see Appendix 4). Computed activity ratios for the waters are plotted on the mineral stability diagrams. Temperatures of 25°C, 150°C, and 250°C were chosen to illustrate relationships at near-surface, mixed water, and deep reservoir conditions, respectively.

No completely convincing studies of alteration assemblages are possible without core samples from deep holes near the hot wells. The use of saturation indices or mineral stability diagrams can only demonstrate the reasonable mineral phases that would be in chemical equilibrium with the waters at the given temperatures. The fact that a water composition indicates "saturation" with respect to a given mineral or plots in the stability field of a mineral neither requires that the mineral be present nor gives any indication of the quantity

of the mineral that might be present. Kinetic relationships and components not treated in the calculations must also be considered. However, the calculations do lead to a model which can be tested by later studies.

Figure 19 is a plot of ($\log a_{K^+}/\log a_{H^+}$) and of ($\log a_{Na^+}/\log a_{H^+}$) against $\log a_{H_4SiO_4}$ on which water compositions with different "best estimate" temperatures have been plotted. There is a clear trend in the data with increasing temperature, indicating that the solutions have changed composition as a function of temperature.

The mineral with which the waters are in chemical equilibrium are also temperature dependent for given compositions. Figures 20 to 22 are mineral stability diagrams (Helgeson and others, 1969) on which the water compositions for the appropriate temperatures have been plotted. Figure 20, for the systems $HCl\text{-}H_2O\text{-}Al_2O_3\text{-}K_2O\text{-}Na_2O\text{-}SiO_2$ at 25°C, indicates that the shallow, cool groundwaters are in equilibrium with kaolinte. Figure 21, for the system $HCl\text{-}H_2O\text{-}Al_2O_3\text{-}K_2O\text{-}Na_2\text{-}SiO_2$ at 150°C and 250°C, shows that Na-montmorillonite is the expected alteration phase in the mixed water region, but that the deep reservoir waters would be in equilibrium with alkali feldspar, probably albite. Figure 22, for the system $HCl\text{-}H_2O\text{-}Al_2O_3\text{-}MgO\text{-}Na_2O\text{-}SiO_2$ at 150°C and 250°C, shows that Mg-montmorillonite and Mg-chlorite are likely phases in the mixed water region, and that Mg-chlorite would be the stable phase in the deep reservoir rocks. This result is consistent with the qualitative argument presented above for the indicated removal of Mg^{2+} and HCO_3^- from solution. As discussed above, all the sampled waters are saturated with respect to calcite. Therefore, at the higher

Figure 19. Plots of (log a_{K^+}/log a_{H^+}) and (log a_{Na^+}/log a_{H^+}) versus log $a_{H_4SiO_4}$ for representative water samples and for calculated geothermal reservoir waters R2, R3, and R4. Temperature groupings are based on best estimate temperatures listed in Table 3.

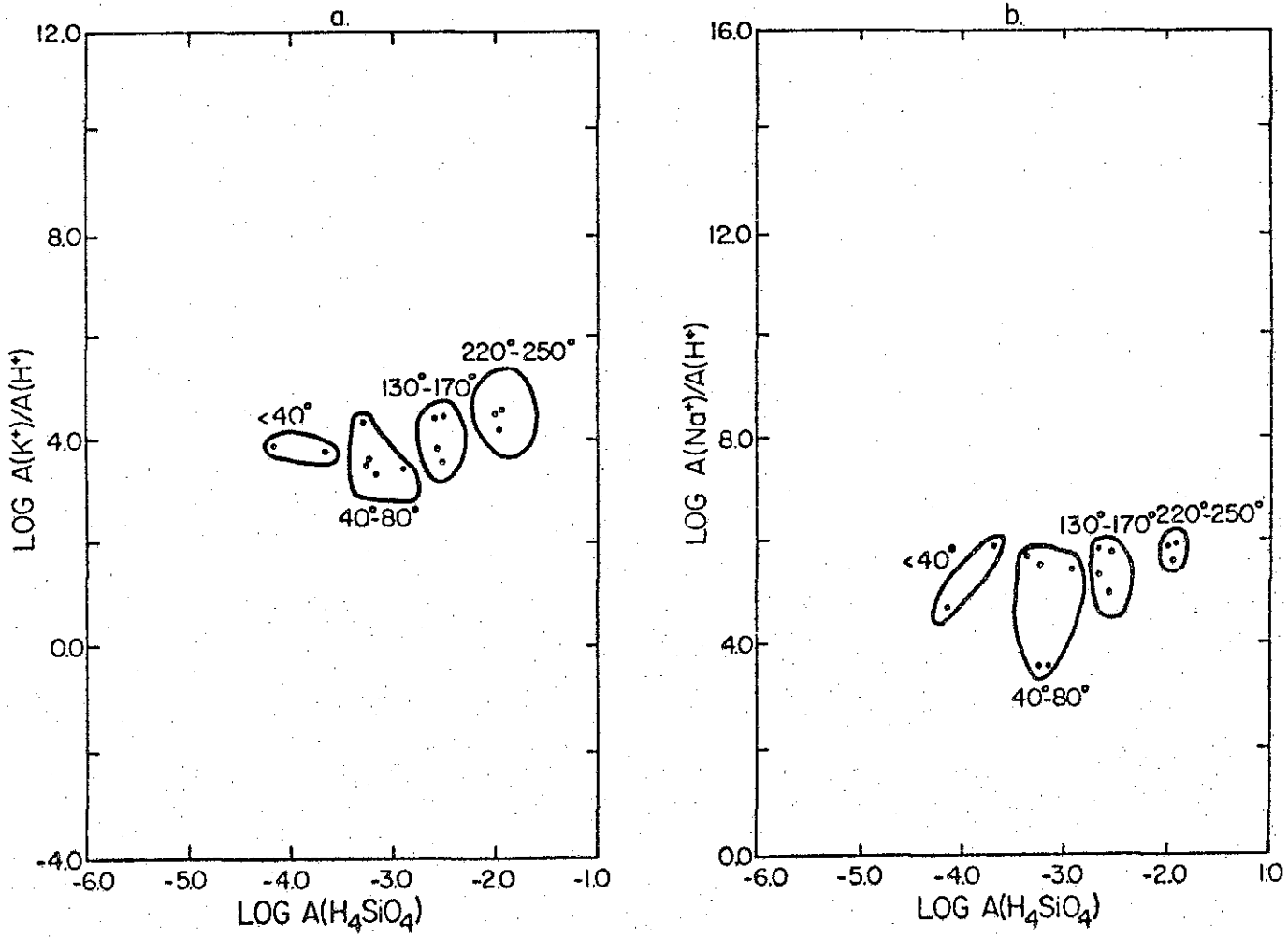
a.
12.0
8.0
4.0
0.0
-4.0
LOG A(K+)/A(H+)
<40°
40°-80°
130°-170°
220°-250°
-6.0
-5.0
-4.0
-3.0
-2.0
-1.0
LOG A(H4SiO4)
b.
16.0
12.0
8.0
4.0
0.0
LOG A(Na+)/A(H+)
<40°
40°-80°
130°-170°
220°-250°
-6.0
-5.0
-4.0
-3.0
-2.0
1.0
LOG A(H4SiO4)

Figure 20. Composition of low-temperature sample waters plotted on the mineral stability diagram for the system HCl-H_2O-Al_2O_3-K_2O-Na_2O-SiO_2 at 25°C and log $a_{H_4SiO_4}$ = -4.00 = quartz saturation (phase boundaries after Helgeson and others, 1969). All P-series values are plotted, but only selected An-series and LD-series values are plotted to avoid clutter.

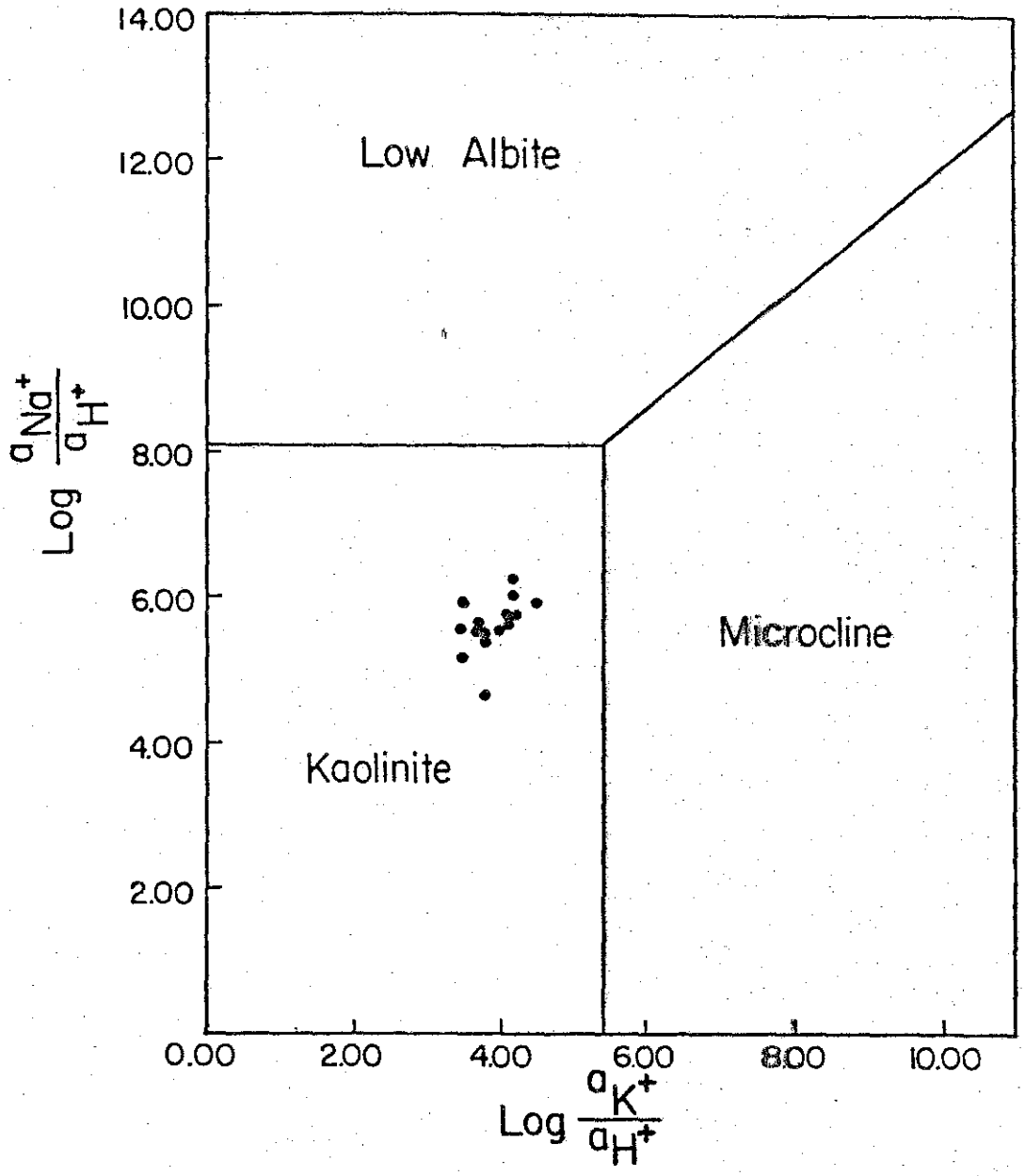
14.00
12.00
10.00
8.00
6.00
4.00
2.00
Low Albite
Microcline
Kaolinite
0.00
2.00
4.00
6.00
8.00
10.00
Log $\frac{a_{Na^+}}{a_{H^+}}$
Log $\frac{a_{K^+}}{a_{H^+}}$

Figure 21. a. Compositions of hot well samples P2, P3, and P4 plotted on the mineral stability diagram for the system HCl-H_2O-Al_2O_3-MgO-Na_2O-SiO_2 at 150°C and log $a_{H_4SiO_4}$ = -2.67 = quartz saturation (phase boundaries after Helgeson and others, 1969).

Figure 21. b. Compositions of geothermal reservoir waters R2, R3, and R4 plotted on the mineral stability diagram for the system HCl-H_2O-Al_2O_3-MgO-Na_2O-SiO_2 at 250°C and log $a_{H_4SiO_4}$ = -2.11 = quartz saturation (phase boundaries after Helgeson and others, 1969).

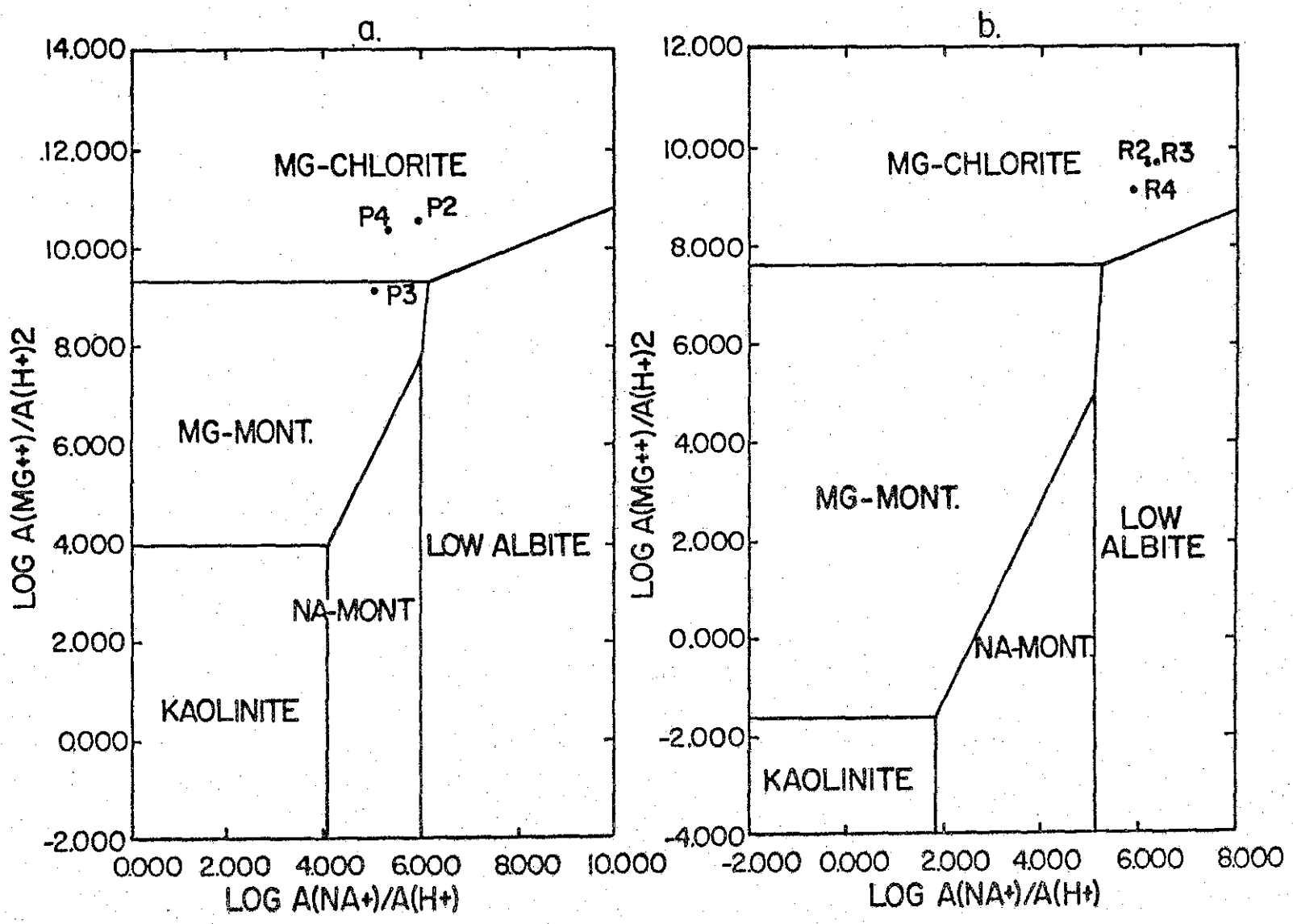
a.
14.000
12.000
10.000
8.000
6.000
4.000
2.000
0.000
-2.000
MG-CHLORITE
P4
P2
P3
MG-MONT.
LOW ALBITE
NA-MONT
KAOLINITE
0.000 2.000 4.000 6.000 8.000 10.000
LOG A(NA+)/A(H+)
LOG A(MG++)/A(H+)2
b.
12.000
10.000
8.000
6.000
4.000
2.000
0.000
-2.000
-4.000
MG-CHLORITE
R2, R3
R4
MG-MONT.
LOW ALBITE
NA-MONT
KAOLINITE
-2.000 0.000 2.000 4.000 6.000 8.000
LOG A(NA+)/A(H+)
LOG A(MG++)/A(H+)2

Figure 22 a. Compositions of hot well samples P2, P3, and P4 plotted on the mineral stability diagram for the system $HCl-H_2O-Al_2O_3-K_2O-Na_2O-SiO_2$ at 150°C and log $a_{H_4SiO_4}$ = -2.67 = quartz saturation (phase boundaries after Helgeson and others, 1969).

Figure 22. b. Compositions of calculated geothermal reservoir waters R2, R3, and R4 plotted on the mineral stability diagram for the system $HCl-H_2O-Al_2O_3-K_2O-Na_2O-SiO_2$ at 250°C and log $a_{H_4SiO_4}$ = -2.11 = quartz saturation (phase boundaries after Helgeson and others, (1969).

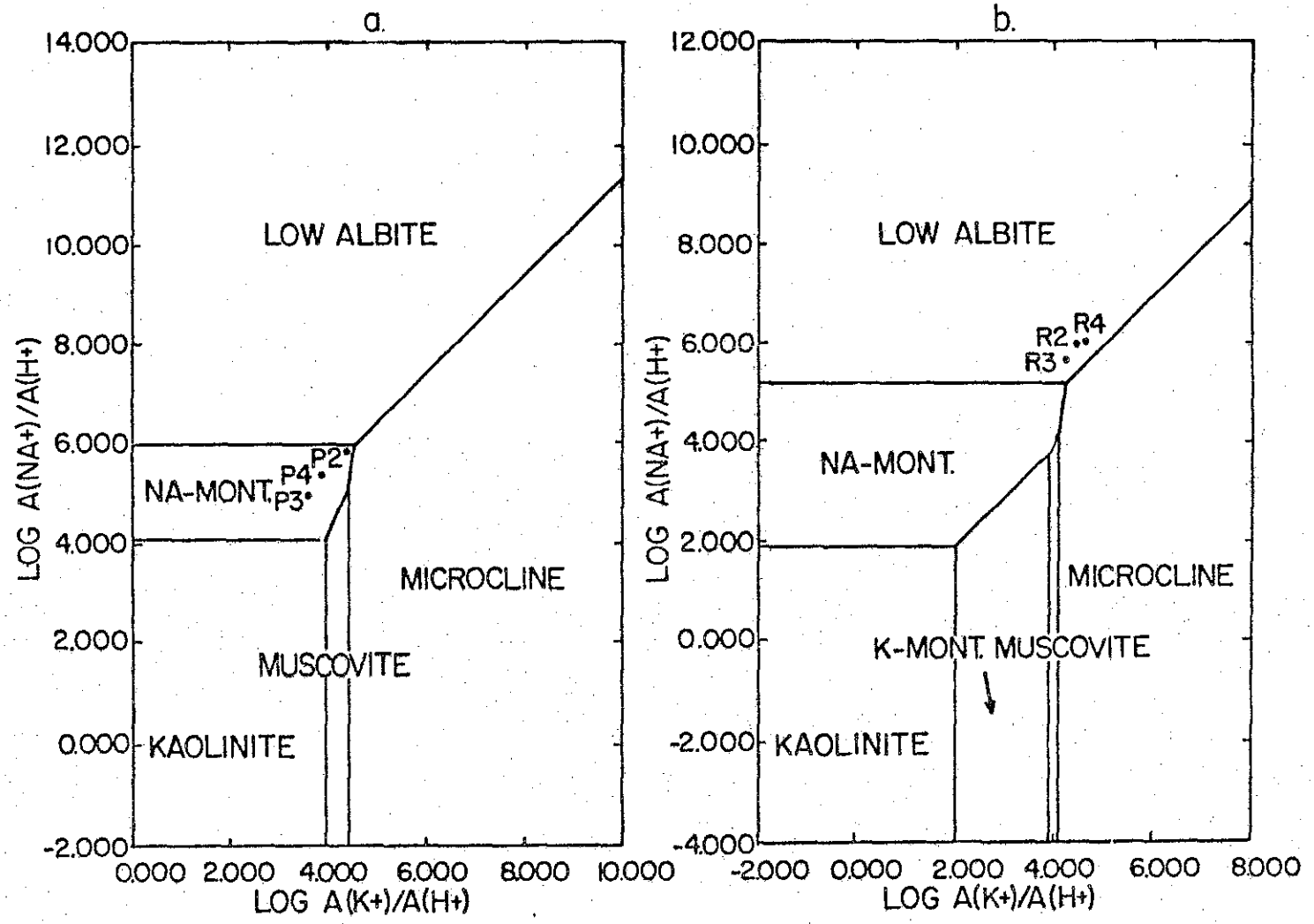
a.
14.000
12.000
10.000
8.000
6.000
4.000
2.000
0.000
-2.000
LOG A(NA+)/A(H+)
LOW ALBITE
NA-MONT.
P4
P3
P2
MICROCLINE
MUSCOVITE
KAOLINITE
0.000 2.000 4.000 6.000 8.000 10.000
LOG A(K+)/A(H+)
b.
12.000
10.000
8.000
6.000
4.000
2.000
0.000
-2.000
-4.000
LOG A(NA+)/A(H+)
LOW ALBITE
R2
R3
R4
NA-MONT.
MICROCLINE
K-MONT.
MUSCOVITE
KAOLINITE
-2.000 0.000 2.000 4.000 6.000 8.000
LOG A(K+)/A(H+)

temperature of the deep system, the waters will also be saturated with respect to calcite. Since the Ca^{2+}/Mg^{2+} ratio is too high to stabilize dolomite, a magnesian calcite is the probable carbonate phase. Although the low-temperature sample waters are undersaturated with respect to anhydrite, the deep waters are saturated with respect to anhydrite, because of the retrograde solubility of the calcium sulfate phases in the temperature range of the LIghtning Dock system.

Integrating the data of Table 4 and Figures 20 to 22, possible alteration phases in the Lightning Dock system include magnesian calcite, montmorillonite, illite, chlorite, zeolites, alkali feldspar, quartz, chalcedony, anhydrite, fluorite, and iron oxides and sulfides. This assemblage is similar to that at the geothermal fields of the New Zealand volcanic zone, particuarly Wairakei (Browne, 1978). Figure 23, after Ellis and Mahon (1977), shows the calculated trend of pH with temperature for three salinities. The measured values and calculated ranges of pH for several explored geothermal systems are shown on the diagram. At 250°C and pH = 7.2, calculated for the deep reservoir at Lightning Dock, the diagram indicates an expected total alkali concentration of 0.01 molal, in reasonably good agreement with the 0.05 value of the calculated Lightning Dock reservoir. Alternatively, the alkali equilibrium at 250°C indicates a reservoir pH of 6.8. The Lightning Dock reservoir limits are plotted on Figure 23 to emphasize the chemical similarity of the system to explored systems of the New Zealand volcanic zone.

Figure 23. Calculated trends of pH with temperature for waters of three salinities (M_a), where $M_a = m_{Na^+} + m_{K^+}$. Open circles and the closed triangles show the pH of waters in several geothermal systems, and the connected arrowheads indicate the pH range calculated for the salinity of the waters. SS: Salton Sea; R: Reykjanes: K: Kawerau; B: Broadlands; W: Wairakei, OL: Olkaria; WT: Waiotapu; OK: Orakeikoraku; LD: Lightning Dock (after Ellis and Mahon, 1977).

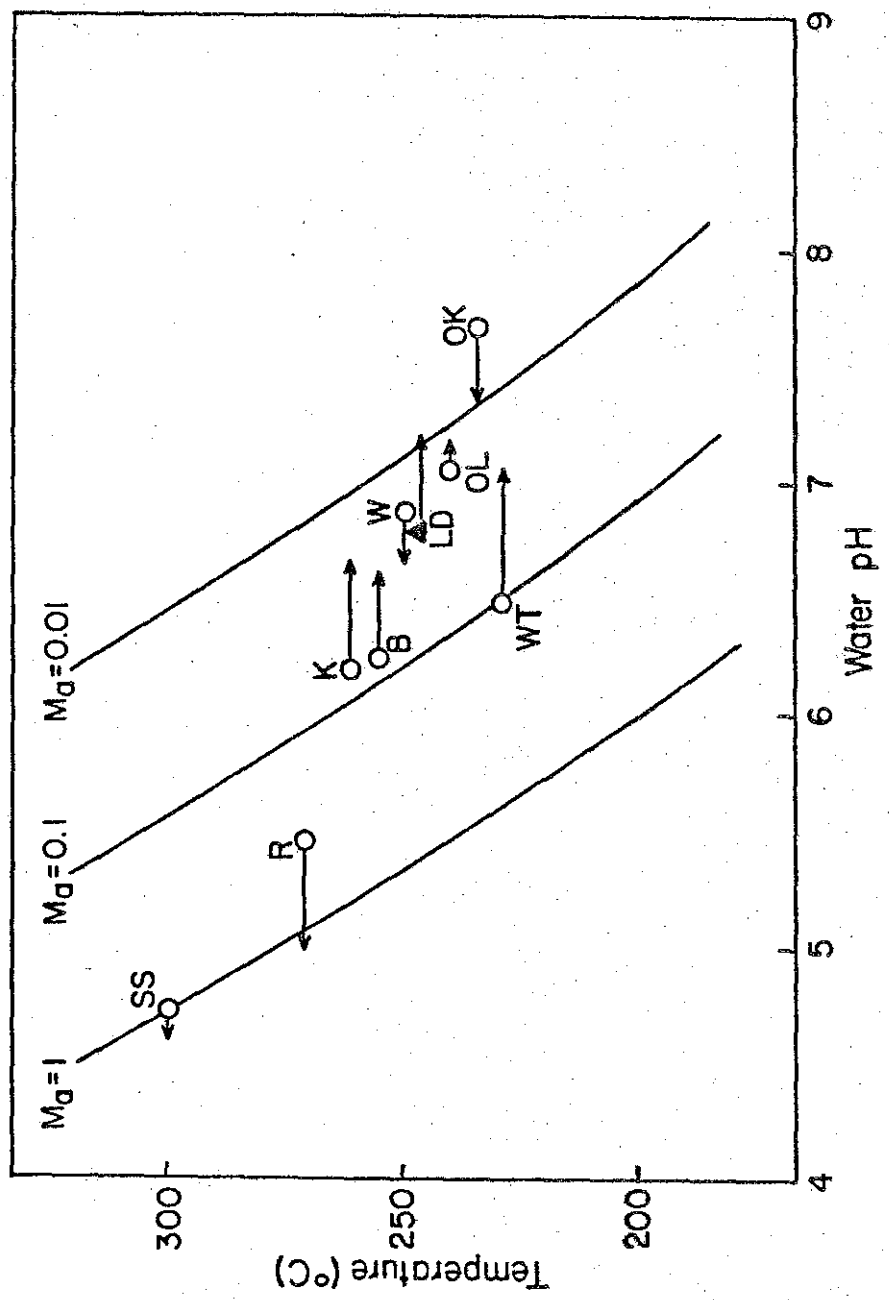
Temperature (°C)
300
250
200
Water pH
4
5
6
7
8
9
M_a=1
M_a=0.1
M_a=0.01
SS
R
K
B
W
LD
OL
OK
WT

Geometry and Hydrodynamics of the Geothermal System

Models of the Lightning Dock KGRA consider the geothermal reservoir to be situated more or less directly beneath the thermal anomaly of the hot wells (Jiracek and Smith, 1976; Smith, 1978). This interpretation of the geometry of the geothermal system is based on a model that the 5 Ω-m isopleth electrical resistivity map represents a conduit-like structure up which the geothermal fluids are ascending from the presumed reservoir. The conduit is presumed to be formed by the intersection of the ring fracture margin of the Muir cauldron with recently active Basin-and-Range faulting.

However, the linear trend in the geochemical isopleth diagrams of Figures 9, 10, and 15 to 17 indicate that this interpretation is too simple. All the wells southwest of the hot wells are hydrologically up gradient from the thermal anomaly. Since their waters show the geochemical signature of deep reservoir water, the main geothermal reservoir must be located southwest of the hot wells.

Gravity and electrical resistivity data, summarized in Figure 24, show anomalies which coincide very closely with the linear trend seen in the geochemical isopleths. The structure responsible for the northeast-trending geophysical anomalies is probably a high-angle fault or fault system. The trace of this fault or fault system intersects very young, perhaps even active, high-angle faults southwest of the hot wells along the western margin of the valley (S. G. Wells, personal communication, 1980). The buried fault in the valley would provide a suitable structure up which small amounts of the deep reservoir fluid could leak into the shallow aquifers which are sampled by the wells southwest of the hot wells. Since the Animas Valley Fault

Figure 24. a. Total field apparent resistivity map of the Lightning Dock KGRA (after Jiracek, in Callender, 1981).

Figure 24. b. Simple Bouguer anomaly gravity map of the Lightning Dock KGRA and vicinity (after Jiracek, in Callender, 1981).

a

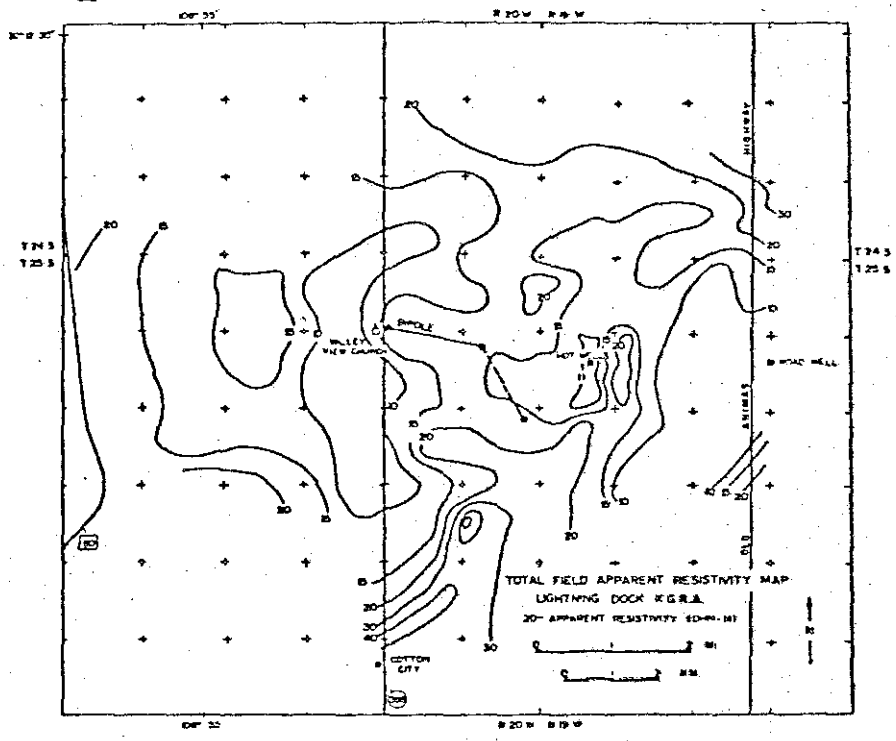
TOTAL FIELD APPARENT RESISTIVITY MAP
LIGHTNING DOCK K.G.R.A.
20m APPARENT RESISTIVITY CONTOURS
COTTON CITY
HIGHWAY

b

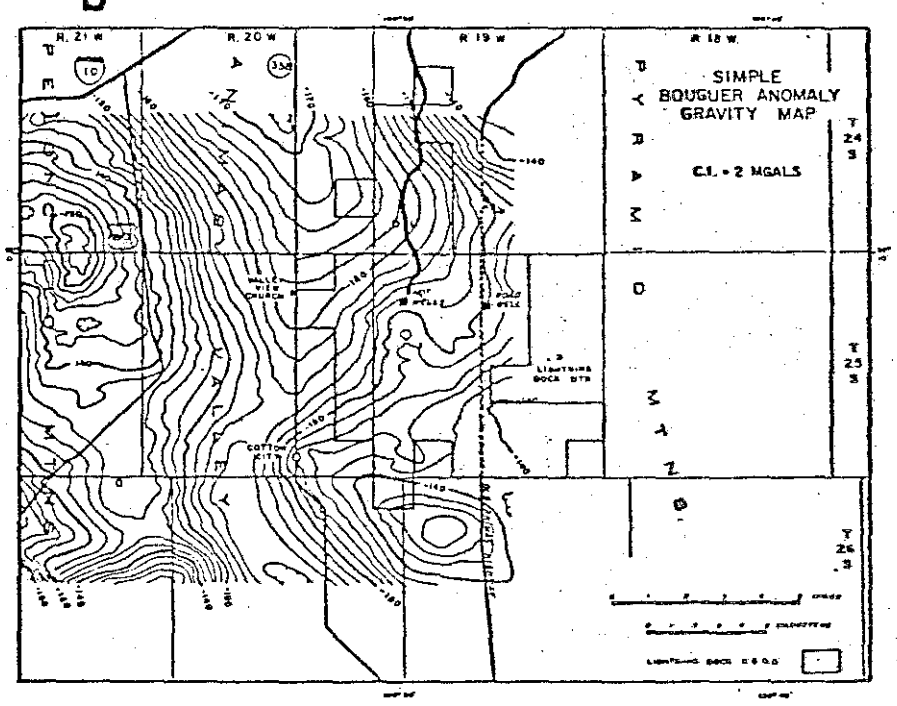
R. 21 W.
R. 20 W.
R 19 W.
R 18 W.
SIMPLE
BOUGUER ANOMALY
GRAVITY MAP
C.I. = 2 MGALS
COTTON CITY
LIGHTNING DOCK DTR

is roughly coincident with the ring fracture zone over a considerable distance (Fig. 2), the hypothesized northeast-trending fault also explains the precise location of the thermal anomaly: the permeable conduit outlined by the 5 Ω-m isopleth is formed by the intersection of two major fault systems with the margin of the ring fracture zone.

The trace of the hypothetical fault intersects the basalt flow west of the village of Animas and is along the trend of the basaltic volcanism which extends from southeastern Arizona into southwestern New Mexico (Fig. 1). While the 140,000-year-old Quaternary flow on the west side of the Animas Valley is too old to be the source of the heat for the Lightning Dock system, the coincidence of trends suggests that the heat source for the deep reservoir geothermal fluid is deep-seated basalt on the liquidus.

A geothermal system which consists entirely of meteoric water in permeable rock must be in a state of forced convection. Cold high-density water infiltrates along the boundaries of the system and circulates downward along interconnected channels to regions of higher temperature at depth. Hot, lower density water at depth rises through the permeable channels in the rock, to be replaced by the cooler, denser water entering the system. Figure 25 illustrates a simple high-temperature liquid geothermal system.

The subsurface flow paths in the Lightning Dock geothermal system must be much more complex than those shown in Figure 25. Geophysical modeling of the electrical resistivity data shows that the body of hot water below the thermal anomaly is located in volcanic rocks of the ring fracture zone of the Muir cauldron (Jiracek and Smith, 1976;

Figure 25. Simple high-temperature hot-spring system with deeply circulating meteoric water assumed to be heated entirely by conduction (after White, 1968).

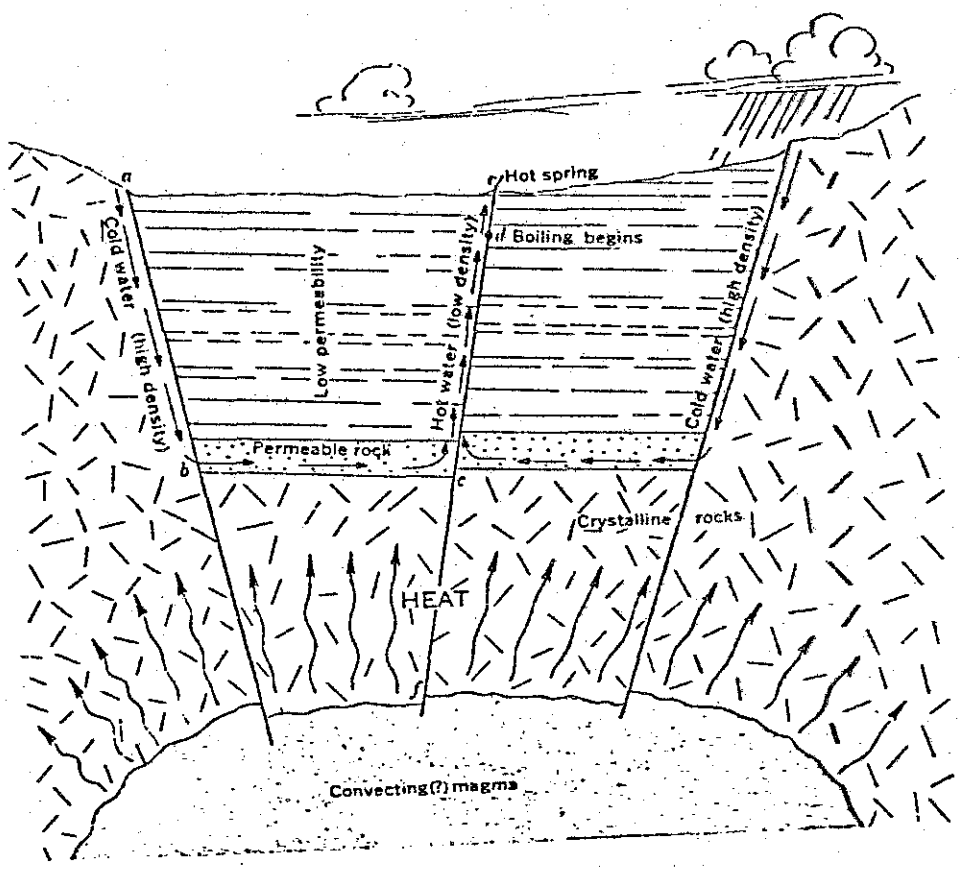
a
Cold water (high density)
Low permeability
Hot water (low density)
Hot spring
Boiling begins
Cold water (high density)
Permeable rock
b
c
Crystalline rocks
HEAT
Convecting(?) magma

Smith, 1978). One-dimensional modeling of a magneto-telluric survey indicates that there is a second, deeper reservoir (Jiracek, in Callender, 1981). The magneto-telluric results are equally consistent with the existence of the high-temperature reservoir to the southwest of the hot wells at a depth that again would place the reservoir below the valley-fill sediments. Figure 26 is probably a more realistic cross-sectional view of the circulation system in the lower Animas Valley than is Figure 25.

Permeabilities of small specimens of the volcanic rocks in this area are probably very low. However, the bulk permeability of the fractured rock may be exceptionally high. Measured permeabilities on fractured welded tuffs from the Nevada Test Site, similar in lithology and tectonic setting to the Animas Valley samples, range from 5,000 to 30,000 millidarcies (Sorey and others, 1978). Field observations and the hydraulic behavior of shallow wells along the western margin of the valley indicate that, at least locally, even the shallow bolson fill has significant fracture permeability (S. G. Wells, personal communication, 1980). Even if the permeability of the rock decreases with depth, decreased density due to thermal expansion of the fluid, decreased viscosity of the hot water, and high-temperature dissolution of silica tend to counterbalance the decreasing permeability. Although the true intrinsic permeability of the crystalline reservoir rocks is not known, the permeabilities are probably sufficient to permit the movement of large volumes of water.

The driving force of a geothermal system is related to two separate factors: (1) differences in altitude between recharge and

Figure 26. Diagrammatic representation of a thermal-spring system largely in fractured crystalline rocks. Permeability decreases downward but is more than offset by decrease in viscosity and increase in driving force related to thermal expansion (after White, 1968).

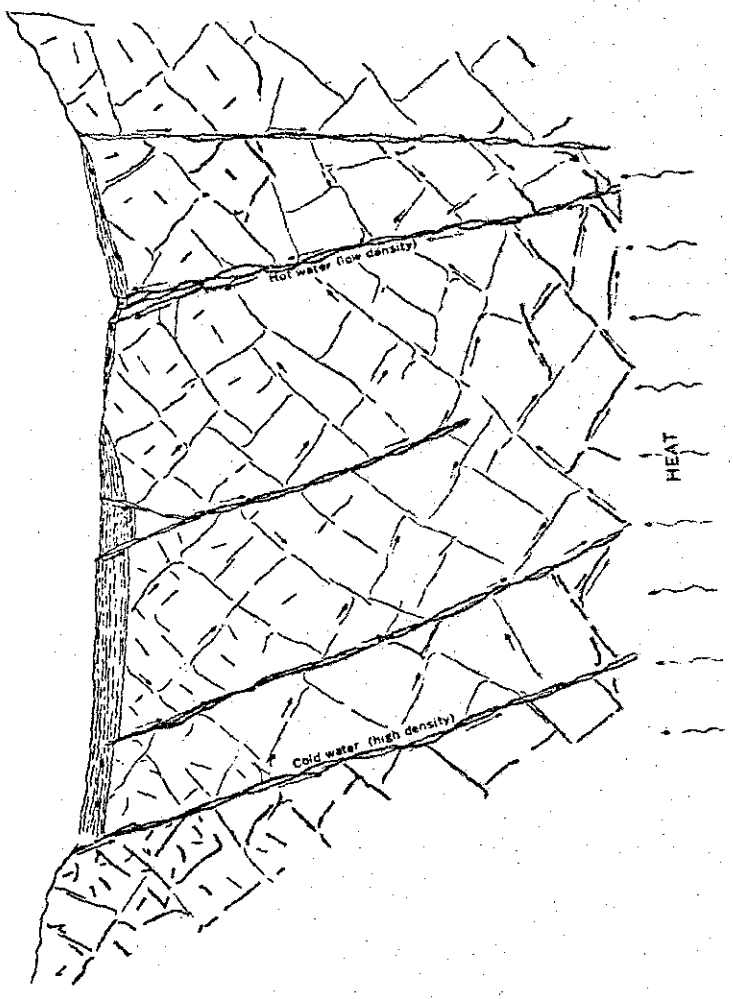
Hot water (low density)
HEAT
Cold water (high density)

discharge areas, and (2) differences in density between the cold, downflowing and the hot, upflowing parts of the system. Groundwater hydrology of the Animas Valley suggests that there is relatively little recharge to the valley at any given point from the immediately adjacent flanking ranges (Reeder, 1957). Therefore, the maximum elevation difference which can affect the recharge in the vicinity of the geothermal system is the difference of approximately 250 m in elevation between the southern end of the San Luis Valley near the Mexican Border and the hot wells. The true recharge is a value integrated over the large area of the valley and the extremely low downward flow required by the recharge rate of 2.5 mm/yr and the condition of steady flow (Reeder, 1957). Therefore, the effective head of cold water is substantially lower than the maximum, probably much closer to 50 m, equivalent to a pressure drive of 500 Pa.

If the downward-flowing cold water in the system is assumed to have an average temperature of 45°C and a density of 0.99, and the upward flowing hot water has a temperature of 250°C and a density of 0.79, the pressure drive related to thermal expansion is equivalent to approximately 200 m of cold water for each 1000 m of depth assumed for the temperature and density difference. For a geothermal reservoir at 1.5 km from which 250°C water rises to a mixing level at 0.5 km and then continues to rise at approximately 150°C, the driving force related to thermal expansion is in the range of 2000-2500 Pa.

These computations are crude, but they indicate that upward flow of water is apt to be much faster than downward flow of cold water and that the principal driving force in the geothermal system at

Lightning Dock is probably related to density differences between the upward-flowing hot water and the downward-flowing cold water. Modeling the true hydrodynamic system of the lower Animas Valley would require detailed information on temperatures and temperature gradients, pressures, salinities, proportions of vapor phase in the system, distribution of permeability, true rates of downflow, and a mathematical model sophisticated enough to treat the system accurately. Such modeling is well beyond the scope of this study.

Figure 27 is a schematic block diagram which shows a hypothetical three-dimensional model of the geothermal system in the lower Animas Valley. The deep geothermal reservoir, containing hot water at approximately 250°C, is located in fractured volcanic rocks at approximately 1.5 km depth about 15 km southwest of the hot wells. The source of the heat is basalt on or near the liquidus. The reservoir is intersected by a northeast-trending high-angle fault system, along which small volumes of the convecting hot water rise and leak into shallow aquifers sampled by irrigation and domestic wells. Where the northeast-trending fault intersects the margin of the Muir Cauldron ring-fracture zone and a north-trending Basin and Range fault, a highly permeable conduit is formed, up which relatively large volumes of hot water move to a zone of mixing at perhaps 0.5 km. In this zone 250°C water mixes with cold groundwater in a ratio of approximately 1 part hot water to 3 parts cold water to produce a mixed water of 150°C-170°C. The mixed water continues to rise along a structurally-controlled high-permeability conduit until it reaches the near surface aquifer, where it is sampled at the hot wells. In this shallow aquifer more mixing occurs, dispersing heat and deep-water chemical

Figure 27. Schematic block diagram of the geothermal system in the lower Animas Valley. In this model the location of the hot wells is structurally controlled by the intersection of two major high angle faults and the margin of the ring fracture zone of the Oligocene Muir cauldron.

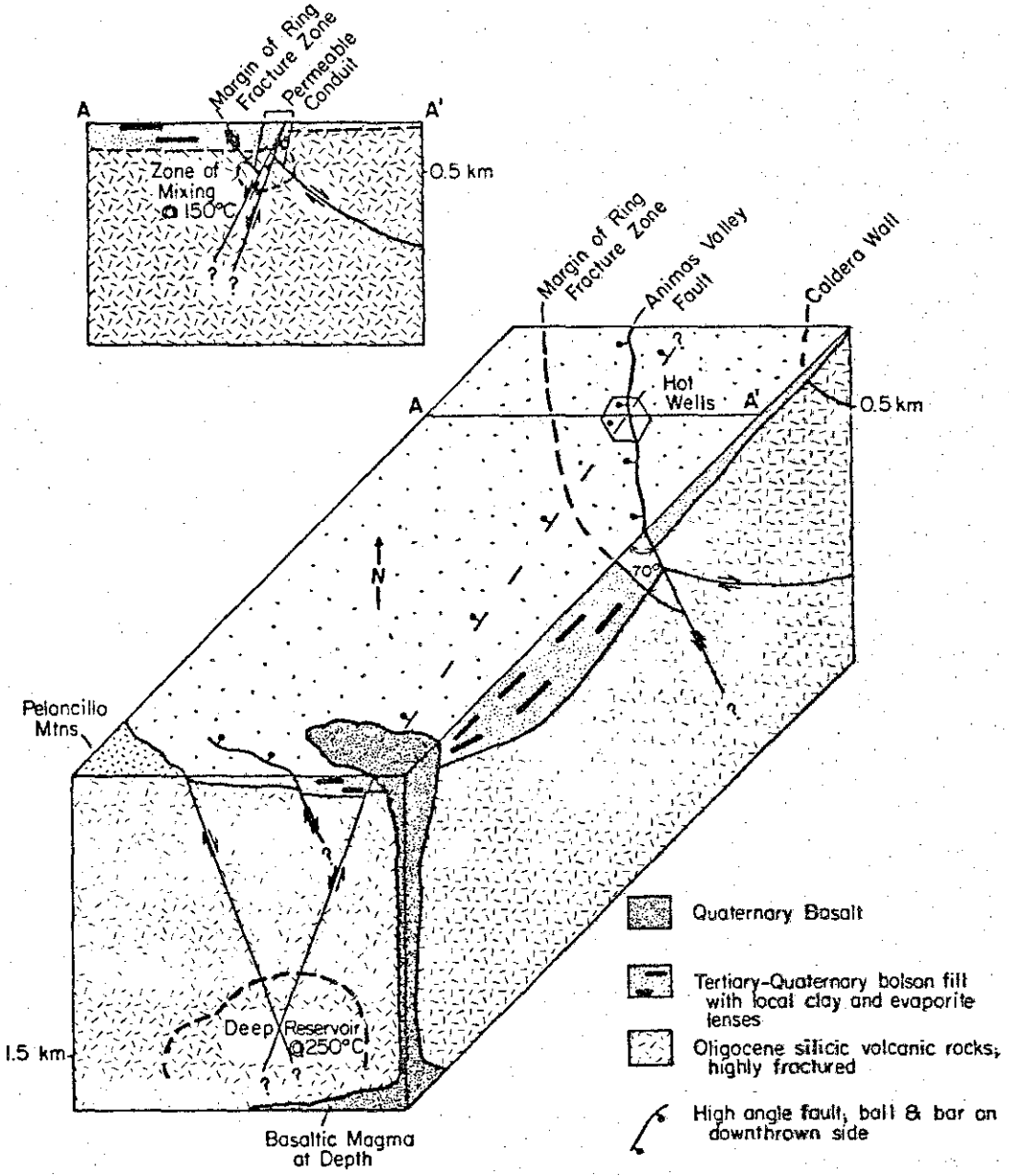
Margin of Ring Fracture Zone
Permeable Conduit
A
A'
Zone of Mixing @ 150°C
0.5 km
Margin of Ring Fracture Zone
Animas Valley Fault
Caldera Wall
Hot Wells
A
A'
0.5 km
N
70°
Peloncillo Mtns
Deep Reservoir @250°C
1.5 km
Basaltic Magma at Depth
Quaternary Basalt
Tertiary-Quaternary bolson fill with local clay and evaporite lenses
Oligocene silicic volcanic rocks, highly fractured
High angle fault, ball & bar on downthrown side

constituents in the pattern seen by Kintzinger (1956) and in many of the figures of this study.

CONCLUSIONS

The waters of the Lightning Dock KGRA hot wells are mixed waters containing about 25 percent deep geothermal fluid at approximately 250°C. Though no thermal manifestation of the deep geothermal reservoir other than the hot wells is known, significant indications of structurally-controlled seepage of chemically distinct reservoir water into the shallow aquifer define a linear trend southwest of the hot wells. The deep water moves up and along a major northeast-trending fault or fault system from a reservoir located southwest of the hot wells, mixing with shallow, cold aquifer waters to produce the samples analyzed for this study. The heat source for the reservoir is probably basaltic magma.

The chemistry of the waters of the Animas Valley is produced by a variety of processes, including evporation and boiling, water-rock interactions at high temperature, and mixing of solutions, including low-temperature groundwaters which have been modified by the dissolution of playa evaporites. The calculated reservoir chemistry suggests that the alteration phases associated with the high-temperature waters could include magnesian calcite, Na- and Mg-montmorillonite, illite, Ca-zeolite, chlorite, alkali, feldspar, quartz, chalcedony, anhydrite, fluorite, and iron oxides and sulfides. The model proposed here can be tested by a drilling program to study alteration mineralogy and to test the physical model of a high-temperature geothermal reservoir southwest of the Lightning Dock KGRA.

APPENDIX 1

Chemical Analyses

Table A1.1 presents the locations of the 55 water samples from the Animas Valley and the adjacent Lordsburg and Playas Valleys used in this study. Tables A1.2-A1.5 list the analyzed chemistry of the samples. In all cases the values are in milligrams per kilogram of solution (parts per million). Table A1.6 lists the gram-formula-weight values used to convert mg/kg to molality. The values, taken from Castellan (1971) are consistent with the IUPAC values. Where meq/l values have been used in the thesis, the values were obtained using the calculated molalities, charges of the ions under consideration, and a solution density of 1.00. Table A1.7 presents whole rock chemical analyses of representative samples from the Oliogcene Muir Cauldron complex of the Pyramid Mountains. Values are in weight percent.

The water chemistry was analyzed at the New Mexico Soil and Water Laboratory, Department of Agronomy, New Mexico State University, under the supervision of Mr. A. L. Bristol. Analytical procedures and error limits are described in Table A1.8. The whole rock chemistry was analyzed in the Analytical Geochemistry Laboratory, Department of Geology, University of New Mexico, under the supervision of Mr. John Husler. Standard spectrophotometric, volumetric, and colorimetric techniques were used.

Table A1.1

Sample Locations of P- An- LD- Series

Sample No.	Latitude	Longitude	Sample No.	Latitude	Longitude
P 1	32° 8.7'N	108° 47.6'W	LD 15	31° 34.2'	108° 52.4'
P 2	32° 8.7'	108° 49.9'	LD 16	31° 37.3'	108° 54.3'
P 3	32° 8.9'	108° 49.9'	LD 17	31° 44.8'	108° 48.6'
P 4	32° 8.7'	108° 50.4'	LD 18	31° 52.9'	108° 48.0'
P 5	32° 8.1'	108° 50.9'	An 1	32° 11.7'	108° 52.2'
P 10	32° 13.6'	108° 49.7'	An 2	32° 12.2'	108° 48.8'
P 13	32° 13.7'	108° 52.4'	An 3	32° 10.1'	108° 52.8'
P 14	32° 10.1'	108° 52.8'	An 4	32° 9.7'	108° 50.7'
P 15	32° 6.1'	108° 50.7'	An 5	32° 8.1'	108° 50.9'
P 20	32° 4.8'	108° 54.0'	An 6	32° 7.3'	108° 51.2'
P 22	32° 4.1'	108° 52.9'	An 7	32° 6.3'	108° 50.8'
P 23	32° 12.2'	108° 48.8'	An 8	32° 7.7'	108° 53.2'
P 24	32° 10.9'	108° 50.7'	An 9	32° 4.8'	108° 52.8'
P 25	32° 9.1'	108° 52.8'	An 10	32° 3.5'	108° 53.5'

Table A1.1 cont'd

Sample No.	Latitude	Longitude	Sample No.	Latitude	Longitude
LD 1	32° 18.9'	108° 38.8'	An 11	32° 3.1'	108° 54.6'
LD 2	32° 13.7'	108° 30.7'	An 12	32° 4.7'	108° 54.0'
LD 3	32° 10.6'	108° 33.6'	An 13	32° 3.1'	108° 52.7'
LD 4	32° 3.9'	108° 34.5'	An 14	32° 2.7'	108° 55.0'
LD 5	31° 55.8'	108° 36.9'	An 15	32° 4.3'	108° 51.2'
LD 6	31° 57.0'	108° 48.5'	An 16	32° 3.6'	108° 53.3'
LD 7	31° 48.6'	108° 46.5'	An 17	32° 4.8'	108° 52.7'
LD 8	31° 50.0'	108° 52.5'	An 18	32° 5.6'	108° 52.2'
LD 9	31° 40.2'	108° 49.9'	An 19	32° 9.1'	108° 46.4'
LD 10	31° 35.8'	108° 52.2'	An 20	32° 5.2'	108° 53.6'
LD 11	31° 24.2'	108° 51.8'	An 21	32° 7.2'	108° 55.3'
LD 12	31° 23.2'	108° 54.9'	An 22	32° 6.3'	108° 51.7'
LD 13	31° 20.4'	108° 47.9'	An 23	32° 9.1'	108° 52.7'
LD 14	31° 28.0'	108° 50.4'			

Table A1.2

Analyses of Total Dissolved Solids, pH, Major Cations, and Major Anions of Samples

mg/kg

Sample	TDS	pH	Ca	Mg	Na	K	CO_3	HCO_3	Cl	SO_4
P 1	484	8.20	28.0	7.3	68.7	1.9	0	183.1	20.5	79.3
P 2	1,116	7.71	22.0	0.5	333.6	23.5	0	106.8	88.3	497.1
P 3	1,024	8.16	23.2	0.8	318.6	21.1	0	103.7	87.6	480.0
P 4	1,608	7.84	67.3	5.3	498.1	27.8	0	118.9	111.3	893.4
P 5	1,660	8.08	159.3	34.9	231.7	9.0	0	209.3	181.9	956.3
P 10	1,708	8.18	67.9	17.1	366.2	6.3	0	255.0	133.6	939.0
P 13	756	7.90	38.3	2.7	105.5	3.1	0	237.9	16.9	298.7
P 14	668	8.00	47.9	4.4	71.0	2.7	0	209.3	23.0	289.6
P 15	868	8.07	78.6	12.6	152.2	5.9	0	201.4	80.5	483.7
P 20	632	8.02	43.2	4.1	97.0	2.3	0	192.2	21.3	305.0
P 22	600	7.90	49.3	4.4	111.3	2.7	0	192.2	38.6	311.7
P 23	640	8.08	18.6	2.4	120.2	1.6	0	250.2	29.1	308.3
P 24	1,348	7.92	38.5	1.8	321.4	18.0	0	275.8	79.1	768.5

Table A1.2 cont'd

Sample	TDS	pH	Ca	Mg	Na	K	CO_3	HCO_3	Cl	SO_4
P 25	604	8.35	38.1	5.7	78.8	3.5	0	183.1	8.9	285.8
LD 1	564	8.09	7.6	1.4	143.2	5.9	0	234.3	27.6	93.7
LD 2	816	7.86	28.0	2.7	216.1	11.7	0	314.8	47.5	223.8
LD 3	740	7.48	117.4	18.7	98.6	10.2	0	218.4	116.6	181.5
LD 4	592	7.94	10.2	1.8	159.3	1.5	0	301.4	33.0	104.2
LD 5	796	7.82	15.6	1.3	234.5	5.5	0	400.3	50.7	154.6
LD 6	208	7.92	22.0	7.3	27.6	2.0	0	147.3	3.5	19.2
LD 7	208	7.82	40.3	4.9	15.2	2.0	0	156.2	2.5	4.3
LD 8	184	7.57	26.0	2.2	21.1	1.2	0	109.8	2.8	4.3
LD 9	176	7.39	21.0	3.2	6.2	4.5	0	65.9	0.7	33.6
LD 10	156	7.31	17.8	3.3	6.9	6.2	0	57.3	1.4	40.3
LD 11	200	7.74	16.5	4.8	35.8	5.1	0	173.3	1.4	3.8
LD 12	136	6.88	15.8	2.9	13.8	3.5	0	37.8	0.7	52.8
LD 13	132	7.00	8.2	1.7	15.2	2.7	0	22.0	1.4	40.3
LD 14	160	8.80	2.4	0.5	54.7	0.4	0	137.9	4.2	16.3

Table A1.2 cont'd

Sample	TDS	pH	Ca	Mg	Na	K	CO_3	HCO_3	Cl	SO_4
LD 15	212	8.11	27.6	3.2	16.3	3.1	0	124.4	1.0	13.4
LD 16	164	7.94	29.4	1.7	11.5	2.3	0	117.1	0.1	5.7
LD 17	168	8.06	21.2	0.7	12.9	1.5	0	98.8	0.1	9.1
LD 18	320	8.15	16.4	0.6	65.3	1.2	0	173.3	4.2	32.7
AN 1	300	7.88	26.2	2.2	54.0	2.0	0	151.3	7.1	42.7
AN 2	360	8.00	13.0	1.6	115.4	2.0	0	241.0	23.7	44.0
AN 3	380	8.29	39.7	3.8	66.9	2.7	0	207.4	15.6	64.8
AN 4	1,372	7.59	79.7	8.3	353.3	14.1	0	228.8	122.7	492.8
AN 5	1,184	7.82	122.0	25.3	178.6	8.2	0	172.1	144.3	351.9
AN 6	1,020	8.00	125.2	14.6	161.4	6.6	0	83.6	117.0	369.0
AN 7	624	7.52	60.5	9.7	134.3	4.3	0	195.2	68.1	167.0
AN 8	272	7.82	28.8	2.7	55.6	2.3	0	170.8	3.5	51.6
AN 9	384	7.85	19.8	4.7	98.2	3.1	0	81.1	59.2	107.3
AN 10	524	7.92	29.8	8.5	112.2	3.5	0	156.8	32.9	111.7
AN 11	688	7.68	81.8	9.1	110.6	4.3	0	202.0	38.3	198.6

Table A1.2 cont'd

Sample	TDS	pH	Ca	Mg	Na	K	CO_3	HCO_3	Cl	SO_4
AN 12	384	7.73	34.5	3.0	77.9	2.7	0	185.5	8.5	74.8
AN 13	420	8.26	25.0	1.8	103.4	3.9	0	167.8	27.3	84.1
AN 14	340	7.75	26.0	1.8	70.3	2.3	0	176.3	1.8	58.8
AN 15	240	7.93	18.2	2.5	49.6	2.0	0	139.1	6.5	38.4
AN 16	384	8.39	30.7	3.0	89.9	2.7	0	178.8	19.8	86.9
AN 17	524	8.17	30.7	5.7	129.2	7.0	0	237.4	29.4	113.3
AN 18	352	8.43	31.3	3.2	67.8	2.7	0	157.4	27.3	58.8
AN 19	675	8.33	81.0	23.5	74.5	2.7	0	181.8	42.5	197.0
AN 20	628	7.41	76.1	7.2	91.7	3.5	0	187.9	64.2	124.9
AN 21	404	8.27	39.9	6.3	74.5	3.5	0	186.7	9.6	88.5
AN 22	396	8.41	25.4	2.5	93.8	2.3	0	172.1	20.9	76.4
AN 23	384	8.44	22.0	2.1	53.4	2.0	0	148.0	2.1	51.6

Table A1.3

Analyses of Iron, Fluoride, Boron, Phosphorus, and Silica in Samples

	mg/kg				
Sample	Fe	F	B	P	SiO_2
P 1	1.10	.35	.08	.01	31.3
P 2	.20	12.6	.48	.02	147.5
P 3	.40	12.0	.50	.02	143.0
P 4	.83	7.25	.42	.01	115.6
P 5	<.10	3.55	.25	.01	42.3
P 10	.53	7.25	.51	.01	60.7
P 13	1.31	3.90	.10	.01	74.1
P 14	.16	.85	.06	.01	48.4
P 15	<.10	2.35	.18	.01	34.3
P 20	<.10	2.54	.10	.01	50.4
P 22	<.10	1.20	.06	.01	43.3
P 23	7.66	1.15	.12	.01	29.3
P 24	21.18	9.35	.50	.01	149.7
P 25	.36	3.55	.12	.01	34.3
LD 1	<.15	3.66	.46	0	33.52
LD 2	<.15	6.90	.46	.01	39.64
LD 3	<.15	.44	.32	.01	43.36
LD 4	.37	2.67	.50	.01	32.30
LD 5	<.15	7.11	.64	.01	47.15
LD 6	.62	.30	.12	.01	38.08
LD 7	4.70	.16	.12	.02	47.62
LD 8	6.39	1.34	.06	.01	45.23

Table A1.3 cont'd

Sample	Fe	F	B	P	SiO_2
LD 9	<.15	.12	.04	.14	47.62
LD 10	.56	.11	.04	.01	39.28
LD 11	5.77	1.12	.12	.01	52.37
LD 12	<.15	.18	.06	.01	35.68
LD 13	<.15	.14	.06	.01	39.28
LD 14	.56	.31	.10	.01	14.23
LD 15	1.49	.42	.08	.01	47.62
LD 16	.22	.22	.08	.01	41.65
LD 17	1.91	.16	.08	0	44.03
LD 18	.78	2.26	.12	0	42.85
AN 1	<.10	1.60	.12	.05	58.5
AN 2	14.3	.95	.17	.01	15.5
AN 3	14.92	.66	.02	.04	68.5
AN 4	<.10	2.85	.59	.01	97.5
AN 5	<.10	3.48	.18	.01	50.5
AN 6	74.58	1.98	.78	0	30.0
AN 7	1.73	2.28	.17	0	29.5
AN 8	3.01	1.14	.05	0	33.5
AN 9	47.69	.84	.01	0	.95
AN 10	8.54	.63	.02	0	37.5
AN 11	<.10	2.85	.19	0	44.5
AN 12	10.31	2.28	0	.01	45.0
AN 13	21.85	3.03	.12	.02	32.0
AN 14	<.10	3.45	.04	.01	44.0

Table A1.3 cont'd

Sample	Fe	F	B	P	SiO_2
AN 15	17.98	.63	0	0	30.0
AN 16	.29	1.32	0	.01	37.0
AN 17	<.10	4.02	.13	.01	30.0
AN 18	<.10	1.71	.18	.01	37.5
AN 19	3.63	not enough sample	.04	.01	40.0
AN 20	.68	.69	.05	0	49.5
AN 21	<.10	3.8.	.04	.01	37.5
AN 22	.83	2.16	.05	.01	32.5
AN 23	.65	.93	0	.01	37.0

Table A1.4

Analyses of Nitrogen Species, Nickel, Lead, Antimony, Selenium, Strontium, and Zinc in Samples

Sample	$NO_3^+NO_2$	Ni	Pb	Sb	Se	Sr	Zn
	mg/kg						
P 3	.66	<.03	.242	<.5	.006	.47	.10
LD 1	4.48	<.16	.005	<.5	.005	.03	<.02
LD 2	.19	<.16	.009	<.5	.009	.15	<.02
LD 3	42.65	<.16	.006	<.5	.016	.46	.21
LD 4	15.30	<.16	.006	<.5	.008	.07	.33
LD 5	15.02	<.16	.008	<.5	.010	.04	.05
LD 6	4.93	<.16	.001	<.5	<.002	.06	.13
LD 7	7.12	<.16	.039	<.5	<.002	.03	2.68
LD 8	22.75	<.16	.006	<.5	.002	.02	1.22
LD 9	9.77	<.16	.001	<.5	.002	<.02	<.02
LD 10	1.47	<.16	.001	<.5	<.002	.03	.20
LD 11	2.15	<.16	.004	<.5	<.002	<.02	.44
LD 12	0	<.16	.001	<.5	<.002	<.03	.04

Table A1.4 cont'd

Sample	$NO_3^+NO_2$	Ni	Pb	Sb	Se	Sr	Zn
LD 13	3.70	<.16	.001	<.5	.002	.02	.03
LD 14	3.59	<.16	.002	<.5	.003	.02	.17
LD 15	4.88	<.16	.002	<.5	<.002	.03	.73
LD 16	7.97	<.16	.001	<.5	<.002	.02	.21
LD 17	1.28	<.16	867.5	3.19	<.002	.03	.63
LD 18	7.53	<.16	.025	<.5	.002	.03	.17

Table A1.5

Analyses of Cadmium, Cobalt, Chromium, Copper, Mercury, Hydrogen Sulfide, Lithium, Manganese, Molybdenum, Ammonium, Silver, Aluminum, Arsenic, Barium, and Bromine in Samples

mg/kg

Sample	Cd	Co	Cr	Cu	Hg	H_2S	Li	Mn	Mo	NH_4	Ag	Al	As	Ba	Br
P 3	<.01	<.15	<.10	<.10	.0006	<.1	.64	.08	<.50	.30	<.03	<2.5	.019	<.70	.56
LD 1	<.02	<.14	<.1		<.0002	<.1	.14	<.05	<.5	<.05	<.06	<1.0	.012	<.20	.53
LD 2	<.02	<.14	<.1	<.10	<.0002	<.1	.31	<.05	<.5	<.05	<.06	<1.0	.017	<.20	.67
LD 3	<.02	<.14	<.1	<.10	.0002	<.1	.09	<.05	<.5	<.05	<.06	<1.0	.008	<.20	1.52
LD 4	<.02	<.14	<.1	<.10	<.0002	<.1	.13	<.05	<.5	<.05	<.06	<1.0	.018	<.20	.56
LD 5	<.02	<.14	<.14	<.10	<.0002	<.1	.23	<.05	<.5	<.05	<.06	<1.0	.017	<.20	.99
LD 6	<.02	<.14	<.1	<.10	.0002	<.1	.03	<.05	<.5	<.05	<.06	<1.0	.003	<.20	0
LD 7	<.02	<.14	<.1	.69	<.0002	<.1	<.02	<.05	<.5	<.05	<.06	<1.0	.003	<.20	.28
LD 8	<.02	<.14	<.1	<.10	<.0002	<.1	.02	<.05	<.5	<.05	<.06	<1.0	.005	<.20	.32
LD 9	<.02	<.14	<.1	<.10	<.0002	<.1	<.02	<.05	<.5	<.05	<.06	<1.0	.003	<.20	.0
LD 10	<.02	<.14	<.1	.11	<.0002	<.1	<.02	<.05	<.5	<.05	<.06	<1.0	.002	<.20	0
LD 11	<.02	<.14	<.1	<.10	<.0002	<.1	.02	<.05	<.5	<.05	<.06	<1.0	.006	<.20	.35
LD 12	<.02	<.14	<.1	<.10	<.0002	<.1	<.02	<.05	<.5	<.05	<.06	<1.0	.003	<.20	.12

Table A1.5 cont'd

Sample	Cd	Co	Cr	Cu	Hg	H_2S	Li	Mn	Mo	NH_4	Ag	Al	As	Ba	Br
LD 13	<.02	<.14	<.1	<.10	.0002	.10	<.02	<.05	<.5	<.05	<.06	<1.0	.017	<.20	.16
LD 14	<.02	<.14	<.1	<.10	.0004	<.1	<.02	<.05	<.5	<.05	<.06	<1.0	.004	<.20	.41
LD 15	<.02	<.14	<.1	<.10	.0006	.13	<.02	<.05	<.5	<.05	<.06	<1.0	.003	<.20	.23
LD 16	<.02	<.14	<.1	<.10	.0004	<.1	<.02	<.05	<.5	<.05	<.06	<1.0	.003	<.20	.25
LD 17	<.02	<.14	<.1	<.10	.0009	<.1	<.02	<.05	<.5	<.05	<.06	<1.0	.031	<.20	.23
LD 18	<.02	<.14	<.1	< .10	.0004	<.1	.11	<.05	<.5	<.05	<.06	<1.0	.007	<.20	.41

Table A1.6

Gram-Formula-Weights Used to Convert Analyzed Concentrations to Molality

Species	Gram-Formula-Weight*
Na	22.9898
K	39.102
Ca	40.08
Mg	24.312
SiO_2	60.0843
HCO_3	61.0173
Cl	35.453
SO_4	96.0616
B	10.811
Br	79.909
F	18.9984
P	30.9738
NO_3	62.0049
NO_2	46.0066
NH_4	19.0383
Fe	55.847
Mn	54.9380
Zn	65.37
Hg	200.59
Pb	207.19
Cu	63.54
As	74.9216

Table A1.6 cont'd

Species	Gram-Formula-Weight*
Sb	121.75
Li	6.939
Sr	87.62
Se	78.96
H_2S	34.0799

*GFW data from Castellan (1971).

Table A1.7

Whole Rock Chemistry of Samples from the Pyramid Mountains
weight percent

	W76-35[1]	W76-89[2]	W76-30[3]	W76-36[4]	W76-24[5]	W76-79[6]	W76-31[7]	W76-27[8]	W76-28[9]
SiO_2	73.59	68.87	59.66	58.96	50.77	51.78	64.40	72.59	66.97
Al_2O_3	12.75	15.25	16.38	16.00	14.25	14.50	15.80	14.45	14.80
Fe_2O_3	1.64	2.73	3.65	3.21	6.78	7.11	3.24	1.41	2.73
FeO	0.18	0.24	2.92	2.24	0.55	0.42	0.52	0.16	0.33
MgO	0.36	0.47	3.61	1.80	2.94	3.00	1.16	0.18	0.68
CaO	0.38	1.85	5.15	5.15	6.90	7.05	2.20	0.70	1.48
Na_2O	3.70	4.25	3.93	3.72	4.12	4.10	5.50	4.08	3.49
K_2O	4.74	4.70	2.62	2.36	2.05	1.98	3.96	5.10	6.49
H_2O^+	1.20	0.67	0.70	3.96	7.56	7.50	1.69	0.71	0.73
H_2O^-	0.67	0.22	0.36	0.42	0.59	0.49	0.17	0.14	0.18
TiO_2	0.28	0.57	0.96	0.90	1.20	1.15	0.75	0.30	0.50
P_2O_5	0.06	0.13	0.26	0.22	0.64	0.61	0.26	0.05	0.13
MnO	0.01	0.03	0.09	0.07	0.12	0.11	0.09	0.008	0.08

Table A1.7 cont'd

	W76-35[1]	W76-89[2]	W76-30[3]	W76-36[4]	W76-24[5]	W76-79[6]	W76-31[7]	W76-27[8]	W76-28[9]
SrO	0.01	0.02	0.05	0.04	0.02	0.03	0.04	0.01	0.02
Total	99.57	100.00	100.34	99.05	98.49	99.83	99.78	99.96	98.61

1. Rhyolite tuff of Woodhaul Canyon.
2. Tuff of Rattler Well.
3. Basaltic andesite of Rimrock Mountain Group.
4. Andesite of Holtcamp Canyon.
5. Andesite of Holtcamp Canyon.
6. "K basalt" of Lasky (1938) near Susie Mine.
7. Tuff of Graham Well.
8. Rhyolite of Pyramid Peak (flow member).
9. Rhyolite tuff of Rimrock Mountain Group.

Table A1.8

Summary of Analytical Techniques for Water Chemistry

Test	Procedure	Reference	Error Limit[a]
pH	Glass and Calomel reference electrode	1	4%
TDS	Evaporation and 105°C drying	2	2%
Hardness	EDTA titration	2	2%
Ca	Atomic absorption Spectrophotometry	1	5%
Mg	Atomic absorption Spectrophotometry	1	5%
Na	Atomic absorption Spectrophotometry	1	5%
K	Atomic absorption Spectrophotometry	1	5%
Cl	Potentiometric titration	2	1%
HCO_3	H_2SO_4 titration	2	2%
CO_3	H_2SO_4 titration	2	2%
SO_4	Nitrochromeazo titration	5	1%

Table A1.8 cont'd

Test	Procedure	Reference	Error Limit[a]
NO_3	Cd reduction	1	5%
NO_2	Diazonium color	1	5%
NH_4	Colorimetric	1	2%
P	Molybdo-blue and persulfate digestion	1	6%
B	Azo-methine-H	3	5%
SiO_2	Molybdate	1	5%
F	Ion selective electrode	1	3%
Metals I[b]	Atomic absorption spectro-photometry	1	5%
Metals II[c]	Atomic absorption spectro-photometry	1	5%
Metals III[d]	Atomic absorption spectro photometry	1	5%
Pb	Graphite furnace-AA	6	5%
Mo	Nitrous oxide-methylisobutl-ketone	6	5%

Table A1.8 cont'd

Test	Procedure	Reference	Error Limit[a]
H_2S	Ion selective electrode	5	N/A
Br	Bromide-phenol red	2	N/A

Notes: a) Error limits calculated from standardized test results as reported by A. L. Bristol (written communication, 1980).

b) Metals I -- Ag, Co, Cu, Fe, Li, Mn, Ni, Sb, Si, Sr, Zn.

c) Metals II -- Al, Ba, Cd.

d) Metals III -- As, Hg, Se

References:
1. Methods for Chemical Analysis of Water and Wastes: EPA, National Environmental Research Center, Cincinnati, OH, 1974.
2. Standard Methods for the Examination of Water and Waste-Water, 14th ed.: APHA-AWWA-WPCF, Washington, DC, 1976.
3. The Determination of Boron in Soil Extracts, Plant Materials, Composts, Manures, Water, and Nutrient Solutions: Benjamin Wolf, Soil Science and Plant Analysis, v. 2, pp 363-374, 1971.
4. Operators' Manual: Orion Research Inc., Cambridge, MA.
5. Nitrochromeazo Titrimetric Determination of Sulfate in Irrigation and Other Saline Waters: B. A. Rasnick and F. S. Nakayama, Communications in Soil Science and Plant Analysis, v. 4, pp 171-174, 1973.
6. A. L. Bristol, written communication, 1980.

APPENDIX 2

Calculating Chemical Equilibrium of Natural Waters

Introduction

The chemistry of water-rock interactions is determined in part by saturation of the solution with respect to solid phases or to gases at a certain pressure. The reaction states of an aqueous phase can be calculated from an equilibrium model of the water and from the stabilities of phases with which it may react. While an inorganic equilibrium model does not completely describe the processes in any natural water, much less a highly dynamic system such as an active geothermal system, the equilibrium model is a useful reference which can indicate processes which are impossible and suggest other processes which may control water compositions.

The practical calculation of multicomponent, multiphase equilibria requires the use of modern electronic computers. The computation of most of the physico-chemical parameters in this thesis was accomplished by using WATEQF, a FORTRAN IV computer program that models the thermodynamic speciation of inorganic ions and complexes in solution for a given water analysis (Plummer and others, 1978). As Nordstrom and others (1979) point out, the aqueous chemical model must be defined separately from the computer program which executes calculations based on the chemical model. The remainder of this appendix will be divided into two parts. Part I will consider the theoretical construction which allows one to predict the thermodynamic properties of natural waters. Part II will consider specific analytical approaches of WATEQF and critically examine the results of those approaches.

Part I: The Aqueous Chemical Model

The discussion of the chemical model closely follows that of Truesdell and Jones (1974), which, in turn, was strongly influenced by the approach of Garrels and Christ (1965) and Denbigh (1955). The simplest approach for a multicomponent aqueous solution is to assume the existence of inorganic complexes whose formation is described by mass-action expressions and to assume that the activity coefficients of simple ions and complexes is described by equations which depend only on temperature and ionic strength, a function of the water composition.

Mass-Action Equilibrium Equations. In a mixture at chemical equilibrium, the activities of the chemical species involved in reactions are related by a set of mass-action equations. Consider a generalized reaction

$$aA + bB = cC + dD, \qquad \text{(A2.1)}$$

where the lower-case letters are the stoichiometric coefficients of the chemical species represented by the upper-case letters. Then, there is a mass-action equation of the form;

$$K = \frac{[C]^c[D]^d}{[A]^a[B]^b}, \qquad \text{(A2.2)}$$

where K is the equilibrium constant for the reaction and the brackets represent activities or other appropriate concentration terms, such as partial pressures for low-pressure gases.

Activity Coefficients. In real solutions with more than a few components of finite concentration, one cannot assume that ionic activities approach ionic concentrations and that activity coefficients approach unity. In treating real solutions, one must use single-ion activities and single-ion activity coefficients, defined by the equation,

$$a_i = \gamma_i m_i, \tag{A2.3}$$

in which a_i, γ_i, and m_i are the activity, the activity coefficient, and the molality of the ith ion, respectively.

Because single-ion activities and single-ion activity, coefficients cannot be exactly measured or defined thermodynamically, WATEQF uses two nonthermodynamic models, the extended Debye-Hückel equation and the MacInnes assumption, to evaluate activity coefficients. The Debye-Hückel equation describes single-ion activity coefficients in dilute solutions; the MacInnes assumption describes activity coefficients at higher concentrations, the so-called mean salt activity coefficients, and permits fitting of the adjustable parameters of the extended Debye-Hückel equation.

By assuming that oppositely charged ions form a spherical shell around a given ion, the Debye-Hückel theory considers the effects of electrical interactions with the surrounding ions on the free energy of the given single ion. The single-ion activity coefficient can be expressed as

$$\log \gamma_{\pm} = - \frac{A z^2 \sqrt{I}}{1 + Ba \sqrt{I}} + b I, \qquad (A1.4)$$

where A and B for a given solution are constants which depend only on the dielectric constant, the density, and the absolute temperature, z is the ionic charge, I is the ionic strength ($\frac{1}{2} \Sigma z_i^2 m_i$), a is a parameter related to the hydrated ion size, and b is a parameter which treats the effect of the decrease of the concentration of the solvent in concentrated solutions (Robinson and Stokes, 1955). In WATEQF the values for a and b for major ions were calculated from mean salt activity coefficients; for minor ions, values of a were taken from Kielland (1937) and b was set to zero.

The MacInnes assumption (MacInnes, 1939), that in symmetrical solutions (for example, 1:1 and 2:2 electrolytes), $\gamma_+ = \gamma_- = \gamma_{\pm}^{1/2}$. allows the use of experimental values of mean molal activity coefficients, $\gamma_{\pm}$, of salts and one calculated single-ion activity coefficient to derive all other activity coefficients in the solution:

If

$$\gamma_{\pm KCl} = \gamma_{K^+} = \gamma_{Cl^-} \qquad (A2.5)$$

then

$$\gamma_{Na^+} = \frac{\gamma_{\pm}^2 \, NaCl}{\gamma_{\pm}^2 \, KCl}, \qquad (A2.6)$$

$$\gamma_{Ca^{2+}} = \frac{\gamma_{\pm}^3 \, CaCl_2}{\gamma_{\pm}^2 \, KCl}, \qquad (A2.7)$$

$$\gamma_{Br^-} = \frac{\gamma_{\pm}^2 \text{ KBr}}{\gamma_{\pm}^2 \text{ KCl}}, \qquad \text{(A2.8)}$$

etc.

These calculated values of single-ion activity coefficients can then be substituted into the extended Debye-Hückel equation to compute values of a and b.

Because of the results of this model are based on experimental measurements of single salt solutions, the final significant assumption is that at a given temperature, activity coefficients in simple solutions are equal to those in complex solutions of the same ionic strenght. Because most of the solutions to which the model has been applied in this study are <<1 molal, this assumption is believed valid.

Solution of Mass Action and Mass Balance Equations. The speciation for a given solution is solved by the method of successive approximations, first applied by Garrels and Thompson (1962), using analytical concentrations, experimental equilibrium constants, mass balance equations for cations and anions, and measured pH and temperature. WATEQF uses the continued fraction method to solve nonlinear equations relating the mass-action and mass balance relations for the free ion concentrations which are initially assumed to be equal to total concentrations. As an illustration, consider a hypothetical solution containing free Ca^{2+} ions, free CO_3^{2-} ions, and only one ion pair, $CaCO_3^0$. Mass balance of the cations and the anions requires that

$$m_{Ca(Total)} = m_{Ca^{2+}} + m_{CaCO_3^0} \qquad \text{(A2.9)}$$

and

$$m_{CO_3(Total)} = m_{CO_3^{2-}} + m_{CaCO_3^0} \quad . \tag{A2.10}$$

Assuming an ideal solution, the mass action equation for the formation of the ion pair will yield an equilibrium constant, often called the "association" or "stability" constant,

$$K = \frac{m_{CaCO_3^0}}{(m_{Ca^{2+}})(m_{CO_3^{2-}})} \quad ,$$

or

$$mCaCO_3^0 = K(m_{Ca^{2+}})(m_{CO_3^{2-}}). \tag{A2.11}$$

Substituting equation (A2.11) into equations (A2.9) and (A2.10),

$$m_{Ca(Total)} = m_{Ca^{2+}} + K(m_{Ca^{2+}})(m_{CO_3^{2-}}) \tag{A2.12}$$

$$m_{CO_3(Total)} = m_{CO_3^{2-}} + K(m_{Ca^{2+}})(m_{CO_3^{2-}}). \tag{A2.13}$$

Rearranging,

$$m_{Ca^{2+}} = \frac{m_{Ca(Total)}}{1 + K(m_{CO_3^{2-}})} \tag{A2.14}$$

$$m_{CO_3^{2-}} = \frac{m_{CO_3(Total)}}{1 + K(m_{Ca^{2+}})}. \tag{A2.15}$$

Equations (A1.14) and (A1.15) give new values for the free ion concentrations, which are then used in the next iteration. The use of single ion activity coefficients allows the treatment to be generalized to nonideal solutions. Iteration continues until the calculated sums of the weak acids, complex ions, and free ions agree with the analytical values to within 0.5 percent. Wigley (1977) has shown that the continued fraction method produces a faster convergence than does the original "brute force" method of Garrels and Thompson (1962), and Nordstrom and others (1979) indicate that the convergence is also faster than for a Newton-Raphson iteration. When the speciation is complete, it is useful to calculate molal concentration ratios and ion activity ratios for use with water composition and mineral stability diagrams.

Ion Activity Products and Solubility Products. Equations (A2.1) and (A2.2) for a mixture at equilibrium are perfectly general. Consider the special case of a solid phase of composition AX in thermodynamic equilibrium with an aqueous solution to form ions A^+ and X^-,

$$AX = A^+ + X^-. \qquad \text{(A2.16)}$$

For equation (A2.16) there exists a characteristic constant,

$$K = \frac{a_{A^+}\, a_{X^-}}{a_{AX}}, \qquad \text{(A2.17)}$$

where K is the thermodynamic equilibrium constant of solubility. If the solid, AX, is a pure substance, then it is in its standard state, and the activity of AX is equal to one. In this case, the equilibrium constant reduces to the solubility product

$$K_{sp} = a_{A^+}\, a_{X^-} \,. \qquad \text{(A2.18)}$$

In hydrolysis reactions, water must be treated explicitly. For example, in the dissolution of quartz to form silicic acid,

$$SiO_{2(Quartz)} + 2H_2O = H_4SiO_4, \qquad \text{(A2.19)}$$

the activity of water appears in the equilibrium expression. Commonly, the activity of water is so close to one that deviations can be ignored in practical applications, such as the computation of mineral stability diagrams (Helgeson and others, 1969).

Waters collected at the well-head are no longer in contact with mineral phases, and the subsurface phases may not be accessible to observation. The calculated activities of dissolved ions in the sample water can be combined to form ion activity products which can be compared with the thermodynamic solubility equilibrium constant to show the degree of saturation for a given phase.

The comparison is most conveniently done by considering the ratio of the ion activity product (IAP) to the equilibrium solubility product (K_{sp}) and the Gibbs free energy change of the reaction (ΔG_r). The quantities are related by the expression

$$\Delta G_r = 2.303\ RT\ \log(IAP/K_{sp}). \qquad \text{(A2.20)}$$

Clearly, when IAP = K_{sp}, $\Delta G_r = 0$, and the water is saturated with respect to the phase being considered. When IAP < K_{sp}, the water is undersaturated; when IAP > K_{sp}, the water is supersaturated.

The principal limitation on this approach is the reliability and consistency of the equilibrium constants used in the calculations. Several sources of uncertainty are obvious. Enthalpies and entropies for most minerals have been measured calorimetrically, and the free energy of formation calculated from these values is usually referred to free energies of formation of the elements or of the oxides rather than to the free energies of formation of the ions formed by dissolution of the mineral. The use of experimental equilibrium constants is free from this inconsistency, but is subject to uncertainties involving exact definitions of reactants and products and difficulities in demonstrating that the reaction was reversed (Walther and Helgeson, 1977, 1979). Because of the uncertainties involved in the basic thermodynamic data, logarithms of the IAP/K_{sp} ratio are used to determine saturation, and the thesis follows the convention of Paces (1973) that values of log (IAP/K_{sp}), also called the saturation index, between -0.25 and +0.25 represent saturated solutions.

Effects of Temperature and Pressure. Most experimental determinations of equilibrium constants and of free energies have been made at 25°C. Where the literature reports the results of experiments at higher temperatures, the equilibrium constant is often expressed as a power function of absolute temperature,

$$\log K = A + BT + C/T + D\log T, \qquad \text{(A2.21)}$$

in which one or more of the coefficients may be zero. WATEQF uses this type of analytical expression whenever it is available from the literature.

In those cases for which high temperature experimental data is limited to two or three temperatures or is lacking all together, the equilibrium constant is corrected by using the Van't Hoff relation,

$$\log K = \log K_{Tr} - \frac{\Delta H_{Tr}}{2.3\ R} \left(\frac{1}{T} - \frac{1}{Tr}\right), \qquad \text{(A2.22)}$$

in which Tr is the reference temperature (298.15 K) and the constants A and C in equation (A1.21) are

$$\log K + \frac{\Delta H_{Tr}}{2.3\ RT}$$

and

$$\frac{\Delta H_{Tr}}{2.3\ R},$$

respectively.

Because the input of measured pH values essentially limits this treatment to near surface waters, the effects of pressure on the equilibrium constant have not been considered. Calculations by Ellis and McFadden (1972) suggest that pressure effects are not large for pressures less than a few hundred atmospheres. Consequently, the treatment of K as a function of temperature alone is believed to be adequate for the purposes of this study.

Redox Reactions. The treatment of redox reactions uses the negative logarithm of the conventional activity of the electron (pE) instead of the oxidation potential (Eh). Eh and pE are related by the expression,

$$pE = Eh/(2.303\ RT/F), \qquad (A1.23)$$

in which F is the faraday and 2.303 RT/F is the Nernst slope. The conventions associated with pE are discussed in depth by Truesdell (1968).

The principal advantage of using the electron activity is that it is not necessary to consider separate redox equilibrium expressions. For example, the equilibrium between Fe^{2+} and Fe^{3+} can be expressed by an equilibrium constant,

$$K = \frac{a_{Fe^{3+}}\ a_{e^-}}{a_{Fe^{2+}}}, \qquad (A1.24)$$

where the value of K can be calculated from $G^\circ_{f(Fe^{3+})}$ and $G^\circ_{f(Fe^{2+})}$, given the convention that $G^\circ_{f(e^-)} = 0$.

Eh values for the waters in this study were not measured in the field. However, separate analyses of reduced and oxidized species allow the computation of pE, based on the assumption of redox equilibrium. Where two such pairs are measured, it is possible to compare the computations as an estimate of the degree of internal redox equilibrium. The pairs which are available in this study are sulfide-sulfate and ammonia-nitrate. The sulfide-sulfate equilibrium can be expressed,

$$H_2S + 4H_2O = SO_4^{2-} + 10H^+ + 8e^- , \qquad (A2.25)$$

The mass-action expression is

$$K = \frac{a_{SO_4^{2-}} \, a_{H^+}^{10} \, a_{e^-}^{8}}{a_{H_2S} \, a_{H_2O}^{4}} . \qquad \text{(A2.26)}$$

Taking common logarithms and using the pH and pE definitions,

$$\log K = \log a_{SO_4^{2-}} - 10pH - 8pE - \log a_{H_2S} - 4\log a_{H_2O}, \qquad \text{(A2.27)}$$

which can be rearranged to solve for pE:

$$pE = \frac{-\log K + \log a_{SO_4^{2-}} - \log a_{H_2S} - 4\log a_{H_2O} - 10pH}{8} \qquad \text{(A2.28)}$$

The implicit assumption of redox equilibrium in the computer calculations will be discussed in Part II of this appendix.

Gas Partial Pressures. Gas partial pressures may be calculated from the gas solubility constants and the water analysis. In WATEQF the partial pressures of CO_2, O_2, and CH_4 are calculated from the following equations,

$$\log P_{CO_2} = -\log K + \log a_{HCO_3^-} + \log a_{H^+} - \log a_{H_2O} \qquad \text{(A2.30)}$$

$$\log P_{O_2} = -\log K' + 2\log a_{H_2O} + 4pH + 4pE \qquad \text{(A2.31)}$$

$$\log P_{CH_4} = -\log K'' + \log a_{HCO_3^-} - 3\log a_{H_2O} - 9pH - 9pE. \qquad \text{(A2.32)}$$

In interpreting the chemistry of the Lightning Dock waters, equations (A1.31) and (A1.32) are relatively unimportant. Further, because the calculated values for P_{O_2} and P_{CH_4} depend on the assumption of redox equilibrium, which may not be valid, the body of the thesis does not consider the partial pressures of O_2 and CH_4. The equations used in the body of the thesis for deriving pH and P_{CO_2} (equations 7-15) are somewhat different in form from equation (A1.30), but the results are virtually identical.

Activity of Water. While the activity of water in dilute solutions is commonly so close to one that it may be treated as a constant (Helgeson and others, 1969), WATEQF computes the activity of water by the approximate relationship of Garrels and Christ (1965),

$$a_{H_2O} = 1 - 0.017 \Sigma m_i, \qquad (A2.33)$$

where Σm_i is the sum of the molalities of dissolved ions and neutral species. The equation is believed to be accurate for $\Sigma m_i < 1$.

Part II: WATEQF

Table A2.1 summarizes the important descriptive program features of WATEQF.

In a recent review Nordstrom and others (1979) have discussed the assumptions, strengths, and limitations of the major schools of computerized chemical models for natural waters, including WATEQF. Using two test cases, low ionic strength (0.0024) river water and high ionic strength (0.6801) sea water, Nordstrom and others (1979) examined the results predicted by the various aqueous models. In a series of

Table A2.1

Descriptive Program Features of WATEQF

Number of Elements	19 [1]
Number of Aqueous Species	105
Number of Gases	3
Number of Redox Species	8
Number of Minerals	101
Number of Organic Species	0
Method of Calculating Activity Coefficients	Extended Debye-Huckel Equation or Davies Equation[2]
Temperature Range (°C)	0-100
Pressure Range (bar)	1
Iteration and Convergence Method	Continued Fraction

[1] Excluding H and O in water.

[2] Only the extended Debye-Huckel equation was used in the computations of the thesis.

tables, they compared the calculated molalities and activity coefficients for major and minor species and the saturation indices for selected minerals. The test cases show significant areas of agreement and of disagreement between the various computer models. In general, there is better agreement between computed concentrations for major species than for minor species, and there is better agreement for the river water case than for the sea water case. There results are consistent with practical expectations: 1) thermodynamic data is much more extensive for major species than for minor species, and 2) dilute solutions are less extensively complexed and yield more consistent and reliable activity coefficients than do more concentrated solutions. For both test cases WATEQF yields results which are generally consistent with all the other computer models; in no case does WATEQF calculate an extremum value. Among the eleven programs considered, WATEQF requires the fewest number of interactions to achieve convergence between calculated and analyzed concentrations. The ease of convergence is believed to reflect the internal consistency of both the data base and the chemical model of WATEQF. Furthermore, on the basis of several years of testing, including the comparison of calculated saturation indices with observed alteration assemblages at Yellowstone, the U.S.G.S. geothermal investigators believe that WATEQF provides a consistent and useful model for water-rock interactions in geothermal systems (R.O. Fournier, personal communication, 1979; L. N. Plummer, written communication, 1980).

However, to observe that WATEQF is internally consistent and useful is not to believe that it provides a complete description of

the inorganic chemistry of natural waters. The discrepencies between the calculations of the various computer models suggest certain limitations of the models. In critically evaluating the results of WATEQF, it is well to consider some of the major limitations.

First, any model is constrained by the assumptions on which it is based. In particular, the chemical model of WATEQF is based on the implicit assumption of the ion association theory (Fuoss, 1935). The reliability of the ion association approach depends on the use of non-thermodynamic models, such as the Debye-Hückel theory, to describe nonideal aqueous electrolytes. While the model certainly does yield useful results, it is worth remembering that the model of real electrolyte solutions uses semi-empirical equations to calculate activity coefficients and that the results of such a model are only as good as the approximations that are used. Fortunately, for the Animas Valley and adjacent areas, solutions are of such low ionic strength that the Debye-Hückel equation can predict very accurately the activity coefficients of the species in solution.

The second principal limitation is the reliability of the thermodynamic data used in the computations. Sources of error and inconsistency have been discussed in Part I of the appendix. Even for such a well-studied phase as calcite, there is substantial disagreement about the value of K_{sp}. (See, for example, Berner, 1976; Thrailkill, 1976). For less well-studied minerals and complexes, particularly low-temperature phases for which reversible equilibrium is difficult to demonstrate, published solubility product constants and complex stability constants reported in the literature commonly vary by as much as three orders of

magnitude. Phases particularly open to this order of uncertainty in WATEQF include hydroxyapatite, goethite, hematite, and kaolinite (Nordstrom and others, 1979).

No single compilation of the thermodynamic data is comprehensive enough to include all the phases, ions, and complexes needed as the data base for a model of natural waters. However, the data base of WATEQF has been chosen critically by Manuel Nathanson of the U.S.G.S. to be as internally consistent and as current as possible. In particular, the data set used for the computations of this thesis during the summer of 1980 reflects the updated thermodynamic data for aluminum as presented by Robie and others (1978) and the data on aqueous silica of Walther and Helgeson (1977), which makes the WATEQF data consistent with the silica geothermometry of section Table 3 in the main body of the thesis.

The distribution of redox species depends on which redox potential is assumed to dominate the chemical equilibrium. As discussed in Part I, for most of the samples from the Animas Valley, the only redox pair measured in the chemical analyses is H_2S-SO_4^{2-}. However, for sample P3, from one of the hot wells, values above background were also found for the redox pair NO_3^--NH_4^+. As a test of the internal consistency of the assumption of redox equilibrium, one can calculate pE for each of the assumed redox potentials. First, consider the S^{2-}/SO_4^{2-} potential to dominate. Equation (A2.28),

$$pE = \frac{-\log K + \log a_{SO_4^{2-}} - \log a_{H_2S} - 4\log a_{H_2O} - 10pH}{8},$$

presents the formula for calculating pE. Since sample P3 has a measured temperature of 81°C, it is necessary to correct the value of K using the Van't Hoff expression,

$$\log K = \log K_{Tr} - \frac{H_{Tr}}{2.303\ R}\left(\frac{1}{T} - \frac{1}{Tr}\right),$$

where $\log K_{Tr} = -40.644$

$H_{Tr} = 65{,}440$ cal mol^{-1}

$R = 1.9872$ cal deg^{-1} mol^{-1}

$T = 354.15$ K

$Tr = 298.15$ K.

Therefore, $\log K = -33.123$.

For P3, $\log a_{SO_4^{2-}} = -2.5992$

$\log a_{H_2S} = -7.2307$

$\log a_{H_2O} = 0.0002$

$pH = 8.160$.

Substituting these values into equation (A2.28), pE = -5.488, or, using equation (A2.23), Eh = -0.386 volts.

Next, consider the NO_3^-/NH_4^+ potential to dominate. Equation (A2.29),

$$pE = \frac{-\log K + \log a_{NO_3^-} - \log a_{NH_4^+} - 3\log a_{H_2O} - 10pH}{8},$$

defines pE for this system. Again using the Van't Hoff expression with

$\log K_{Tr} = -119.007$

$H_{Tr} = 187.055$ cal mol^{-1}

$R = 1.9872 \text{ cal deg}^{-1} \text{ mol}^{-1}$

$T = 354.15 \text{ K}$

$Tr = 298.15,$

pE = 2.009, or Eh = +0.141 volts.

The implication of these calculations is that redox equilibria are not attained in the Lightning Dock waters, even at the relatively elevated temperature of 81°C. This conclusion is coroborated by the results of other workers in the field (R. O. Fournier, personal communication, 1979; L. N. Plummer, written communication, 1980).

The inconsistency of pE results introduces an uncertainty in the speciation of the redox elements, especially iron and manganese. Table A2.2 summarized the results of the redox calculations given above and compares the calculated values of Fe^{2+} and Fe^{3+} for the two imposed potentials given the total concentration of iron in sample P3. The variation of almost nine orders of magnitude in the calculated concentrations of Fe^{2+} is clearly unsatisfactory, in that it implies gross uncertainties in the saturation indices for all the iron-bearing phases.

Three approaches to this problem have been considered. The first is to assume that since the total concentration of sulfur in the system is orders of magnitude greater than the concentrations of any other redox species, the redox reactions will be dominated by the sulfur systems. This assumption may be supported by the results of Nordstrom and others (1979) who, in examining the assumptions of redox equilibrium, compared the variations in redox species speciation for several imposed redox potentials for the river water test case using WATEQ2, a program related to WATEQF in assumptions, computational methods, and data base.

Table A2

Comparison of pE, Eh, and Calculated Concentrations of Fe^{2+} and Fe^{3+} of Sample P3 for Imposed Redox Potentials. Concentration of Fe^{2+} and Fe^{3+} are Given as -log (molality) (pm).

Imposed Redox Potential	pE	Eh(volts)	$pm_{Fe^{2+}}$	$pm_{Fe^{3+}}$
S^{2-}/SO_4^{2-}	-5.488	-0.386	5.57	22.72
NO_3^-/NH_4^+	2.009	+0.141	14.39	5.56

In the WATEQ2 calculations, the concentration, expressed as -log molality (pm), of Fe^{2+} using the S^{2-}/SO_4^{2-} couple is 6.56, compared to a measured value of 6.49. The second approach is to assume that the redox conditions in solution are not represented by any imposed potential and to introduce several pE values to determine the effects on calculated saturation indices for minerals. The third approach is to handle the speciation without regard to redox equilibria by setting the pE equal to 0.

Varying the pE between -5 and +5 has relatively little effect on the results of the WATEQF calculations, primarily because of the low concentration of total iron in solution. The most significant effects are observed for siderite, goethite, hematite, amorphous $Fe(OH)_2$, mackinawite, amorphous FeS, and several minor Mn phases. Variation between calculated supersaturation and undersaturation with respect to these phases is troublesome in theory, but less so in practice. For some of the phases, particularly siderite and rhodchrosite, it is unrealistic to expect that the solutions have been in contact with the pure phases. Almost certainly, the iron or magnanese present in carbonate phases in the Lightning Dock system is present as a trace substitution for Ca^{2+} and/or Mg^{2+} in calcite or dolomite. Furthermore, given the uncertainties in the thermodynamic data, it is probably unreasonable to believe that an equilibrium model would adequately describe low temperature phases such as goethite or mackinawite, much less amorphous iron oxides, oxyhydroxides, or sulfides.

Given these considerations and the general failure of equilibrium chemical modeling of natural waters to successfully describe actual

redox conditions (Nordstrom and others, 1979; L. N. Plummer, written communication, 1980), the third approach, setting pE = 0, seems the most reasonable. The calculated saturated phases are all reasonable, consistent with calculated and observed assemblages at other geothermal locales, and consistent with the X-ray examination of the drill chips from Cockrell #1.

A fourth limitation is the way in which WATEQF handles the concentration of aluminum. In the pH range of the Lightning Dock waters ($7 < pH < 9$), aluminum is almost totally insoluble. Therefore, the water analyses (Appendix 1, Table A1.5) all show aluminum below detection limits. If one introduces an analyzed chemistry which includes no aluminum, then no aluminous species will be calculated by WATEQF (or any other computer program). In particular, the calculated saturation indices will include no feldspars, micas, clays, or zeolites, which would correspond to our expectation for phases in a hydrothermally altered igneous or detrital sedimentary reservoir. The "saturated" phases would include such unlikely phases as magadiite, sepiolite, and greenalite. Two approaches are possible. First, one could assume that since aluminum is below detection limits, its input value should be zero. This is the approach taken by Dellachaie (1978). A reasonable interpretation of the computer results then requires that the reseacher by cognizant of the assumption and be familiar enough with low temperature mineralogy to interpret sepiolite as the probable equivalent of chlorite, magadiite as the probable equivalent of an alkali feldspar, etc. Dellachaie (1978) seems to have taken the calculated "saturated"

values as indicative of actual phases with which the water was in contact. Clearly, this approach is hazardous.

The second approach is to recognize that clay minerals and zeolites probably do not precipitate from ionic solutions. Experimental and theoretical results indicate that the hydrolysis of feldspar and micas produces a metastable amorphous aluminosilicate phase of variable composition as an intermediate step in the formation of clays and zeolites (Helgeson, 1969; Paces, 1973). The Muir Cauldron rocks, andesitic to rhyolitic in composition, contain approximately 13 to 16 weight percent Al_2O_3 (Appendix 1, Table A1.7). Aluminum is certainly present in the Lightning Dock geothermal system and available for the formation of authigenic minerals, including feldspars, chlorite, clay minerals, and zeolites. Since the overwhelming bulk of the Ca, Na, and K in solution is due to water-rock reactions, particularly the hydrolysis of feldspars, it seems likely that the concentration of Al available in some reactive state (though not as Al^{3+} ions) should be of approximately the same order of magnitude as the concentrations of the major cations. For example, in sample P3 the analyzed concentrations of the major cations is in the range 1×10^{-2} to 5×10^{-4} molal and the dissolved silica is 2×10^{-3} molal. Introducing an aluminum concentration of 4×10^{-6} molal (0.1 ppm) produces calculated saturation with respect to at least some mineral phases of the feldspar, mica, clay, and zeolite groups. An order of magnitude increase in aluminum stabilizes a wide range of phases of each of these groups. These inputs are probably overly conservative in terms of the actual concentration of aluminum available in the system, but since they

produce results that are consistent with geochemical experience and interpretable, they have been used in the calculations of the thesis.

The final, and probably most critical, limitation involves the basic assumption of the chemical model: chemical equilibrium between a solution and the phases which are precipitating from or dissolving into that solution. The fact that a geothermal water has a saturation index greater than or equal to zero for a given mineral does not require that the mineral be present nor give any indication of the quantity of the mineral. Kinetic factors, such as nucleation and growth rates, must also be considered. Certainly, indicated saturation with respect to a given phase does not require that the solution has ever interacted with a mass of that phase, as is clear from the widespread formation of pedogenic caliche in the Southwest. Hence, Dellachaie's conclusion that calculated saturation with respect to calcite requires the geothermal solutions to have circulated through the Paleozoic sedimentary rocks underlying the Animas Valley is without geochemical foundation. However, misinterpretation of the results of a computer program should be considered a limitation of scientists rather than of the program. The only proper use of a computer model such as WATEQF is to demonstrate the reasonable mineral phases that would be in equilibrium with a given water composition. Interpretation of the results must rest on sound geologic interpretations and must ultimately be tested by petrologic alteration studies of reservoir rocks.

In summary, as with all models, WATEQF has certain limitations which grow out of the assumptions of the chemical model on which the

program is based. However, when the assumptions are understood, the limitations can be understood and dealt with reasonably. The results of such a computer model are sufficiently interesting and consistent to justify its use in helping to interpret the geochemistry of natural waters.

APPENDIX 3

Computer-Modeled Geothermometry

Three computer programs related to calculating geothermal reservoir temperatures were developed during the early stages of the thesis research. All programs were developed in FORTRAN IV for use on a PDP 11/MNC computer (64 Kbyte) with two RL01 (10 Megabyte) disks. A Tektronix 4025 terminal and 4662 X-Y digital plotter provided interactive and hardcopy graphics. A DECwriter III (LA-120) served as the console terminal. The three programs are described in detail and fully documented in Landis and Logsdon (1979). Computer programs ALKALI and ALKFIT use the chemical and temperature data sets of Fournier and Truesdell (1973) to determine statistical best-fit equations for the alkali geothermometer. Such equations have the form

$$Y = A + BX, \qquad \text{(A3.1)}$$

where $Y = 1000/T$ (°K),

$$X = \log [Na^+]/[K^+] + \beta \log [Ca^{2+}]^{1/2}/[Na^+],$$

and A, B, and β are empirically derived constants. The differences between the statistical approaches of the two programs results in slightly different values for the constants and slightly different values for the calculated reservoir temperatures. The results of ALKALI and ALKFIT are presented and compared with the original results of Fournier and Truesdell (1973) in Table A3.1.

Computer program GEOTHM calculates Na-K, Na-K-Ca, and SiO_2 temperatures for geothermal and related waters. An interactive option

of the program is the choice of alkali fit parameters from ALKALI, ALKFIT, or Fournier and Truesdell (1973). While the statistically generated geothermometry curves are more precise, the Fournier and Truesdell values have been used in all my calculations to make the results as compatible as possible with published values from other geothermal areas where the Fournier and Truesdell analysis has been used. The most recent comprehensive silica solubility data are used to calculate SiO_2 temperatures (Walther and Helgeson, 1977).

A variety of assumptions are involved in the geothermometry models used by GEOTHM. It is important to review and evaluate the assumptions. The use of dissolved silica in geothermal waters as a geothermometer was first proposed by Fournier and Rowe (1966); recent applications include Arnórsson (1975), Truesdell (1976), and Swanberg and Morgan (1978). The solubility of SiO_2 in aqueous solutions is essentially independent of the concentration of dissolved salts except near the lower critical end point (Krauskopf, 1956; Kitahara, 1960). Furthermore, for the most of the geochemically relevant range, silica solubility is also independent of pH. This behavior can be understood in terms of the solution chemistry of silica. In aqueous solution dissolved silica is present as one or more monomer of the generalized form $SiO_2 \cdot nH_2O$. For the concentration range seen in the Lightning Dock waters, even at 25°C, the silica monomer is probably an uncharged $SiO_2 \cdot 2H_2O$ which is in equilibrium with silicic acid. The value of the first ionization constant,

Table A3.1

Na-K-Ca Alkali Geothermometer Curve Fitting Data

Source	Temperature Boundary °C	Beta $T>T_B$	Beta $T\geq T_B$	$Y + A + B * Y$ $A(\pm\sigma)$	$B(\pm\sigma)$	R_{xy}
Fournier & Truesdell	100	0.333	1.333	1.3502	0.6101	---
ALKALI	100	0.217	1.360	1.3778 (0.169)	0.6188 (0.094)	0.94
ALKFIT	100	0.105	---	1.2441 (0.302)	0.6812 (0.063)	0.95
		---	0.100	3.8168 (0.360)	-0.4739 (0.058)	-0.84

$$K = \frac{[H^+]\cdot[H_3SiO_4^-]}{[H_4SiO_4]} = 10^{-9.9} \quad , \qquad (A3.2)$$

shows that the solubility does not depend significantly on pH below a value of approximately 9 (Yariv and Cross, 1979). The uncharged nature of the $SiO_2 \cdot 2H_2O$ monomer explains the lack of influence of ionic strength on silica solubility (Holland Malinin, 1979).

Two critical questions remain: 1) which silica polymorph controls the concentration, and 2) does the concentration of silica in solution change rapidly during flow of the aqueous phase from the high temperature reservoir to the lower temperature collection site. It is very difficult to make a priori predictions about the mineralogy of the silica polymorph to be expected in a given system. The SiO_2 phase which precipitates will be controlled by the degree of supersaturation and by the specific kinetics of the given system, particularly the availability of nucleation sites (Barnes and Rimstidt, 1978). Field studies indicate that at temperatures above approximately 100°C, quartz is the most common polymorph; between 100°-50°C, chalcedony is the most common polymorph; and below 50°C, amorphous silica becomes increasingly important (R. O. Fournier, personal communication, 1980). These temperature ranges are not absolute: chalcedony has been reported up to 160°C (R. O. Fournier, personal communication, 1980) and authigenic quartz is known from waters trapped in the Nubian Sandstone at less than 50°C (C. A. Swanberg, personal communication, 1979). Although authigenic cristobalite has been reported from some geothermal systems (Browne, 1978), given the controversy which

surrounds the validity of cristobalite solubility measurements (Walther and Helgeson, 1977), I have chosen to ignore cristobalite in the silica geothermometry. As shown in Figure A3.1, samples P2, P3, and P4 lie between the saturation cruves for chalcedony and amorphous silica. Therefore, one would expect chalcedony to be the SiO_2 precipitate from these waters. The waters are also supersaturated with respect to quartz. Landis and Logsdon (1979) have shown that a comparison of silica temperatures with alkali temperatures is most consistent if quartz is assumed to be the silica phase above 100°C and chalcedony the silica phase below 100°C.

The final assumption of silica geothermometry is that the silica concentration does not change rapidly during circulation within the geothermal system. I have already presented the equilibrium arguments for the stability of aqueous silica. Barnes and Rimstidt (1978) have shown that the kinetics of silica precipitation can be expressed as a first order expression,

$$\left[\frac{\partial\ (SiO_2)}{\partial\ t}\right]_T = K_p\ (SiO_2)(s/v), \qquad \text{(A3.3)}$$

where (SiO_2) = concentration of silica; t = time; T = temperature; K_p = rate constant for precipitation; and (s/v) = ratio of surface area of silica to the volume from which it is precipitating. The Barnes and Rimstidt experiments show that the precipitation of an ordered silica phase is so slow at low temperatures that even moderate flow rates should preserve evidence of the reservoir silica form.

Figure A3.1. Silica solubility along the liquid-vapor water pressure curve for alpha quartz (A), chalcedony (B), and amorphous silica (C). Note that values along the abscissa are given in terms of the enthalpy of liquid water in cal/gm. Points P1, P2, P3, and P4 and the lines through them are described in the body of the thesis and in Figure 18. Data for the curves are from Walther and Helgeson (1977).

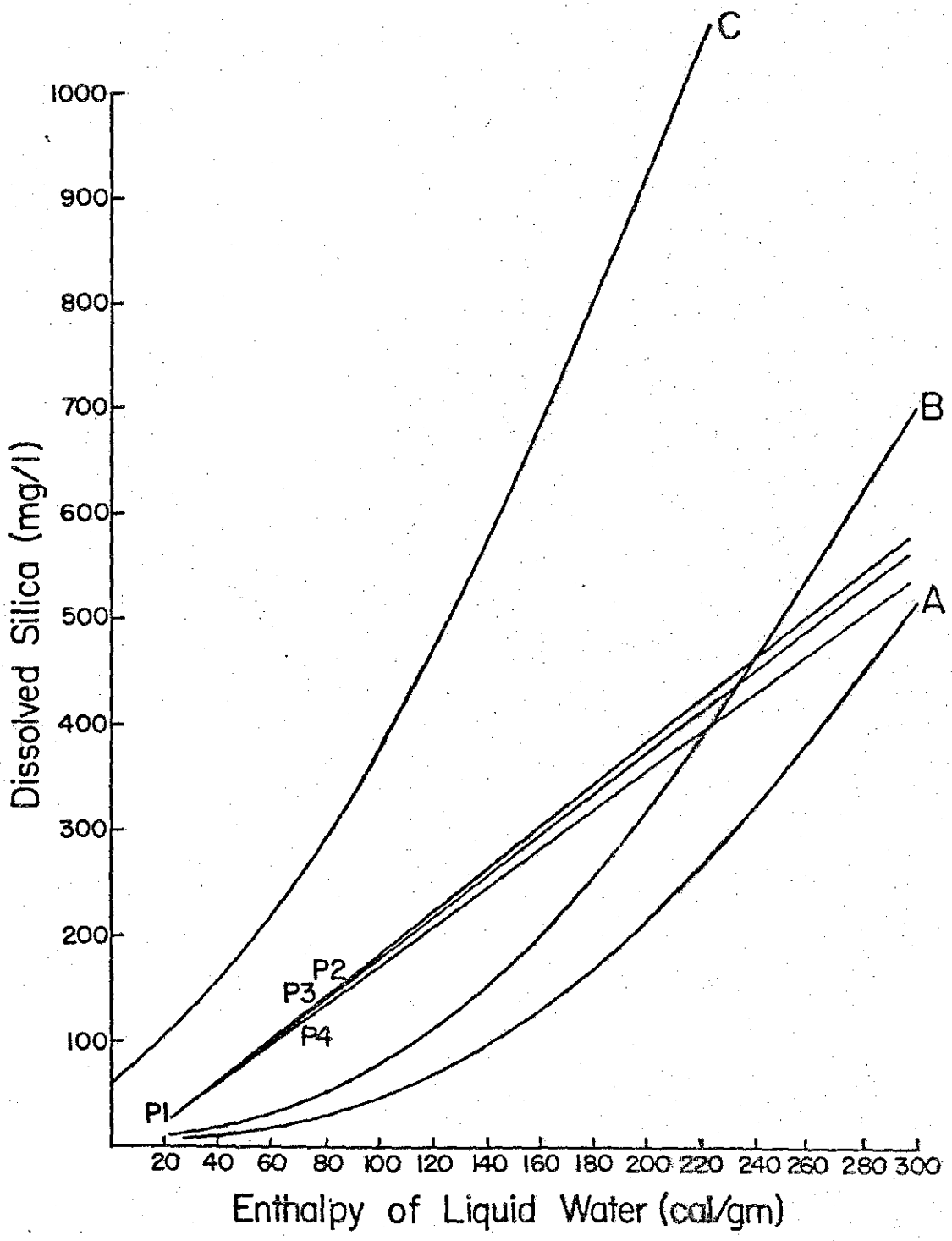
C
B
A
P1
P2
P3
P4
1000
900
800
700
600
500
400
300
200
100
Dissolved Silica (mg/l)
20 40 60 80 100 120 140 160 180 200 220 240 260 280 300
Enthalpy of Liquid Water (cal/gm)

Although the system SiO_2-H_2O has been extensively studied, there is still considerable controversy about the solubility of quartz below 300°C and about the solubility of cristobalite and amorphous silica in general. Experimentally, these systems are non-trivial because of the difficulty in completely characterizing the fine-grained phases and in completely reversing the reactions. I have chosen the Walther and Helgeson (1977) data because they are consistent with the thermodynamic properties of aqueous silica and with reversed solubility measurements for quartz. It is important to note that the Walther and Helgeson data predict higher temperatures of equilibration than do the earlier data of Fournier and Rowe (1966).

The alkali temperatures are functions of the Na-K and Na-K-Ca concentrations of the waters, theoretically based on cation exchange equilibria between aqueous solutions and feldspar. For the Na-K geothermometer, consider the exchange reaction

$$K^+ + \text{Na-feldspar} \rightleftharpoons Na^+ + \text{K-feldspar}, \qquad \text{(A3.4)}$$

where

$$K = \frac{a_{Na^+} \; a_{K\text{-fsp}}}{a_{K^+} \; a_{Na\text{-fsp}}} .$$

Given that the activity of a solid phase is one, and assuming that for dilute solutions activity is approximately equal to concentration,

$$K \simeq \frac{[Na^+]}{[K^+]} . \qquad \text{(A3.6)}$$

At equilibrium the Gibbs-Helmholtz equation holds, and for pure

substances in the standard state,

$$\frac{d \log K}{d T} = \frac{\Delta H^\circ}{2.303\ RT^2} . \qquad \text{(A3.7)}$$

Rearranging equation (A3.7)

$$d \log K = \frac{\Delta H^\circ}{2.303\ R} \frac{d T}{T^2}$$

$$= \frac{\Delta H^\circ}{2.303\ R} d\ (1/T). \qquad \text{(A3.7a)}$$

Since $K \simeq ([Na^+]/[K^+])$, $\log ([Na^+]/[K^+])$ is a function of $(1/T)$. The function has been calibrated empirically and experimentally as

$$\log \frac{[Na^+]}{[K^+]} = -1.2172 + (1.149 \times 10^3)\ T^{-1} \qquad \text{(A3.8)}$$

(Truesdell, 1975).

Fournier and Truesdell (1973) showed that for most geologic systems one must also consider exchange equilibria involving plagioclase feldspars. Using the same logic as above and a schematic exchange reaction,

$$Na^+ + \text{Ca-feldspar} \rightleftharpoons 1/2Ca^{++} + \text{Na-feldspar}, \qquad \text{(A3.9)}$$

where

$$K' \simeq \frac{[Ca^{2+}]^{1/2}}{[Na^+]} ,$$

and $\log \frac{[Ca^{2+}]^{1/2}}{[Na^{+}]}$ is also a function of temperature. Fournier and Truesdell (1973) combined both reactions to produce a temperature function of the form

$$10^3/T = A + B \left(\log \frac{[Na^{+}]}{[K^{+}]} + \beta \log \frac{[Ca^{2+}]^{1/2}}{[Na^{+}]} \right) \qquad (A3.10)$$

where A, B, and β are the empirically determined values referred to in the preceding discussion of computer programs ALKALI and ALKFIT. Numerous studies show that the Na-K-Ca temperature fits measured systems better than the Na-K temperature (Truesdell, 1975; Fournier, 1977; Swanberg, 1978). Hence, all references in the thesis to alkali temperatures will refer to the Na-K-Ca temperature unless otherwise specified.

Mg-rich waters, including seawater, have an adverse effect on calculated alkali temperatures (Fournier and Potter, 1979). Although the theoretical basis for the Mg-correction is obscure, the explanation probably lies in Mg-Ca exchange in carbonates and smectites which interfere with the interpretation of $[Ca^{2+}]^{1/2}/[Na^{+}]$ as controlled by feldspar equilibria. The Mg-correction, which is substracted from the alkali temperature, is a complex function of the alkali temperature and the ratio Mg/Mg+Ca+K. Table A3.2 shows the corrected alkali geothermal temperature for selected samples based on the Mg-correction curves of Fournier and Potter (1979). Where the Fournier and Potter criteria indicate that it can be usefully applied, the Mg-correction improves the agreement between the silica and the alkali geothermometers.

Table A3.2

Reservoir Temperature After Applying Mg^{++} Correction

	Ca	Mg	K	Na	R%[1]	Δt_{Mg}[2]	T°C[3] Mg Corr.	T°C[4] Silica	T°C[5] Na-K-Ca
	mg/l								
Lightning Dock: Estimate = 170°C									
P 2	22.0	0.5	23.5	333.6	2.36	0.0	169	168*	169
P 3	23.2	0.8	21.1	318.6	3.73	3.5	162	165*	165
P 4	67.3	5.3	27.8	493.1	9.68	27.3	129	122#	156
P 24	38.5	1.8	18.0	321.4	5.85	8.7	145	153↑	154

1. R% = Mg/Mg + Ca + K) in equivlanet units.

2. $\Delta t_{Mg} = 10.66 - 4.7415\ R + 325.87(\log R)^2 - 1.032*10^5(\log R)^2/T - 1.988*10^7(\log R)^2/T^2 + 1.605*10^7(\log R)^3/T^2$ [5_R_50] -- $\Delta t_{Mg} = -1.03 + 59.971(\log R) + 145.05(\log R)^2 - 36711(\log R)^2/T - 1.67*10^7(\log R)/T^2$ [0.5 R 5.0].

3. T°C Mg Corr. = T°C Na-K-Ca - Δt_{Mg}.

4. T°C Silica = silica solubility controlled by * = alpha quartz, liquid-vapor curve of water, ↑ = alpha quartz at 500 bar, # = chalcedony,

5. T°C Na-K-Ca = alkali temperature, UNM.

APPENDIX 4

Mineral Stability Diagrams

Mineral stability diagrams, using the computer-calculated logarithms of activities and of ratios of activities, have been calculated using the methods of Helgeson and others (1969). The thermodynamic data for the computation are taken from Robie and others (1978), in which the G_f° values are in J mol^{-1}, standard temperature and pressure are 298.15 K and 1 bar, and R, the universal gas constant, is 8.314 J mol^{-1} K^{-1}.

Helgeson and others (1969) define a chemical system which includes the rock forming minerals (phases defined by the oxide components MgO-CaO-FeO-Na_2O-K_2O-Al_2O_3-SiO_2-CO_2-H_2O), natural aqueous solutions (the oxides given above, plus HCl), and hydrothermal ore-forming solutions (the oxides and HCl, plus H_2S-H_2SO_4-Cu_2S-PbS-ZnS-Ag_2S-etc.). Not all of the potential components are of equal interest in any given situation, and it is possible to define a subsystem of the system of Helgeson and others. For the Lightning Dock area there now exist too little data on the concentrations of base and precious metal cations in solution or on the redox systematics of sulfur and iron to apply mineral stability diagrams in predicting the possible occurrence of sulfide minerals. Therefore, the chemical system defined for the purposes of this thesis consists of the components MgO-CaO-Na_2O-K_2O-Al_2O_3-SiO_2-CO_2-H_2O-HCl. For convenience in presentation, even smaller subsystems may be considered.

Unlike WATEQF, in which all reactions are written as associations, this approach treats mineral equilibria in terms of dissocation. Under

most natural conditions, SiO_2, CO_2, and H_2O do not dissociate appreciably; they will occur as neutral molecules or as complexes with other ions in solution (Helgeson and others, 1969). At temperatures below 300°C, HCl and the metal oxides are nearly completely dissociated in aqueous solutions (Helgeson, 1970). Consider a generalized reaction,

$$M_{\nu+}O_{\nu-} + \nu+zH^+ \rightleftharpoons \nu+M^z + \frac{\nu+z}{2} H_2O, \qquad \text{(A4.1)}$$

where M = cation in the oxide component; O = oxygen; H = hydrogen; $\nu+$ = number of moles of cation in one mole of oxide; $\nu-$ = number of moles of oxygen in one mole of oxide; and z is the charge on the cation. For example,

$$Ca_1O_1 + 1\cdot2\cdot H^+ \rightleftharpoons 1Ca^{2+} + \frac{1\cdot2}{2} H_2O.$$

In a manner exactly analogous to equation (A2.2), the Law of Mass Action for equation (A4.1) may be written,

$$K_{1(i)} = \frac{a_i^{+(i)} \; a_{H_2O}^{(\nu+(i)z(i)/2)}}{a_i \qquad a_{H^+}^{(\nu+(i)z(i))}}, \qquad \text{(A4.2)}$$

where a_i = activity of the ith species in aqueous solution and $K_{1(i)}$ = the equilibrium constant for reaction (A4.1) involving the ith oxide component.

For two oxide components and $a_{H_2O} = 1$, it can be shown that,

$$\frac{d \log (a_{M_{(1)}}/a_{H^+}^{z(1)})}{d \log (a_{M_{(2)}}/a_{H^+}^{z(2)})} = \frac{\nu+(2)\ d \log a_1}{\nu+(1)\ d \log a_2} = \frac{\nu+(2)\ d \log f_1}{\nu+(1)\ d \log f_2} = \frac{\nu+(2)\ d \mu_1}{\nu+(1)\ d \mu_2}, \quad \text{(A4.3)}$$

where f_i = fugacity of the ith component and μ_i = chemical potential of the ith component (Helgeson, 1967). On this basis one may construct equilibrium mineral stability diagrams normalized to pH in which slopes of the mineral boundaries are proportional to boundaries of the corresponding log fugacity or chemical potential diagrams.

As an example, consider the incongruent hydrolysis of microcline in the system K_2O-Al_2O_3-SiO_2-H_2O-HCl to form kaolinite, aqueous silica, and K^+ ion. The balanced reaction may be written,

$$2KAlSi_3O_8 + 2H^+ + 9H_2O \rightleftharpoons Al_2Si_2O_5(OH)_4 + 2K^+ + 4H_4SiO_{4(aq)} \quad \text{(A4.4)}$$

For reaction (A4.4) the equilibrium constant is given by,

$$K_4 = \frac{a_{K^+}^2 \ a_{H_4SiO_4}^4}{a_{H^+}^2}, \quad \text{(A4.5)}$$

which can be rewritten to give

$$\frac{a_{K^+}^2}{a_{H^+}^2} = \frac{K_4}{a_{H_4SiO_4}^4} .$$

Taking common logarithms and rearranging, and dividing by 2 to clear the left-hand side,

$$\log \left(\frac{a_{K^+}}{a_{H^+}}\right) = \frac{\log K_4 - 4 \log a_{H_4SiO_4}}{2} , \qquad \text{(A4.6)}$$

which is a linear equation in slope-intercept form with slope = -2 and intercept = (log K_4/2).

In the absence of experimental values for K_4, one may derive the value from $\Delta G^\circ_{reaction}$ and the standard relation,

$$K = e^{-\Delta G^\circ/RT} .$$

Consider reaction (A4.4) at 25°C and 1 bar. $\Delta G^\circ_{reaction} = \Sigma n_i \Delta G^\circ_{(formation,i)} - \Sigma n_J \Delta G^\circ_{(formation,j)}$, where i indicates product species, j represents reactant species, and n represents the stoichiometric coefficient for the appropriate species. Taking the Gibbs free free energy data from Robie and others (1978), for the products,

Species	ΔG_f°	$n_i \Delta G_f^\circ$
kaolinite	-3,799,464	-3,799,364
K^+	-282,490	-564,980
H_4SiO_4	-1,308,000	-5,232,000
		= -9,596,344

and for the reactants,

Species	ΔG_f°	$n_i \Delta G_f^\circ$
microcline	-3,742,330	-7,484,660
H^+	0	0
H_2O	-273,141	-2,134,269
		= -9,618-929

Therefore, $\Delta G^\circ_{reaction}$ = +22,585,

$-(\Delta G^\circ/RT)$ = -9.11, and

K = -.0001106.

Therefor, log K = -3.956, and substituting this value into equation (A4.6), the log (a_{K^+}/a_{H^+}) intercept is -1.978.

At each temperature of interest, one proceeds through analogous calculations for each appropriate reaction to calculate the mineral stability boundaries. The other reactions to be considered at 25°C, include gibbsite-kaolinite, gibbsite-muscovite, kaolinite-muscovite, kaolinite-illite, muscovite-microcline, and illite-microcline. The resulting diagram for the system K_2O-Al_2O_3-SiO_2-H_2O-HCl is shown in Figure 20 in the body of the thesis with calculated values of

low-temperature groundwaters plotted on the diagram. Similar constructions for several chemical systems at various temperatures are shown in Figures 21 and 22.

Several miscellaneous considerations remain. The diagrams are all calculated using the conventions that $a_{solid} = 1$ and that $a_{H_2O} = 1$. Calculations by Helgeson and others (1969) show that pressure has little effect on the positions of the phase boundaries up to 500 bars. Therefore, all the calculations have been made for a pressure of 1 bar. The presence of an aqueous phase is implicit in all diagrams. That is, the aqueous phase coexists with the minerals in all stability fields, and one is to consider the aqueous phase to be saturated with respect to the minerals shown in the diagrams (Helgeson and others, 1969). All equilibrium reactions are written to conserve aluminum among the solid phases. This treatment is consistent with the low solubility of aluminum in natural waters and with the theoretical and experimental considerations of Helgeson (1969) and Paces (1973) which were discussed in Appendix 2.

The water samples of the Animas Valley range in measured temperature from 18°C to 85°C. As shown in the body of the thesis, chemical geothermometers imply that the higher temperature waters from the hot wells were last at chemical equilibrium in the model system at approximately 150°C. Mixing models suggest that the 150°C water is a mixture of shallow ground water (23°C) and a deep reservoir water ($\sim$ 250°C). Given the wide range of observed and calculated temperatures, it is neither practicable nor meaningful to calculate mineral stability diagrams for each temperature. Instead, I have chosen to

use diagrams at 25°C, 150°C, and 250°C, to represent shallow groundwater, mixed water, and reservoir water temperatures, respectively.

As was proposed in Appendix 2, for interpreting saturation indices, caution must be exercised in interpreting the mineral stability diagrams. The fact that a water composition falls in the stability field of a mineral in one of the diagrams does not require that the mineral be present, either in the original country rock or as an alteration phase, nor give any indication of the quantity of the mineral. In particular, for a case such as that shown by equation (A4.4), if components other than those shown in the equation are present, then either kaolinite or microcline, or both, may not be stable with respect to other minerals that might coexist with the aqueous phase (Helgeson and others, 1969). The only appropriate use of such diagrams is to demonstrate the reasonable phases which would be in equilibrium with the respective water compositions.

APPENDIX 5

Oxygen and Hydrogen Isotope Relationships in Geothermal and Related Groundwaters

Given the extremely low salinity of all of the groundwater samples from the Animas Valley, it is clear that H_2O is the dominant constituent of the fluids in the system, including the deep reservoir fluid. Therefore, knowledge of the origin of the water in the geothermal system is a crucial piece of information in a study of such a system. While variations in dissolved salts in aqueous solutions yield information on the physicochemical history of the solution and on the minerals with which the solution interacted, they do not give any information about the origin of the solvent, water. The origin of the water, and some aspects of its history, can be determined only by examining the water molecules.

Both hydrogen and oxygen have stable isotopes which show variable but systematic abundances in natural waters. The purpose of this appendix is to discuss the principles of the isotope geochemistry of hydrogen and oxygen as it applies to using D/H and $^{18}O/^{16}O$ analyses as indicators of the origin and history of H_2O in the waters of the Animas Valley.

Isotopic Notation and Standards

The isotopic data are reported as δD or $\delta^{18}O$ in the conventional permil/notation,

$$\delta = \frac{Rspl-Rstd}{Rstd} \times 10^3, \qquad (A5.1)$$

where Rspl = D/H or $^{18}O/^{16}O$ ratio in the sample and Rstd is the corresponding ratio in the standard. The standard for both hydrogen and oxygen in water as Standard Mean Ocean Water (SMOW), first defined by Craig (1961) as an arbitrary standard in terms of a National Bureau of Standards water reference sample, NBS-1, and later redefined as a stable water reference sample, Vienna SMOW (V-SMOW), by the International Atomic Energy Agency (IAEA). Craig's 1961 SMOW and V-SMOW are not identical (Friedman and O'Neil, 1977), but differences between the two systems are smaller than the limit of precision of the analyses. In calibrating the mass spectrometer for hydrogen and oxygen isotopic analyses, V-SMOW, NBS-1, NBS-1A, and SLAP (Standard Light Antarctic Precipitation), another IAEA standard, were used. All values reported in the thesis are relative to SMOW.

Analytical Methods

D/H ratios were determined on H_2 gas produced from the sample waters following the general technique of Bigeleisen and others (1952), as adapted by Robert Rye of the U.S.G.S. Isotope Branch in Denver, Colorado. A 25 µl aliquot of well-mixed sample water is injected by syringe through a latex membrane into a "cold-finger" on the vacuum manifold. The water is frozen at liquid nitrogen temperature to permit the pumping away of all noncondensible gases. The ice is melted and slowly warmed to room temperature. The water is than passed over uranium metal at approximately 800°C to reduce the water and produce H_2 gas:

$$U^0 + 2H_2O \longrightarrow UO_2 + 2H_2. \qquad (A5.2)$$

At 800°C the reaction is rapid and quantitative, producing H_2 gas with the same D/H ratio as was present in the sample water. Aliquots of the H_2 sample are taken directly to the mass spectrometer and analyzed within 30 minutes of extraction to minimize any possible loss of H_2 by diffusion through the stopcock grease on the sample tubes. In addition to calibrating the mass spectrometer with recognized standards (V-SMOW, NBS-1, NBS-LA, SLAP) at the beginning and end of each analytical session, internal laboratory standards were run after each set of four sample analyses to maintain calibration. Blanks and duplicates were analyzed at irregular intervals. While the sample preparations were done by persons familiar with the samples, the mass spectrometry was done by a laboratory technician totally unfamiliar with the Animas Valley project and my numbering system. Therefore, the actual analyses of D/H ratios have all the salient features of a blind experiment.

$^{18}O/^{16}O$ ratios were measured on CO_2 gas prepared by the CO_2-H_2O equilibration method of Epstein and Mayeda (1953) as adapted by Gary P. Landis at the stable isotope laboratory at the University of New Mexico. Twenty ml of sample water at ambient temperature and pressure are pipetted into a 200 ml round bottom flask. Next, 0.25 ml of 6N HCl is added to the sample to lower the pH below 6 to facilitate equilibration. The acid is diluted from stock concentrated HCl using distilled local water, which has a $\delta^{18}O$ value close to average meteoric water in southwestern New Mexico. The addition of approximately 1 percent of such water to the sample has no significant effect on the measured isotopic values reported in the thesis. A

stopcock attachment is fitted to the flask and the assembly is then fitted to the vacuum manifold. The water is frozen in a solid carbon dioxide (dry ice) -- ethylene glycol monobutyl ether bath, and the air is pumped away. After the water is melted to release any trapped gases, the water is refrozen and pumped again to remove all remaining noncondensible gases. The ice is remelted and commercial cylinder CO_2 of known isotopic composition is introduced into the flask at a pressure approximately 2 cm Hg below ambient atmospheric pressure. The flask is closed at the stopcock, removed from the manifold, and equilibrated in a water bath thermostated at 25°C for four days. After equilibration the flask is returned to the vacuum manifold, the water frozen, and the CO_2 transferred to sample tubes for analysis on the mass spectrometer. Since the CO_2-H_2O exchange is occurring at equilibrium and at a constant temperature, one can consider a model exchange reaction

$$C^{16}O_2 + 2H_2{}^{18}O \rightleftharpoons C^{18}O_2 + 2H_2{}^{16}O \qquad \text{(A5.3)}$$

which can be characterized by an equilibrium fractionation factor

$$\alpha_{CO_2\text{-}H_2O} = \frac{1 + \frac{\delta^{18}CO_2}{1000}}{1 + \frac{\delta^{18}O_{H_2O}}{1000}} . \qquad \text{(A5.4)}$$

Rearranging equation (A5.4) yields

$$\delta^{18}O_{H_2O} = \left[\frac{1 + \frac{\delta^{18}O_{CO_2}}{1000}}{\alpha_{CO_2\text{-}H_2O}} - 1 \right] 10^3. \qquad \text{(A5.5)}$$

$\alpha_{CO_2\text{-}H_2O}$ at 25°C is 1.0412 (Friedman and O'Neil, 1977) and $\delta^{18}O$ is measured in the mass spectrometer. The mass, and therefore, the number of moles, of the sample water is calculated from the volume and density. Treating low pressure (< 1 atm) CO_2 as an ideal gas, the number of moles of CO_2 introduced can be calculated from the measured pressure and temperature and the known volume of the system. The number of moles of oxygen of each species follows from stoichiometry. From the known $\delta^{18}O_{CO_2}$, the measured $\delta^{18}O_{H_2O}$, and the mass balance, one can calculate the $\delta^{18}O_{H_2O}$ of the sample water.

The hydrogen isotope analyses were performed on a standard 3-inch 60° sector Nier-type gas ratio mass spectrometer at the U.S.G.S. Isotope Branch laboratory in Denver, Colorado. The oxygen isotope analyses were performed on a 3-inch 60° sector Nier-type gas ratio mass spectrometer at the University of New Mexico. In both bases data were interpreted graphically and numberically by means of a digital integrator interfaced to a mini-computer. The precision of the δD data is better than $\pm$ 2% the precision of the $\delta^{18}O$ data is better than $\pm$ 0.2%. The H_3^+ correction problem in the hydrogen analyses has been circumvented at the Denver laboratory by accepting Craig's (1961) δD values of -47.6% and -183.3% for NBS-1 and NBS-1A, respectively.

Isotope Fractionation Processes

The variability of the O and H isotope abundances in natural waters is due to isotope fractionation during chemical reactions and during such physical processes as changes of state and molecular diffusion. The following discussion will present some basic information on the isotopes of hydrogen and oxygen, review fractionations due to equilibrium chemical reactions in some detail, and then consider some aspects of kinetic chemical fractionations and physical fractionations. The approach draws heavily from Broecker and Oversby (1970), Hoefs (1980), and personal communications from C. J. Yapp.

Isotopes are defined to be atoms of an element whose nuclei contain the same number of protons but a different number of neutrons. Isotopes are conventionally denoted in the form

$$^{m}_{n}E,$$

where the superscript m represents the mass number and the subscript n represents the atomic number of element E. For example, $^{16}_{8}O$ is the isotope of oxygen with 8 protons and 8 neutrons in the nucleus. Since all isotopes of a given element have the same atomic number, it is convenient to drop the subscripted n from the denotation. Thus, one discusses variations in the abundances of ^{18}O and ^{18}O or ^{1}H and ^{2}H (more commonly, H and D, for protium and deuterium).

Average natural abundances of the stable isotopes of hydrogen are

H: 99.9844 atom %

D: 0.0156 atom % (Hoefs, 1980),

and the natural terrestrial range of D/H variation is $82.6 \times 10^{-6} \leq D/H \leq 171.2 \times 10^{-6}$ (C. J. Yapp, personal communication, 1980). The average natural abundances of the stable isotopes of oxygen are

^{16}O: 99.763 atom %
^{17}O: 0.0375 atom %
^{18}O: 0.1995 atom % (Hoefs, 1980),

and the natural terrestrial range of $^{18}O/^{16}O$ variation is $1.8848 \times 10^{-3} \leq {}^{18}O/^{16}O \leq 2.0854 \times 10^{-3}$ (C. J. Yapp, personal communication, 1980). The average natural molecular abundances of the hydrogen isotopic species of water are

$H_2{}^{16}O$: 0.99732
$HD^{16}O$: 155.6×10^{-6}
$D_2{}^{16}O$: 0.0243×10^{-6};

analogous ratios can be calculated with respect to ^{18}O (C. J. Yapp, personal communication, 1980). In addition to providing basic information about the stable isotopes of hydrogen and oxygen, these figures point out three important concepts. First, D and ^{18}O are present as trace constituents of natural hydrogen and oxygen and their compounds. Second, the natural variation in D/H and $^{18}O/^{16}O$ is remarkably small, but is easily distinguished with modern mass spectrometry. Third, since the natural abundance of HDO is 6400 times that of D_2O, HDO is the only important source of deuterium in natural waters.

Because all the isotopes of a given element are atoms of the element, they are usually considered to have identical electronic structures and will form identical bonds in any given compound. However, differences in the physicochemical properties of isotopes arise from the quantum mechanical implications of the differences in mass. Because translational, rotational, and vibrational energies are all functions of mass, the replacement of an atom in a molecule by one of its isotopes will result in a molecule which differs in chemical and physical behavior from the original molecule. Important thermal properties which vary with mass as a consequence of these considerations include internal energy, heat capacity, and entropy. Consideration of the relationship between zero-point energy and mass for isotopes of any element in a diatomic gas indicates that the bonds formed by lighter isotopes are more easily broken than bonds of the heavier isotopes (Broecker and Oversby, 1970). These quantum mechanical effects will be reflected also in such physical properties of a compound as density, melting point, and vapor pressure. Since the analytical data given in the form of δ values, that is in the form measured of $^{18}O/^{16}O$ or D/H, one must be able to develop a mathematical expression for the ratio of the species of interest in terms of the thermodynamics and/or statistical mechanics if one is to quantitatively understand the processes of stable isotope fractionation. The analysis will begin with a consideration of processes under equilibrium for the oxygen isotopic system.

As a model, consider the reaction of nitrogen gas with isotopically pure oxygen gas,

$$N_2 + {}^{16}O_2 \rightleftharpoons 2N{}^{16}O, \tag{A5.6}$$

with

$${}^{16}K_{eq} = \frac{[N{}^{16}O]^2}{[N_2][{}^{16}O_2]}\ ; \tag{A5.7}$$

$$N_2 + {}^{18}O_2 \rightleftharpoons 2N{}^{18}O, \tag{A5.8}$$

with

$${}^{18}K_{eq} = \frac{[N{}^{18}O]^2}{[N_2][{}^{18}O_2]}\ , \tag{A5.9}$$

where ${}^{n}K_{eq}$ is the equilibrium constant for the reaction of nitrogen with oxygen of pure isotopic composition n and the brackets indicate an appropriate concentration term. Reactions (A5.6) and (A5.8) can be combined into a model equilibrium exchange reaction,

$${}^{18}O_2 + 2N{}^{16}O \rightleftharpoons {}^{16}O_2 + 2N{}^{18}O, \tag{A5.10}$$

with

$$K_{ex} = \frac{\{[N{}^{18}O]/[N{}^{16}O]\}^2}{[{}^{18}O_2]/[{}^{16}O_2]} = \frac{{}^{18}K_{eq}}{{}^{16}K_{eq}}\ , \tag{A5.11}$$

where K_{ex} is the equilibrium constant for the exchange reaction.

From statistical mechanics, it can be shown that all thermodynamic functions can be written in terms of Q, the partition function for a chemical system, and that Q can be written in terms of q, the molecular partition function (Castellan, 1970). Given the relations

$$A = -kT\ln Q$$

and

$$\mu_a = (\partial A/\partial N_a)_{T,V} ,$$

where A = the Helmholtz function, k = Boltzman's constant, T = absolute temperature, μ_a = chemical potential of species a in mixture, and N_a = number of molecules of species a, and the Sterling formula, which related Q and q,

$$\mu_a = -kT\ln \left(\frac{q_a}{N_a}\right) , \qquad \text{(A5.13)}$$

which expresses the chemical potential of an ideal gas in terms of the molecular partition function per molecule (Castellan, 1970).

At low pressure the gases of reaction (A5.10) can all be considered as ideal diatomic gases. Therefore, for the exchange reaction, the equilibrium condition is

$$\mu^{18}O_2 + 2\mu N^{16}O = \mu^{16}O_2 + 2\mu N^{18}O. \qquad \text{(A5.14)}$$

Rewriting the chemical potentials in the form given by equation (A5.13) and dividing both sides of the equation by (-kT),

$$\ln\left(\frac{q_{^{18}O_2}}{N_{^{18}O_2}}\right) + \ln\left(\frac{q_N{}^{16}O}{N_N{}^{16}O}\right)^2 = \ln\left(\frac{q_{^{16}O_2}}{N_{^{16}O_2}}\right) + \ln\left(\frac{q_N{}^{18}O}{N_N{}^{18}O}\right)^2 \qquad \text{(A5.14a)}$$

Taking exponents and rearranging, this becomes,

$$\frac{(N_N{}^{18}O/N_N{}^{16}O)^2}{N_{^{18}O_2}/N_{^{16}O_2}} = \frac{(q_N{}^{18}O/q_N{}^{16}O)^2}{q_{^{18}O_2}/q_{^{16}O_2}} . \qquad \text{(A5.14b)}$$

The concentration of the ith component can be expressed as

$$[i] = \frac{Ni}{V} ,$$

where V is volume in cm^3, and the concentration unit is molecules/cm^3. Multiplying the left-hand side of equation (A5.14b) by $[(\frac{1}{V^2}/\frac{1}{V^2})/(\frac{1}{V}/\frac{1}{V})]$,

$$\frac{\{[N^{18}O]/[N^{16}O]\}^2}{[^{18}O_2]/[^{16}O_2]} = \frac{(q_N{}^{18}O/q_N{}^{16}O)^2}{q_{^{18}O_2}/q_{^{16}O_2}} , \qquad \text{(A5.15)}$$

where the ratio of the concentrations on the left-hand side of the equation is the equilibrium constant for reaction (A5.10) in concentration units of molecules/cm^3. Therefore,

$$K_{ex} = \frac{(q_N{}^{18}O/q_N{}^{16}O)^2}{q_{^{18}O_2}/q_{^{16}O_2}} . \qquad \text{(A5.16)}$$

For an ideal diatomic gas, it can be shown that the molecular partition function, q, is the product of the partition functions for the translational, rotational, and vibrational degrees of freedom in the molecule (Castellan, 1970). The statistical mechanical expressions for q_{trans}, q_{rot}, and q_{vib} can be found in any standard physical chemistry text. Since q_{trans} and q_{rot} are functions of mass and temperature and q_{vib} is a function of temperature and vibrational frequency, then q and K_{ex} must also be functions of mass, temperature, and vibrational frequency.

The problem reduces to relating K_{ex} to the isotopic ratios actually measured in the mass spectrometer. One begins by defining a new function, called the isotope fractionation factor,

$$\alpha_{A-B} = \frac{R_A}{R_B} , \qquad \text{(A5.17)}$$

where R_A is the isotopic ratio of interest in substance A and R_B is the isotopic ratio of interest in substance B. For reaction (A5.10)

$$\alpha_{NO-O_2} = \frac{(^{18}O/^{16}O)_{NO}}{(^{18}O/^{16}O)_{O_2}} = \frac{[N^{18}O]/[N^{16}O]}{\frac{2[^{18}O^{18}O] + [^{18}O/^{16}O] + [^{16}O/^{18}O]}{2[^{16}O^{16}O] + [^{18}O/^{16}O] + [^{16}O/^{18}O]}} , \qquad \text{(A5.17a)}$$

assuming that the molecules $^{18}O^{16}O$ and $^{16}O^{18}O$ are distinguishable.

Now let x = abundance of ^{18}O in NO,

y = abundance of ^{16}O in NO,

x' = abundance of ^{18}O in O_2,

y' = abundance of ^{16}O in O_2.

Treating these abundances in the ideal gas as random variables, one can consider the probabilities of molecular combination and atomic ratios in terms of the four random variables. For example, $p(^{18}O^{18}O) = x^2$; $(^{18}O/^{16}O)_{NO} = x/y$; and $(^{18}O/^{16}O)_{O_2} = \frac{2(x')^2 + 2(x'y')}{2(y')^2 + 2(x'y')}$. Therefore,

$$\alpha_{NO\text{-}O_2} = \frac{x/y}{\frac{x'}{y'}\frac{2x' + 2y'}{2y' + 2x'}} = \frac{x/y}{x'y'} . \qquad \text{(A5.18)}$$

But

$$K_{ex} = \frac{(x/y)^2}{(x')^2/(y')^2} = \left[\frac{(x/y)}{(x'/y')}\right]^2 . \qquad \text{(A5.19)}$$

Therefore,

$$K_{ex} = \alpha^2,$$

or

$$\alpha_{NO\text{-}O_2} = K_{ex}^{1/2} . \qquad \text{(A5.20)}$$

In general, for any two species A and B for which the isotopes of interest are randomly distributed over all possible positions,

$$\alpha = K^{1/n} , \qquad \text{(A5.21)}$$

where n is the number of atoms exchanged (Friedman and O'Neil, 1977). Thus, one can demonstrate that at equilibrium the stable isotopes of a given element are fractionated as known functions of mass and temperature and that the thermodynamics of the fractionation can be

related quantitatively to ratios of the isotopes which are measurable in the mass spectrometer.

There are some mathematical aspects of the fractionation factor, α, which are of practical importance. Combining equations (A5.1) and (A5.17), it is clear that α_{A-B} is related to the δ values by the expression

$$\alpha_{A-B} = \frac{1 + \frac{\delta_A}{1000}}{1 + \frac{\delta_B}{1000}}, \qquad \text{(A5.22)}$$

For a system at equilibrium, one can consider the variation of α with temperature by applying the Gibbs-Helmholtz equation in the form

$$\frac{d \ln \alpha^n}{d T} = \frac{H^\circ}{RT^2}, \qquad \text{(A5.23)}$$

where $\alpha^n = K_{ex}$. Since values of α are usually $\simeq 1.00i$, $\ln(1.00i) \simeq 0.00i$, and $1000 \ln i \simeq i$, the permil fractionation. For ideal gases, $\ln\alpha$ varies as $1/T$ at low temperature and as $1/T^2$ at high temperatures. For most systems of geologic interest, there are linear relationships between $1000 \ln\alpha$ and $1/T^2$ over large temperature ranges for experimentally determined values. An important exception to this is the case of hydrogen in water, ${}^{D}\alpha_{H_2O_{(l)}-H_2O_{(v)}}$, for which there is a crossover point in the $1000 \ln\alpha$ - $1/T^2$ plot at approximately 221°C (Friedman and O'Niel, 1977).

One can go on to consider fractionations due to kinetic chemical reactions and physical processes. This section of the appendix will present some of the major conclusions related to nonequilibrium fractionations. If equations (A5.6) and (A5.8) are rewritten as irreversible reactions, for each of which there is a characteristic rate constant, then, when the isotopic ratios of the products are determined, it can be shown that: 1) the light isotope generally reacts faster than the heavy isotope at a given temperature; 2) early in the reaction, there will be a kinetic isotope fractionation due strictly to the different rate constants; and (3) if the reactions are run to completion and products are not separated during the reaction, there is no net fractionation of isotopes (C. J. Yapp, personal communication, 1980). The third conclusion is particuarly important in sample preparation -- as in the preparation of H_2 gas from H_2O, where 100% conversion is needed to avoid experimental fractionation. The physical processes of greatest geologic interest are changes of state and molecular diffusion. Since HDO and $H_2{}^{18}O$ have lower vapor pressures than does $H_2{}^{16}O$, there will be isotopic fractionation during evaporation or condensation, with the liquid phase enriched in the heavier isotopes. As one might expect from the considerations of kinetic reactions, light isotopes move more quickly than heavy isotopes in diffusive processes, setting up isotopic diffusion gradients.

δD and $\delta^{18}O$ Systematics in Groundwater

From hydrologic, geologic, and geochemical evidence, there can be no doubt that the overwhelming mass of groundwater is meteoric in origin. Therefore, the isotopic composition of groundwater must be

controlled primarily by processes in the hydrologic cycle, particularly condensation and evaporation. Water-rock interaction, mixing with nonmeteoric water, and other factors, such as postinfiltration changes in state, may be superimposed, but the original meteoric signature of groundwater should be decipherable.

Craig (1961) demonstrated that there is a very systematic variation of δD and $\delta^{18}O$ in meteoric waters,

$$\delta D = 8\ \delta^{18}O + 10, \tag{A5.24}$$

which is conventionally plotted on graphs of δD versus $\delta^{18}O$ and labeled as the "meteroic water line", as in Figure 7 in the body of the thesis. The only meteoric waters in Craig's data set for which this relationship does not hold are samples from closed basins in evaporating settings and East African rivers and lakes, for which evaporation is also an important hydrologic condition.

Virtually all researchers working with stable isotopes in meteoric waters have recognized that precipitation can be described in terms of the Rayleigh distillation model, in which condensed water forms in instantaneous equilibrium with water vapor and is subsequently removed from the cloud (e.g., Craig, 1961; Dangsgaard, 1964; Eriksson, 1965). The Rayleigh model can be expressed by the relation

$$\frac{1 + \frac{\delta_c}{1000}}{1 + \frac{\delta_{c_0}}{1000}} = f^{\alpha c - v - 1}, \tag{A5.25}$$

where δ_c is the δD or $\delta^{18}O$ value of the condensate, δ_{c_0} is the δD or $\delta^{18}O$ value of the initial condensate, f is the fraction of vapor remaining, and α_{c-v}, the isotope fractionation fractor for $H_2O_{(v)} \rightleftharpoons H_2O_{(l)}$ at the temperature of interest; is considered to be constant. At 25°C, $^{18}\alpha_{c-v} = 1.0093$ and $^{D}\alpha_{c-v} = 1;0790$ (Majzoub, 1971, in Friedman and O'Neil, 1977). Taking the natural logarithm of both sides of equation (A5.25), using the approximations that

$$\frac{1 + \frac{\delta_c}{1000}}{1 + \frac{\delta_{c_0}}{1000}} \simeq 1 + \left[\frac{(\delta_c - \delta_{c_0})}{1000}\right]$$

and

$$1000 \ln(1 + .00z) = z,$$

multiplying both sides of the modified Rayleigh equation by 1000, and taking the ratio of the resulting expressions for δD and $\delta^{18}O$ yields,

$$\frac{\delta D_c - \delta D_{c_o}}{\delta^{18}O_c - \delta^{18}O_{c_o}} \equiv \frac{\Delta D}{\Delta^{18}O}$$

$$= \frac{^{D}\alpha_{c-v} - 1}{^{18}\alpha_{c-v} - 1} \qquad \text{(A5.26)}$$

For the 25°C α values given above, the Rayleigh model indicates that there is an expected linear relationship between δD and $\delta^{18}O$ in precipitation with a slope of 8.49, in excellent agreement with Craig's

measured values, particularly given the assumptions and the approximations of the model and the computations.

Craig (1961) proposed that the process of free evaporation at temperatures close to the ambient temperatures of the earth's surface was controlled by kinetic factors which offset the closed basins and the East African waters from the meteoric water line along slopes of approximately 5. Craig, Gordon, and Horibe (1963) experimentally confirmed the earlier proposal and demonstrated that for evaporation under conditions of natural relative humidity ranges, ΔD and $\Delta^{18}O$ approach steady state values. A more detailed theoretical analysis of steady-state evaporating reservoirs shows that the δ value of the reservoir is a function of equilibrium and kinetic fractionation factors (which are temperature dependent), relative humidity, the δ value of the atmosphere into which the reservoir is evaporating, the δ value of inlet water, if any exists, and the fraction of water left to flow out of the reservoir if there is an outlet (Eriksson, 1965; C. J. Yapp, personal communication, 1980). For natural systems, the slope of the evaporation trend in a δD - $\delta^{18}O$ plot will increase from approximately 5 to approximately 8 as the relative humidity increases toward 1 (C. J. Yapp, personal communication, 1980).

Except under conditions of exceptionally low relative humidity, most evapotranspiration, which takes place from capillary systems, does not effectively fractionate meteoric water (Eriksson, 1965). Therefore, groundwater should acquire the isotopic composition of the precipitation which is recharging the system. Spatial and temporal surveys of stable isotope variations of precipitation and other meteoric waters can be used to distinguish seasonal recharge, to

recognize geographic sources of recharge, and to identify nonmeteoric processes in groundwater histories. Particularly relevant to this thesis are isotope studies related to arid regions hydrology and to geothermal systems. Simpson and others (1970) used deuterium analyses to distinguish seasonal recharge to the Tucson groundwater basin in southern Arizona. Gat and Dansgaard (1972) and Gat and Issar (1974) used integrated δD - $\delta^{18}O$ studies to identify recharge areas and to distinguish between paleo-meteoric waters and evaporated modern waters in Israel. Craig (1963, 1966), using integrated δD - $\delta^{18}O$ studies on geothermal waters, described the so-called "oxygen shift" and attributed the variable $\delta^{18}O$ but essentially constant δD values to equilibration of oxygen in water with silicate and/or carbonate rocks at elevated temperatures. Truesdell and others (1977), using both stable isotopes and some aspects of the aqueous geochemistry of the system, described the effects of subsurface boiling and dilution on the isotopic composition of geothermal waters at Yellowstone. Most of the ideas and approaches used to interpret the isotopic data in the body of the thesis are drawn from these studies.

Apparent and True Fractionation Factors for a Mixture of Waters

Consider a two-component mixture of coexisting waters, each with a characteristic $\delta^{18}O$ value, in which one of the waters is derived from the other by separation and recondensation of a steam phase. Let water (1) be the parent water, with isotopic value $\delta^{18}O_{(1)}$; let water (2) be the condensate of boiled water (1), with isotopic value $\delta^{18}O_{(2)}$. The coexistance of the two isotopically distinct waters defines an apparent fractionation factor,

$$\alpha_{app} = \frac{1 + \frac{\delta^{18}O_{(2)}}{1000}}{1 + \frac{\delta^{18}O_{(1)}}{1000}} \qquad (A5.27)$$

The process of boiling is continuous over some time interval during which a fraction of the original liquid water (1) is converted to steam and recondensed as liquid water (2). Therefore, the isotopic value of water (2) represents an integrated value dependent on the fractionation between liquid and vapor water during the boiling interval. Because isotopic equilibrium between steam and water is established virtually instantaneously (Giggenbach, 1971), the fractionation that occurs during the boiling process can be represented by an equilibrium, or true α value. If one treates the boiling process as a Rayleigh distillation, it is possible to derive a simple relationship between the apparent α and the true α. Having derived the equilibrium α, one can use the known temperature dependence of α to establish a model temperature at which the boiling process occurred.

For the given condition of Rayleigh distillation,

$$\frac{^{18}R_{(2)}}{^{18}R_{(2)_o}} = f^{\alpha-1}, \qquad (A5.28)$$

where $^{18}R_{(2)}$ is the $^{18}O/^{16}O$ ratio in water (2), $^{18}R_{(2)_o}$ is the $^{18}O/^{16}O$ ratio of the initial water (2), f is the fraction of water (1) remaining, and α is the equilibrium fractionation factor for $H_2O_{(1)} \rightleftharpoons H_2O_{(2)}$. Using the basic definition of α, equation (A5.28) can be rewritten,

$$f^{\alpha-1} = \frac{1 + \frac{\delta^{18}O_{(2)}}{1000}}{1 + \frac{\delta^{18}O_{(2)o}}{1000}} . \qquad \text{(A5.29)}$$

Algebraically rearranging (A5.29),

$$^{18}O_{(2)f} = [f^{\alpha-1}(1 + \frac{\delta^{18}O_{(2)o}}{1000} - 1[\times 10^3, \qquad \text{(A5.30)}$$

where $\delta^{18}O_{(2)f}$ is the $\delta^{18}O$ value of water (2) when f is the fraction of water (1) remaining.

Since the observed $\delta^{18}O_{(2)}$ is a value integrated over the duration of the boiling process, one can consider an average $\delta^{18}O_{(2)}$ over the interval of boiling,

$$\overline{\delta^{18}O_{(2)f_1,f_2}} = \frac{\int_{f_1}^{f_2} [f^{\alpha-1}(1 + \frac{\delta^{18}O_{(2)o}}{1000}) - 1] \times 10^3 \, df}{\int_{f_1}^{f_2} df}, \qquad \text{(A5.31)}$$

where f_1 is the fraction of original water (1) which is left when boiling begins and f_2 is the fraction of water (1) which is left when boiling ends. Integrating equation (A5.31) can be rewritten,

$$\overline{\delta^{18}O_{(2)f_1,f_2}} = \frac{10^3[\frac{1}{\alpha} f^{\alpha} (1 + \frac{\delta^{18}O_{(2)o}}{1000})]_{f_1}^{f_2} - (f_2 - f_1)}{f_2 - f_1} . \qquad \text{(A5.32)}$$

Substituting (A5.32) into equation (A5.27),

$$\alpha_{app} = \frac{1 + [(1 + \frac{\delta^{18}O_{(2)o}}{1000})(\frac{f_2^{\alpha} - f_1^{\alpha}}{\alpha\ (f_2 - f_1)}) - 1]}{(1 + \frac{\delta^{18}O_{(1)f_2}}{1000})} \qquad \text{(A5.33)}$$

Given that there exists an equilibrium α, one can rewrite $\delta^{18}O_{(1)}$ in terms of α and $\delta^{18}O_{(2)}$ and substitute into equation (A5.33) to yield,

$$\alpha_{app} = \frac{1 + [(1 + \frac{\delta^{18}O_{(2)o}}{1000})(\frac{f_2^{\alpha} - f_1^{\alpha}}{\alpha\ (f_2 - f_1)}) - 1]}{\frac{1}{\alpha}\ (1 + \frac{\delta^{18}O_{(2)f_2}}{1000})} . \qquad \text{(A5.34)}$$

But, using the Rayleigh model,

$$(1 + \frac{\delta^{18}O_{(2)f_2}}{1000}) = f_2^{\alpha-1}\ (1 + \frac{\delta^{18}O_{(2)o}}{1000}) . \qquad \text{(A5.34)}$$

Therefore,

$$\alpha_{app} = \frac{(f_2^{\alpha} - f_1^{\alpha})}{f_2^{\alpha-1}\ (f_2 - f_1)} , \qquad \text{(A5.36)}$$

which gives the required relationship between the apparent isotopic fractionation factor defined by the samples and the true equilibrium factor of the boiling process. The equilibrium fractionation factor, α, can be related to temperature by using the experimentally derived relationship,

$$10^3 \ell n\alpha = +0.7.664(10^8 T^{-2}) + 1.2051(10^3 T^{-1}) - 3.493$$

and the graphical solution presented in Friedman and O'Neil (1977).

The derivation of equation (A5.36), reproduced as equation (3) in the body of the thesis, was suggested by a discussion of the isotopic systematics of sulfur in coexisting sulfides and sulfates by C. J. Yapp (personal communication, 1980).

REFERENCES

Arnorsson, S., 1975, Application of the Silica Geothermometer in Low Temperature Hydrothermal Areas in Iceland: American Journal of Science, v. 275, p. 763-784.

Barnes, H. L. and Rimstidt, J. D., 1978, Chemistry of Scale Formation, in Collies, M. J. (ed.), Geothermal Energy - Recent Developments: Park Ridge, New Jersey, Noyes Data Corp., p. 274.

Berner, R. A., 1976, The Solubility of Calcite and Aragonite in Seawater at Atmospheric Pressure and 34.5% Salinity: American Journal of Science, v. 276, p. 713-730.

Bigeleisen, J., Perlman, M. L. and Prosser, H. C., 1952, Conversion of Hydrogenic Materials to Hydrogen for Isotopic Analysis: Analtyical Chemistry, v. 24, p. 1356-1357.

Broecker, W. S. and Oversby, V. M., 1971, Chemical Equilibria in the Earth: New York, McGraw-Hill, 318 p.

Browne, P. R. L., 1978, Hydrothermal Alteration in Active Geothermal Fields: Annual Review of Earth and Planetary Science, v. 6, p. 229-250.

Browne, P. R. L. and Ellis, A. J., 1970, The Ohaki-Broadlands Hydrothermal Area, New Zealand: Mineralogy and Related Geochemistry: American Journal of Science, v. 269, p. 97-131.

Callender, J. F., 1981, Final Report of "Evaluation of Geothermal Potential of the Basin and Range Province of New Mexico," Grant Nos. 117, 264, and 350 of the New Mexico Energy Research and Development Program of the New Mexico Energy and Minerals Department - Geothermal Institute; for co-investigators D. G. Brookins,

W. E. Elston, G. R. Jiracek, A. M. Kudo, G. P. Landis, C. A. Swanberg, and L. A. Woodward.

Castellan, G. W., 1971, Physical Chemistry: Reading, Massachussetts, Addison-Wesley, 866 p.

Craig, Harmon, 1961, Isotopic Variations in Meteoric Waters: Science, v. 133, p. 1702-1703.

Craig, Harmon, 1963, The Isotopic Geochemistry of Water and Carbon in Geothermal Areas, in Tongiorgi, E. (ed.), Nuclear Geology on Geothermal Areas - Spoleto, 1963: Pisa, Consiglio Nationale delle Ricerche, Laboratorio di Geologia Nucleare, p. 17-53.

Craig, Harmon, 1966, Isotopic Composition and Origin of the Red Sea and Salton Sea Geothermal Brines: Science, v. 154, p. 1544-1548.

Craig, Harmon, Gordon, L. I., and Horibe, Y., 1963, Isotopic Exchange Effects in the Evaporation of Water; 1. Low Temperature Experimental Results: Journal of Geophysical Research, v. 68, p. 5079-5087.

Dansgaard, W., 1964, Stable Isotopes in Precipitation: Tellus, v. 16, p. 436-468.

Deal, E. G., Elston, W. E., Erb, E. E., Peterson, S. L., Reiter, D. E., Damon, P. E., and Shafiquallah, M., 1978, Cenozoic Volcanic Geology of the Basin and Range Province in Hidalgo County, Southwestern New Mexico: New Mexico Geological Society, Guidebook to the 29th Field Conference, p. 219-229.

Dellechaie, Frank, 1977, A Geologic and Hydrogeochemical Study of the Animas Geothermal Area, Hidalgo County, New Mexico: Geothermal Resources Council, Transactions, v. 1, p. 73-75.

Denbigh, Kenneth, 1955, The Principles of Chemical Equilibrium: Cambridge, England, University Press, 491 p.

Elder, John, 1976, The Bowels of the Earth: London, Oxford University Press, 272 p.

Ellis, A. J., 1977, Chemical and Isotopic Techniques in Geothermal Investigations: Geothermics, v. 5, p. 3-12.

Ellis, A. J. and Mahon, W. A. J., 1964, Natural Hydrothermal Systems and Experimental Hot Water/Rock Interactions: Geochimica et Cosmochimica Acta, v. 28, p. 1323-3157

Ellis, A. J. and Mahon, W. A. J., 1977, Chemistry and Geothermal Systems: New York, Academic Press, 392 p.

Ellis, A. J. and McFadden, I. M., 1972, Partial Molal Volumes of Ions in Hydrothermal Solutions: Geochimica et Cosmochimica Acta, v. 36, p. 413-426.

Elston, W. E., Damon, P. E., Coney, P. J., Rhodes, R. C., Smith, E. I., and Mikerman, M., 1973, Tertiary Volcanic Rocks, Mogollon-Datil Province, New Mexico, and Surrounding Region: K-Ar Dates, Patterns of Eruption and Periods of Mineralization: Geological Society of America Bulletin, v. 54, p. 2259-2274.

Elston, W. E. and Deal, E. G., 1978, Geology of the Lightning Dock KGRA and Vincity, Pyramid Mountains and Animas Valley, Hidalgo County, New Mexico: Report to the New Mexico Geothermal Energy Institute and the U.S. Geological Survey on Grants Nos. 75-109, 75-117, 76-264, 76-350, 14-08-001-G-255, and 14-08-001-G-348, 49 p.

Epstein, S. and Mayeda, T., 1953, Variation of O^{18} Content of Waters from Natural Sources: Geochimica et Cosmochimica Acta, v. 4, p. 213-224.

Eriksson, Erik, 1965, Deuterium and Oxygen-18 in Precipitation and Other Natural Waters -- Some Theoretical Considerations: Tellus, v. 17, p. 498-512.

Fleischauer, H. L., 1978, Summary of the Late Quaternary Geology of Lake Animas, Hidalgo County, New Mexico: New Mexico Geological Society, Guidebook to the 29th Field Conference, p. 283-284.

Fournier, R. O. and Potter, R. W., II, 1979, Magnesium Correction to the Na-K-Ca Chemical Geothermometer: Geochimica et Cosmochimica Acta, v. v. 43, p. 1543-1550.

Fournier, R. O. and Rowe, J. J., 1966, Estimation of Underground Temperatures from the Silica Content of Water from Hot Springs and Wet Steam Wells: American Journal of Science, v. 264, p. 685-697.

Fournier, R. O. and Truesdell, A. H., 1970, Geochemical Indicators of Subsurface Temperature Applied to Hot Spring Waters of Yellowston National Park, Wyoming, USA: Geothermics Special Issue 2, v. 2, p. 529-535.

Fournier, R. O. and Truesdell, A. H., 1973, An Empirical Na-K-Ca Geothermometer for Natural Waters: Geochimica et Cosmochimica Acta, v. 37, p. 1255-1275.

Fournier, R. O. and Truesdell, A. H., 1974, Geochemical Indicators of Subsurface Temperature - Part II, Estimation of Temperature and Fraction of Hot Water Mixed with Cold Water: Journal of Research of the U.S. Geological Survey, v. 2, p. 263-270.

Fournier, R. O., White, D. E., and Truesdell, A. H., 1974, Geochemical Indicators of Subsurface Temperature -- Part I, Basic Assumptions: Journal of Research of the U.S. Geological Survey, v. 2, p. 259-262.

Fuoss, R. M., 1935, Properties of Electrolyte Solutions: Chemical Reviews, v. 17, p. 27-42.

Friedman, Irving and O'Neil, J. R., 1977, Compilation of Stable Isotope Fractionation Factors of Geochemical Interest: U.S. Geological Survey, Professional Paper 440-KK, 110 p.

Garrels, R. M. and Christ, C. H., 1965, Solutions, Minerals, and Equilibria: New York, Harper and Row, 450 p.

Garrels, R. M. and Thompson, M. E., 1962, A Chemical Model for Seawater at 25°C and One Atmosphere Total Pressure: American Journal of Science, v. 260, p. 57-66.

Gat, J. R. and Dansgaard, W., 1972, Stable Isotope Survey of the Fresh Water Occurences in Israel and the Northern Jordan Rift Valley: Journal of Hydrology, v. 16, p. 177-212.

Gat, J. R. and Issar, Arie, 1976, Desert Isotope Hydrology: Water Sources of the Sinai Desert: Geochimica et Cosochimica Acta, v. 38, p. 1117-1131.

Giggenbach, W. F., 1971, Isotopic Composition of Waters of the Broadlands Geothermal Field: New Zealand Journal of Science, v. 14, p. 959-970.

Harned, H. S. and Davis, R. O., 1943, The Ionization Constant of Carbonic Acid in Water and the Solubility of Carbon Dioxide in Water and Aqueous Salt Solutions from 0° to 50°C: Journal of the American Chemical Society, v. 65, p. 2030-2037.

Helgeson, H. C., 1967a, Solution Chemistry and Metamorphism, in Abelson, P. H. (ed.), Research in Geochemistry: v. 2: New York, John Wiley & Sons, p. 362-404.

Helgeson, H. C., 1967b, Thermodynamics of Complex Dissociation in Aqueous Solution at Elevated Temperature: Journal of Physical Chemistry, v. 71, p. 3121-3136.

Helgeson, H. C., 1969, Thermodynamics of Hydrothermal Systems at Elevated Temperature and Pressure: American Journal of Science, v. 267, p. 729-804.

Helgeson, H. C., 1970, A Chemical and Thermodynamic Model of Ore Deposition in Hydrothermal Systems: Mineralogical Society of Ameica Special Publication 3, p. 155-186.

Helgeson, H. C., Brown, T. H. and Leeper, R. H., 1969, Handbook of Theoretical Activity Diagrams Depicting Chemical Equilibrium in Geologic Systems Involving an Aqueous Phase at One Atmosphere and 0° to 300°C: San Francisco, Freeman, Cooper, 253 p.

Helgeson, H. C. and Kirkham, D. H., 1974, Theoretical Prediction of the Thermodynamic Behavior of Aqueous Electrolytes at High Pressures and Temperatures: II. Debye-Huckel Parameters for Activity Coefficients and Relative Partial Molal Properties: American Journal of Science, v. 274, p. 1199-1261.

Hemley, J. J. and Jones, W. R., 1964, Aspects of the Chemistry of Hydrothermal Alteration with Emphasis on Hydrogen Metasomatism: Economic Geology, v. 59, p. 538-569.

Hoefs, J., 1980, Stable Isotope Geochemistry, 2nd ed.: Heidelberg and New York, Springer-Verlag, 140 p.

Holland, H. D. and Malinin, S. D., 1979, The Solubility and Occurrence of Nonore Minerals, in Barnes, H. L. (ed.), Geochemistry of Hydrothermal Ore Deposits, 2nd ed.: New York, J. Wiley & Sons, p. 461-508.

Jiracek, G. R. and Smith, C., 1976, Deep Resistivity Investigations at Two KGRAs in New Mexico: Radium Springs and Lightning Dock, in Woodward, L. A. and Northrop, S. A. (eds.). Tectonics and Mineral Resources of Southwestern North America: New Mexico Geological Society Special Publication 6, p. 71-76.

Kielland, J., 1937, Individual Activity Coefficients of Ions in Aqueous Solutions: American Chemical Society Journal, v. 59, p. 1675-1678.

Kintzinger, P. R., 1956, Geothermal Survey of Hot Ground Near Lordsburg, New Mexico: Science, v. 124, p. 629-630.

Kitahara, S., 1960, The Solubility of Quartz in Water at High Temperatures and High Pressures: Reviews of Physical Chemistry, Japan, v. 30, p. 109-114.

Klotz, I. M., 1956, Chemical Thermodynamics: Englewood Cliffs, New Jersey, Prentice-Hall, 331 p.

Krauskopf, K. B., 1956, Dissolution and Precipitation of Silica at Low Temperatures: Geochimica et Cosmochimica Acta, v. 10, p. 1-29.

Landis, G. P., 1976, Final Technical Report of "Evaluation of Geothermal Potential of the Basin and Range Province of New Mexico," Grants No. 14-08-001-G-225 of the U.S. Geological Survey; for co-investigators D. G. Brookins, J. F. Callender, W. E. Elston, G. R. Jiracek, A. M. Kudo, C. A. Swanberg, and L. A. Woodward, 117 p.

Landis, G. P. and Logsdon, M. J., 1979, Computer-Based Chemical and Stable Isotope Modeling of Geothermal Systems in New Mexico: Report to New Mexico Energy and Minerals Department, Energy Research and Development Program, Grant No. 78-2120, 83 p.

Langmuir, D., 1971, The Geochemistry of Some Carbonate Groundwaters in Central Pennsylvania: Geochimica et Cosmochimica Acta, v. 35, p. 1023-1045.

Latimer, W. M., 1952, The Oxidation States of Elements and Their Potentials in Aqueous Solutions: Englewood Cliffs, New Jersey, Prentice-Hall, 392 p.

Lewis, G. N. and Randall, M., 1923, Thermodynamics: New York, McGraw-Hill, 381 p.

Lynch, D. J., 1978, The San Bernardino Volcanic Field in Southeastern Arizona: New Mexico Geological Society, Guidebook to the 29th Field Conference, p. 261-268.

MacInnes, D. A., 1939, The Principles of Electrochemistry: New York, Reinhold, 478 p.

MacKenie, F. T. and Garrels, R. M., 1966, Chemical Mass Balance Between Rivers and Oceans: American Journal of Science, v. 264, p. 507-525.

Majzoub, M., 1971, Fractionnement en Oxygen-18 et en Deuterium Entre L'eau et sa Vapeur: Journal of Chemical Physics, v. 68, p. 1423-1436.

Mariner, R. H. and Willey, L. M., 1976, Geochemistry of Thermal Waters in the Long Valley, Mono County, California: Journal of Geophysical Research, v. 81, p. 792-800.

Marvin, R. F., Naeser, C. W., and Mehnert, H. H., 1978, Tabulation of Radiometric Ages -- Including unpublished K-Ar and fission-track ages -- for Rocks in Southeastern Arizona and Southwestern New Mexico: New Mexico Geological Society, Guidebook to the 29th Field Conference, p. 243-253.

Mottl, M. J. and Holland, H. D., 1978, Chemical Exchange During Hydrothermal Alteration of Basalt by Seawater - I. Experimental Results for Major and Minor Components of Seawater: Geochimica et Cosmochimica Acta, v. 42, p. 1103-1115.

Nordstrom, D. K., Plummer, L. N., Wigley, T. M. L., Wolery, T. J., Ball, J. W., Jenne, E. A., Bassett, R. L., Crerar, D. A., Florence, T. M., Fritz, B., Hoffman, M., Holdren, G. R., Lafon, G. M., Mattigod, S. V., McDuff, R. E., Morel, F., Reddy, M. M., Sposito, A., Thrailkill, J., 1979, A Comparison of Computerized Chemical Models for Equilibrium Calculations in Aqueous Systems, in Jenne, E. A. (ed.), Chemical Modeling in Aqueous Systems: New York, American Chemical Society, p. 857-892.

Paces, Tomas, 1973, Steady-State Kinetics and Equilibrium Between Groundwater and Granitic Rocks: Geochimica et Cosmochimica Acta, v. 37, p. 2641-2663.

Plummer, L. N., Jones, B. F., and Truesdell, A. H., 1978, WATEQF - a FORTRAN IV Version of WATEQ, a Computer Program for Calculating Chemical Equilibrium of Natural Waters: U.S. Geological Survey, Water Resources Investigations, 76-13, 63 p.

Reeder, H. O., 1957, Ground Water in Animas Valley, Hidalgo County, New Mexico: State of New Mexico State Engineer Office, Technical Report 11, 101 p.

Robie, R. A., Hemingway, R. S., and Fischer, J. R., 1978, Thermodynamic Properties of Minerals and Related Substances at 298.15 K and 1 Bar (10^5Pa) Pressure and at Higher Temperatures: U.S. Geological Survey Bulletin 1452, 456 p.

Robinson, R. A. and Stokes, R. H., 1955, Electrolyte Solutions: London, Butterworths, 559 p.

Smith, Christian, 1978, Geophysics, Geology, and Geothermal Leasing Status of the Lightning Dock KGRA, Animas Valley, New Mexico: New Mexico Geological Society, Guidebook to the 29th Field Conference, p. 343-348.

Sorey, M. L., Lewis, R. E., and Olmstead, F. H., 1978, The Hydrothermal System of Long Valley Caldera, California: U.S. Geological Survey Professional Paper 1044-A, 60 p.

Simpson, E. S., Thorud, D. B., and Friedman, Irving, 1972, Distinguishing Seasonal Recharge to Groundwater by Deuterium Analysis in Southern Arizona, in UNESCO, World Water Balance, v. 3, p. 623-633.

Summers, W. K., 1965, Prelimineary Report on New Mexico's Geothermal Energy Resources: New Mexico Bureau of Mines and Mineral Resources Circular 80, 41 p.

Swanberg, C. A. and Morgan, Paul, 1978, The Linear Relationship Between Temperatures Based on Silica Content of Groundwater and Regional Heat Flow: A New Heat Flow Map of the U.S.: PAGEOPH, v. 117, p. 227-241.

Truesdell, A. H., 1968, The Advantage of Using pE Rather than Eh in Redox Equilibrium Calculations: Journal of Geological Education, v. 16, p. 17-20.

Truesdell, A. H., 1975, Summary of Section III: Geochemical Techniques in Exploration, in Procedings of the 2nd U.N. Symposium on the Development and Use of Geothermal Resources, San Francisco, 1975: Washington, U.S. Government Printing Office, p. LIII-LXXIX.

Truesdell, A. H., 1976, Chemical Evidence of Subsurface Structure and Fluid Flow in Geothermal System, in Procedings of the 1974 International Symposium on Water-Rock Interactions: Praha, Ustredni Ustav Geologicky, p. 250-257.

Truesdell, A. H. and Fournier, R. O., 1977, Procedure for Estimating the Temperature of a Hot-Water Component in a Mixed Water by Using a Plot of Dissolved Silica Versus Enthalpy: Journal of Research of the U.S. Geological Survey, v. 5, p. 49-52.

Truesdell, A. H. and Jones, B. F., 1974, WATEQ, A Computer Program for Calculating Chemical Equilibrium of Natural Waters: Journal of Research of the U.S. Geological Survey, v. 2, p. 233-248.

Truesdell, A. H., Nathenson, M., and Rye, R. O., 1977, The Effects of Subsurface Boiling and Dilution on the Isotopic Compositions of Yellowstone Thermal Waters: Journal of Geophysical Research, v. 82, p. 3694-3704.

Van Devender, T. R. and Spaulding W. F., 1979, Development of Vegetation and Climate in the Southwestern U.S.: Science, v. 204, p. 701-710.

Walther, J. V. and Helgeson, H. C., 1977, Calculation of the Thermodynamic Properties of Aqueous Silica and the Solubility of Quartz and its Polymorphs at High Pressure and Temperature: American Journal of Science, v. 277, p. 1315-1351.

Wells, S. G., 1977, Geomorphic Controls of Alluvial Fan Deposition in the Sonoran Desert, Southwestern Arizona, in Doehring, D. O., (ed.), Geomorphology in Arid Regions: Fort Colins, Colorado, Publications in Geomorphology, p. 27-50.

Wells, S. G., 1978, Geomorphology and Neo-Tectonics, in Elston, W. E. and Deal, E. G., Geology of Lightning Dock KGRA and Vicinity, Pyramid Mountains and Animas Valley, Hidalgo County, New Mexico: Report to the New Mexico Energy Institute and the U.S. Geological Survey on Grants Nos. 75-109, 75-117, 76-264, 76-350, 14-08-001-G-255, and 14-08-001-G-348, p. 24.

White, D. E., 1957, Magmatic, Connate, and Metamorphic Waters: Geological Society of America Bulletin, v. 68, p. 1659-1682.

White, D. E., 1968, Hydrology, Activity, and Heat Flow of the Steamboat Springs Thermal System, Washoe County, Nevada; U.S. Geological Survey Professional Paper 458-C, 104 p.

White, D. E. and Williams, D. L., (eds.), 1975, Assessment of Geothermal Resources of the U.S.: U.S. Geological Survey Circular 726, 155 p.

Wigley, T. M. L., 1977, WATSPEC: A Computer Program for Determining the Equilibrium Speciation of a Aqueous Solutions: British Geomorphology Research Group Technical Bulletin, v. 20, 48 p.

Yariv, S. and Cross, H., 1979, Geochemistry of Colloid Systems for Earth Scientists: New York, Springer-Verlag, 450 p.